POLITECNICO
MILANO 1863

School of Industrial and Information Engineering

Master of Science in Aeronautical Engineering
Track in Propulsion

Estimating the Effects of Electric Propulsion for Aircraft in terms of Acoustic and Atmospheric Emissions

Supervisor
Prof. Carlo E. D. Riboldi

Co-Supervisors
Prof. Lorenzo Trainelli
Prof. Alberto L. M. Rolando

Author
Luca Mariani
ID 876407

Academic Year 2018-2019

Abstract

The studies on hybrid-electric propulsion for General Aviation have so far dealt with aircraft design, with the modelling of the propulsive unit and with the infrastructural change. In line with these analyses, the current work focuses on the environmental comparison between a hybrid-electric powertrain and a conventional propulsive unit based on an internal combustion engine (ICE). The acoustic and atmospheric effects are studied thanks to two innovative prediction procedures, derived from validated estimation methods and applied to both hybrid-electric and conventional aircraft.

The estimation of sound exposure is based on the contributions of the airframe, the propeller and the engine; when present, the gearbox and the electric motor have proven to be negligible. The sound pressure levels relative to the cited sources are combined through an innovative formula using three dimensionless coefficients, obtained on the basis of the error with respect to real noise data. Atmospheric pollution is instead predicted through a simpler method exploiting the segmentation of flight trajectory for a more accurate estimation of the transit times.

The two procedures are then applied to study the standard traffic pattern at Milan Bresso airport. At first, the influence of power management is investigated considering two existing airplanes retrofitted with serial hybrid-electric power-trains. Apart from the all-electric mode, the best results are obtained with the ICE activation in the base and final legs. In a second analysis, a real hybrid-electric aircraft is compared with two conventional airplanes considering actual engine activation. The sound exposure map relative to the hybrid-electric aircraft presents values at least one order of magnitude smaller than those of the conventional airplanes. Moreover, the hybrid-electric aircraft shows a promising 80% reduction in social cost deriving from pollutant emissions.

Keywords — emissions; estimation; hybrid-electric propulsion; noise; pollutants

Contents

List of Figures

List of Tables

List of Acronyms

2-D Two-Dimensional.

3-D Three-Dimensional.

ACRP Airport Cooperative Research Program.

AEA Atomic Energy Authority.

AEDT Aviation Environmental Design Tool.

AEED Aircraft Engine Emission Databank.

AEM Advanced Emission Model.

AGL Above Ground Level.

AIAA American Institute of Aeronautics and Astronautics.

AIR Aerospace Information Report.

ALAQS Airport Local Air Quality Studies.

AMSL Above Mean Sea Level.

ANCON Aircraft Noise CONtour.

ANOPP Aircraft NOise Prediction Program.

ANOPP-PAS Aircraft NOise Prediction Program - Propeller Analysis System.

ANP Aircraft Noise and Performance.

ASCENT Aviation Sustainability CENTer.

AST Advanced Subsonic Technology.

ATC Air Traffic Control.

ATM Air Traffic Management.

ATZ Aerodrome Traffic Zone.

AUSTAL Ausbreitungsrechnung nach Technische Anleitung zur reinhaltung der Luft.

AVGAS AViation GASoline.

AVT Applied Vehicle Technology.

AzB Anleitung zur Berechnung von lärmschutzbereichen.

BADA Base of Aircraft DAta.

BEM Boundary Element Method.

BFFM2 Boeing Fuel Flow Method 2.

CAA Computational AeroAcoustics.

CAA Civil Aviation Authority.

CAEP Committee on Aviation Environmental Protection.

CAN Committee on Aircraft Noise.

CCD Climb/Cruise/Descent.

CEAS Council of European Aerospace Societies.

CFD Computational Fluid Dynamics.

CORINAIR CORe INventory AIR.

CPA Closest Point of Approach.

CPI Consumer Price Index.

CTR Controlled Traffic Region.

DEFRA Department for Environment, Food and Rural Affairs.

DLR Deutsches zentrum für Luft- und Raumfahrt.

DORA Directorate of Operational Research and Analysis.

DOT Department Of Transportation.

EASA European Aviation Safety Agency.

EC European Community.

ECAC European Civil Aviation Conference.

EEA European Environment Agency.

EEC EUROCONTROL Experimental Centre.

EMEP European Monitoring and Evaluation Programme.

EPN Effective Perceived Noise.

ESDU Engineering Sciences Data Unit.

EU European Union.

EUCASS EUropean Conference for AeroSpace Sciences.

FAA Federal Aviation Administration.

FEM Finite Element Method.

FLULA FLUgLAerm.

FOCA Federal Office of Civil Aviation.

IC Internal Combustion.

ICA Independent Component Analysis.

ICAO International Civil Aviation Organization.

ICE Internal Combustion Engine.

ICSV International Congress on Sound and Vibration.

ID IDentification.

IESTA Infrastructure d'Évaluation des Systèmes de Transport Aérien.

IFR Instrument Flight Rules.

IHS Information Handling Services.

INM Integrated Noise Model.

ISA International Standard Atmosphere.

LTO Landing and Take-Off.

MAHEPA Modular Approach to Hybrid Electric Propulsion Architecture.

MATLAB MATrix LABoratory.

MOGAS MOtor GASoline.

MTOW Maximum Take-Off Weight.

NASA National Aeronautics and Space Administration.

NATS National Air Traffic Services.

NETCEN National Environmental Technology CENtre.

NLR Nationaal Lucht- en Ruimtevaartlaboratorium.

NO_x Nitrogen Oxides.

NORTIM NORwegian Topography Integrated Model.

NPD Noise Power Distance.

ONERA Office National d'Etudes et de Recherches Aérospatiales.

PANAM Parametric Aircraft Noise Analysis Module.

PEM Proton Exchange Membrane.

PM10 Particulate Matter of 10 microns in diameter or smaller.

PM2.5 Particulate Matter of 2.5 microns in diameter or smaller.

PNL Perceived Noise Level.

QGIS Quantum Geographic Information System.

R&D Research & Development.

RMS Root Mean Square.

RSS Root Sum Square.

RTO Research and Technology Organization.

SAE Society of Automotive Engineers.

SAGE System for assessing Aviation's Global Emissions.

SEL Sound Exposure Level.

SESAR Single European Sky ATM Research.

SN Smoke Number.

SOR Start Of Roll.

SPL Sound Pressure Level.

STAPES SisTem for AirPort noise Exposure Studies.

TEFC Totally Enclosed Fan Cooled.

TNO nederlandse organisatie voor Toegepast Natuurwetenschappelijk Onderzoek.

TRL Technology Readiness Level.

UHC Unburned HydroCarbons.

UK United Kingdom.

US United States.

VDI Verein Deutscher Ingenieure.

WADC Wright Air Development Center.

WP Working Paper.

Chapter 1

Introduction

One of the main challenges in current intergovernmental policies concerns the reduction of acoustic and atmospheric pollution as both of them prove to be related to serious health diseases. Aviation plays a crucial role with respect to these highly important issues since aircraft emissions in terms of noise and chemical pollutants are significant. Moreover, the global amount of movements is expected to undergo substantial growth over the next decades, as highlighted in the most recent EUROCONTROL estimate [1]. According to this document, a 53% increase in the number of European IFR flights is expected in 2040 with respect to 2017 in the most likely perspective; even in the most critical scenario of a fragmenting world, a 12% increment is foreseen.

The future of European aviation has seriously been tackled through the *Flightpath 2050*, a series of goals that need to be achieved inside the European Union by 2050. Among all Flightpath 2050 objectives, environmental protection requirements involve a 65% perceived noise reduction and a decrement fixed at 75% for CO_2 production, at 90% for NO_x; the reference conditions are represented by the emissions of a typical aircraft produced in 2000. Other important points concern an emission-free taxiing, the design of recyclable air vehicles and a massive research in sustainable alternative fuels on one side, in new environmental action plans and standards on the other.

Though continuous and tremendous efforts have been produced in the last 15 years, the ambitious environmental goals of the Flightpath 2050 are likely not to be reached with conventional power-train configurations. Consequently, several concepts of hybrid-electric or even full-electric aircraft have been introduced over the last years not only in Europe, but all over the world: examples of such innovative propulsive configurations are presented in detail in the work of Gaspari et al. [2].

1.1 The MAHEPA project

In order to explore the potential of the new power-train concepts, on 1st May 2017 the European Union funded the Modular Approach to Hybrid Electric Propulsion Architecture (MAHEPA) project. As its name suggests, the problem of atmospheric pollution is addressed through the introduction of hybrid-electric aircraft with a modular propulsive configuration, characterized by the combination and/or repetition of some fixed components.

The MAHEPA approach to hybrid propulsion will give the possibility for a more eased and more extended fleet replacement, ranging from General Aviation airplanes to regional commuters, and

possibly heavier passenger aircraft, when battery capacities will be large enough at some future time.

The main objective of MAHEPA lies in the design, development and testing of two hybrid-electric four-seat airplanes, which are scheduled to fly in 2020. Both of them feature a series architecture since the propeller, which is responsible for thrust, is driven by a single source of mechanical power, the electric motor. In the first prototype (*Panthera Hybrid*), batteries are supported by an internal combustion engine, while the second one (*HY4*) is totally emission-free thanks to the presence of hydrogen fuel cells.

The final tests will be necessary to understand the actual feasibility of current General Aviation and regional fleet replacement with hybrid-electric aircraft, in the light of a greener future for aviation and for the entire world. Moreover, the testing procedures will emphasize the strengths and weaknesses of such radical and innovative transition towards the electrification of the aeronautical sector. Indeed, a further goal of the project is to derive design methodologies and scenario studies devoted to the transition of short-haul regional air transportation to hybrid-electric fleets, in order to provide guidance for future investments and regulatory actions.

The deadline of the MAHEPA project is fixed at the beginning of 2021 after the analysis of the experimental outcomes, which will give a more practical idea of the direction to follow for future development.

Led by the Slovenian aircraft manufacturer Pipistrel, the project brings together different European universities among which Politecnico di Milano plays a very important role. To date professors and Master's candidates have been focusing on the power-train modelling and simulation [3], on the conceptual [4] and preliminary [5] design of the aircraft, on the weight sizing [6] and on the infrastructural change [7].

1.2 The MAHEPA testbeds

As previously stated, major efforts inside the MAHEPA project are finalized to the integration and testing of two prototypes, manufactured by Pipistrel Vertical Solutions[1] and based on the previously cited hybrid-electric concepts.

1.2.1 Pipistrel Panthera Hybrid

Panthera is a four-seat lightweight aircraft featuring an innovative all-composite airframe made from carbon fibres, glass fibres and Kevlar, while the retractable landing gear features titanium and aluminium elements [8].

Since the beginning of the manufacturing in May 2011, Pipistrel planned for a Panthera release in three versions characterized by different propulsive technologies. All the main performance characteristics of this airplane in its three versions can be found in the official Panthera website [9], from which Figure 1.1 has been obtained.

[1] Pipistrel Vertical Solutions d.o.o. is the company name for the R&D department previously operating inside Pipistrel d.o.o. Ajdovščina. Founded in 2017, Pipistrel Vertical Solutions is specialized in the development of all Pipistrel's two seat models and the four-seater Panthera from the conceptual design phase to the preparation for serial production. Its headquarters is in Goriška cesta 50a, 5270 Ajdovščina, Slovenia.

Figure 1.1: Pipistrel Panthera in flight [9]

The first design is built around an internal combustion engine fed by Motor Gasoline (MOGAS), which is cheaper and more widely available than the traditional Aviation Gasoline (AVGAS). The original choice was centred on the use of a Lycoming IO-390, a four-cylinder piston engine capable of producing 210-hp power.

The first engine start and taxi tests were successfully completed on 29th March 2013 and six days later, on 4th April, Panthera made its first flight. It lasted approximately forty minutes and allowed for the estimation of the basic performance characteristics. Several other tests were performed in the following months for stability, controllability and landing gear retraction.

However, the Panthera development was abruptly interrupted because the low Octane quality of MOGAS prevented from the certification of Lycoming IO-390. In March 2014, Pipistrel was forced to shift towards the heavier and more powerful Lycoming IO-540-V, to the point that the original version is currently produced just for experimental purposes.

The design based on a conventional piston engine actually serves as a solid basis for the study and development of the other two Panthera versions, highlighting Pipistrel's intentions to move towards a more environmentally-friendly aviation.

Panthera Hybrid features a hybrid-electric power-train with a Rotax 914 internal combustion engine and two lithium-ion batteries capable of supplying up to 200 kW. Such high power enables the aircraft to take-off and climb in all-electric, while the piston engine serves as a range extender and is activated just above a certain altitude. In this way, atmospheric pollution in the aerodrome area is zeroed since the aircraft is powered by the batteries in all terminal flight modes including approach and landing.

The further development is represented by Panthera Electro, a full-electric aircraft featuring just the 200-kW battery packs: since the TRL of this project is still quite low, it is not part of the MAHEPA project, but it is still destined to pave the way for the future of aviation.

1.2.2 Pipistrel/DLR/H2Fly HY4

HY4 is an all-electric airplane designed by H2Fly[2] with the aim to develop a new electric air taxis regional network inside Germany. The official HY4 website [10] provides more details about this innovative means of transport, which is shown in Figure 1.2.

Figure 1.2: H2Fly HY4 in flight [2]

As can be seen, the most evident feature is represented by the configuration with double fuselage, each capable of carrying two passengers and derived from Pipistrel *Taurus Electro G2*. Despite the twin fuselages, the thrust-generation mechanism consists of a unique propeller driven by an 80-kW electric motor: the energy sources are represented by four low-temperature PEM fuel cells and two lithium-polymer batteries used when high powers are required, i.e. during take-off and climb.

1.3 Purpose and structure of the present work

The MAHEPA studies mentioned in the last part of Section 1.1 have focused on the main design and infrastructural changes related to the application of electric propulsion to the aeronautical world.

The present work aims to investigate methodologies for the prediction of noise and pollutant emissions with application to all-electric, hybrid-electric and conventional power-trains as well. Such procedures can be exploited in turn to assess the potential of newer power-trains in reducing emissions with respect to conventionally-propelled aircraft.

Furthermore, a key driver of the MAHEPA project is the interest in previsions for the extension of hybrid-electric powertrains to micro-feeders and regional commuters. In this sense, the current thesis represents a first important step for the prediction of the environmental effects even in relation to these future applications.

Being an early environmental study, the focus is on the General Aviation sector as it represents the first segment of civil aviation in which a significant colonization of hybrid-electric aircraft is expected in the near future, and for which a high number of design and performance data is available thanks to Pipistrel's prototypes.

[2]H2Fly is a spin-off from the DLR Institute of Engineering Thermodynamics specifically developed as a service provider for the implementation of quite and emission-free propulsion technology. Founded in 2014, its headquarters is in Äxtlestraße 6, 70599 Stuttgart, Germany.

The development of the new estimation procedures essentially starts from the investigation of the techniques and methods currently available for pollution computation. This extensive model collection is presented in Chapter 2, while Chapter 3 is specifically devoted to the prediction of acoustic pollution according to a peculiar estimation procedure.

In the first part, a model complying with the directives suggested by ECAC is presented and described in all its aspects since it serves as a solid basis for future sound exposure computation.

The second half of the chapter is instead centred on a general method for noise prediction applicable to conventional and hybrid-electric aircraft as well. The greatest number of aspects relative to the ECAC model is inherited in this new estimation procedure, which starts from the acoustic contribution of the different sources in order to estimate the overall aircraft noise. A comparison between the results of this approach and real noise data is presented in Appendix A for two radically different conventional airplanes.

Chapter 4 instead addresses all issues related to the prediction of atmospheric pollution, including the most innovative aspect connected to the segmentation of flight trajectory. The two models for the prediction of noise and pollutant emissions have been applied then to two different comparative analyses described in Chapter 5.

In a first phase, attention is posed on the investigation of power management between the battery and the internal combustion engine; extra results concerning the influence on noise emission maps are provided in Appendix B.

The second application study is instead devoted to a more direct pollution comparison between a real hybrid-electric aircraft and two existing airplanes of similar size.

Finally, the last chapter recalls the basic features of the estimation procedures and synthetically collects the main results; the final part of the chapter is instead devoted to the possible developments of the current work.

Chapter 2

State of the art

The quantification of acoustic and atmospheric pollution is an extremely difficult task and the simulation of sound propagation and pollutant dispersion is one of the most challenging engineering issues. It indeed implies the need for a numeric solution of Navier-Stokes equations over the large domain enclosed by the airport area and its surroundings.

Several efforts have been made since the very beginning of the aviation industry in order to simplify the problem through less sophisticated prediction models. However, the validation of these procedures is itself quite a complex issue because the measurements needed for model check require a proper sensor tuning and positioning in order to capture just the sound or concentration coming from the airplane and not from the other sources.

2.1 Prediction of acoustic pollution

The history of noise prediction methods in all engineering fields has always been characterized by the distinction between simple formulas based on experimental results and more sophisticated theoretical approaches. Despite the gradual shift towards more accurate sound estimations, in many practical applications the earliest, less sophisticated, empirical models are still preferred to the analytical and numerical procedures, whose higher level of accuracy does not always justify the larger computational cost.

Nowadays, numerous models exist for the sound coming from the different airplane components and the estimation of aircraft noise is performed in a great variety of methods. In the following paragraphs, a brief overview of such issues is performed on the basis of the work done by Filippone [11], one of the major experts in the aero-acoustic field.

2.1.1 Noise sources

Since no acoustic data are available for hybrid-electric aircraft, the model for sound prediction needs to start from the contribution of the most significant noise sources. Since the contribution of the single component is assumed independent of the others, the entire aircraft spectrum is obtained through the combination of the different SPL values belonging to the same frequency band. Furthermore, this *modus operandi* is particularly suited to the modularity concept intrinsic to the MAHEPA project.

Propeller noise

The prediction of noise coming from propellers has been performed since the early years of aviation as it is the first technique used for thrust generation. Despite the gradual shift towards jet propulsion, propeller noise is still deeply under investigation since turboprops and piston engines are nowadays used in short-haul routes. A complete review of the methods used for propeller noise prediction up to 1995 is available in the work by Metzger [12].

The typical characteristic of a propeller spectrum is the superposition of a tonal component, generated by the regular rotation of the blades, and a broadband noise resulting from the turbulent flow conditions at the leading edge, at the trailing edge and at the tip of each blade. As for the former, it can be furtherly split into thickness noise, related to the regular air displacement at the blade passage, and the loading contribution produced by the aerodynamic blade loading.

The first model dates back to 1919 with the work by Lynam and Webb [13], who focused on the theoretical prediction of the discrete noise component. In the following years, several other methods were introduced, but the lack of computer resources and the poor experimental equipment did not allow for a significant progress until the 1950's. Thanks to the introduction of the first computers, the period up to the 1970's was mainly devoted to the refinement of the theoretical prediction models developed up to that time.

A further improvement of the methods for tonal noise was made from the 1970's with the introduction of new prediction procedures centred on Lighthill's acoustic analogy [14], subsequently developed into Ffowcs Williams-Hawkings (FW-H) equation [15]. This constitutes the basis of practically all works and studies by Farassat, one of the most prolific noise researchers in the period from the 1970's to the 2000's. In cooperation with Succi, in 1980 he published an important work [16] in which two prediction procedures are introduced for the estimation of propeller noise starting from blade geometry, the aerofoil section description, the aerodynamic and operating data. While the Langley method for supersonic tip speeds brought to poor results, the MIT program has proven to be so successful to be currently used even for helicopter rotor noise in *ANOPP-PAS*, one of NASA's computer codes.

Another important author of the same period is Hanson, who also studied the shielding effects of fuselage on tone noise [17] and focused on the counter-rotation of propellers as well [18]. Concerning the estimation of propeller tonal noise, his most important work was the paper presented with Parzych in 1992 and published as a NASA report in the following year [19]. In this work, the authors describe a frequency-domain method for the prediction of thickness and loading noise starting from Goldstein's derivation of Lighthill's equations [20].

Although the sound levels typical of broadband noise are sensibly lower than the discrete tones, several studies have been made in this field since 1932 [21, 22]. The most significant source is represented by the turbulent flow at the trailing edge of the blade, whose effects can be modelled according to two different methods. A first prediction approach, based on the work of Ffowcs Williams and Hall [23], relies on the study by Curle [24] for pressure field estimation, while in the method originally used by Chase [25] the surface pressure distribution at the trailing edge is known a priori.

The most sophisticated predictions belong to the CFD-based Computational Aero-Acoustics (CAA) methods, which are able to capture the non-linear effects and are particularly recommended for near-field predictions. However, the level of accuracy of these methods is still too low at the largest distances, for which the less sophisticated theoretical or empirical approaches are preferable.

Besides the theoretical methods, empirical propeller noise prediction relies on a more restricted number of parameters related to macroscopic quantities. These techniques are therefore advisable

in the design and study of new concepts since a preliminary estimation of the emitted noise is performed through simple calculations with an acceptable accuracy degree.

The earliest empirical models were substantially based on graphs for the estimation of a reference sound level and of the corrective terms applied to it. Examples of this kind are the work by Franken et al. [26], the studies by Marte et al. [27] and by Dunn et al. [28] for the computation of noise spectrum; the more recent SAE AIR1407 [29] provides an estimation of the overall sound pressure level, obtained after the integration of the different spectral contributions.

An important turning point is represented by Smith's work [30] since his estimate is provided by means of a simple equation, whose number of parameters was furtherly reduced by Rathgeber [31].

The last transition goes into the direction of computer programs in place of equations, as evidenced by ESDU 11005 [32]: this procedure is nevertheless based on more sophisticated and numerous inputs with respect to the previous empirical formulations.

Airframe noise

While the studies about propeller noise began in 1919, research on airframe sound started around fifty years later from the interest to quantify the minimum aircraft noise or the one generated by gliders. The main parts involved in airframe noise generation are the wings, the high-lift systems (flaps and slats) and the landing gear: for this reason, airframe noise plays a significant role especially in the terminal phases of the flight, when it often overcomes propulsive noise above all in modern aircraft.

One of the first works about airframe noise prediction was made by Munson [33], who derived an analytical expression for sound pressure level based on a semi-empirical method of noise generation and propagation. The main drawbacks of this approach are the lack of generality on one side since the equations' constants depend on the airplane type; on the other side, the impossibility to predict noise coming from the single components prevents it from being used as a design tool. A few years later, Fink made an important development [34, 35] by adopting a general procedure which considers the different airframe noise sources independent from each other.

Yamamoto and others made a comparison between these two methods [36] and found that Munson's approach is generally more accurate. However, Fink's airframe model is more widespread thanks to its generality and the possibility to consider different aircraft configurations. Even the most recent works on airframe noise substantially refer to Fink's model and still rely on a massive use of experimental data due to the high complexity of the problem.

Clean wing noise is mainly related to the turbulent kinetic energy scattering at the trailing edge and was studied in depth by Amiet [37] and Howe [38] through fully analytical methods.

Noise generated by flap extension is instead caused by the interaction between the primary and the secondary unsteady tip vortices in the downstream region. Guo tried to reduce flap-edge noise to a single algebraic equation in many of his works [39, 40, 41], while Brooks and Humphreys relied on a more complex procedure [42].

The estimation of slat noise is even more demanding since it involves numerous noise sources such as flow separation in the cove area, vortex shedding in the slat gap and lateral flow separation at the two edges. Dobrzynski proposed a simple algebraic equation for slat-noise estimation [43], while Guo's formulation is analogous to the one for flap-edge noise [44].

Besides high-lift devices, the other main source of airframe noise is represented by landing gear, for which only empirically-based models exist. The spectrum is typically characterized by tonal

components related to vortex shedding from struts and bars, superposed to a large broadband content caused by the wake and the vast turbulent flow separation region. Even for the estimation of landing gear noise, Guo proposed a single algebraic equation, which is declined into the low, medium and high-frequency range [45]: in this formulation, the entire system is split into its main components, each of which is responsible for a specific spectral contribution. Other important studies about landing gear noise have focused on the interaction with an extended flap, responsible for a sound level increase from 5 to 10 dB.

While the class of empirical or semi-empirical models is quite widespread, fully analytical methods are applied just to canonical shapes and in the simplest cases. Other options currently under development are represented by CFD methods coupled with acoustic analogies and the fully numerical procedures, which are even more complex.

Fink's most important works not only represent the basis for most theoretical approaches, but also provide some simple formulas and graphs for preliminary noise calculation. A more recent estimation method is the computer program proposed in ESDU 90023 [46], which is largely based on Fink's theory, but is applicable just to large airplanes.

Internal combustion engine noise

Since the novelty of hybrid and full-electric aircraft lies in a new propulsion concept, the prediction of piston engine noise is crucial for the acoustic comparison with a conventional power-train. Despite being the first type of motor used in aviation, internal combustion engines have progressively been replaced with the more powerful jets, which are nowadays installed in most airplanes. The only aeronautical applications of reciprocating engines are limited to General Aviation, where power demands are sensibly lower.

The gradual substitution with jets reflects in the poor number of studies for the prediction of aircraft piston engine noise. Considerable research has been performed in the automotive world, but the engines used in the aeronautical sector are radically different machines as they are less sophisticated, but much more reliable.

In general, the assessment of sound coming from an internal combustion engine is an extremely difficult task and basically refers to three main sources, namely the combustion, the mechanical and the aerodynamic noise, as pointed out by Yao et al. [47]. The first two mechanisms are at the basis of the sound radiated by the engine external surfaces according to the path reported in Figure 2.1.

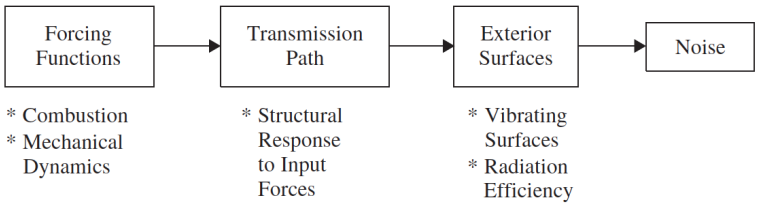

Figure 2.1: Piston engine noise generation [48]

Combustion noise is caused by the tremendous pressure increment occurring with the ignition of the mixture, while mechanical noise is related to the contact between all parts in relative motion.

However, ESDU 09009 [49] clearly states that the great majority of piston engine noise is of aerodynamic nature and connected to the intake and exhaust periodical variation of the gas flow

through the valves and piping. Davies et al. [50] showed a sound dependency on the fourth power of the local flow velocity at the lower frequencies and on the sixth at the highest tones; as a result, considerable attention has been made to exhaust noise in particular.

According to Bodén [51], the entire world of theoretical prediction models can essentially be distinguished between the linear time-invariant, the linear time-varying, the hybrid and the fully non-linear methods in increasing order of complexity.

An electro-acoustic analogy introduced by Russell et al. [52] lies at the basis of linear systems, which are solved for source pressure and impedance. The fundamental distinction between the two categories is connected to the time dependence of the coefficients, which is usually taken into account to mirror the effects of the reciprocating motion. Time-varying models were solved by Soedel et al. [53, 54, 55] in time domain for the study of Helmholtz resonators, while Wang developed a frequency-domain time-varying model for a piston-engine inlet system [56, 57, 58].

As their name suggests, hybrid methods instead rely on a combination between a non-linear model for noise generation and a linear frequency-domain method for sound propagation. The most critical aspect of these procedures lies in the system coupling, which brings to the distinction between two different approaches. The first class of methods refers to the iterative procedures, used by Gupta et al. [59] and Albertson et al. [60] among others; the more stable coupling methods are instead based on convolution integrals, as in the work by Davies et al. [61].

Finally, the application of fully non-linear models leads to the most accurate results above all for the prediction of exhaust noise, which is extremely powerful and related to highly non-linear effects. Besides the work of Takagi et al. [62], few other non-linear models have been introduced since the computational cost is extremely high and just the simplest geometries can be taken into account.

Despite the high complexity typical of theoretical procedures, simpler empirical models are not so widespread, particularly in the aeronautical sector. The Handbook of Noise and Vibration Control provides some formulas which are valid just for Diesel and natural-gas industrial engines [63] or in the automotive sector [48].

In the aviation context instead, a very simple expression based on the shaft power has been introduced by Thurston in 1978 [64]. A more refined formula based on the actual and maximum rotational speed as well as on the rated engine power was introduced by Dobrzynski in the mid '90s [65] and subsequently reported by Tada [66]. In the last years, Moshkov et al. [67] proposed an empirical expression for sound power prediction, which is however based on engine-dependent coefficients and therefore lacks of generality.

Electric motor noise

The electric motor represents the other distinguishing feature for the acoustic comparison between hybrid-electric aircraft and conventionally-propelled airplanes.

Although the most primitive examples of electric motors date back to the 1830's, the first book on noise estimation appeared only 120 years later with Jordan [68]. Another milestone is the work of Heller and Hamata in 1977 [69] about harmonic field analysis, while the book published by Timar et al. in 1989 [70] focuses on the effects of vibrations in sound generation.

The book by Gieras et al. [71] is one of the most recent publications providing a global overview of the past and current methods for the prediction of electric motor noise. According to the authors, the most novel techniques can be split into the deterministic and the statistical methods, where the first are more suitable at the lowest frequencies, the second at the highest ones.

Deterministic techniques indeed rely on an acoustic model based on the Finite Element Method (FEM) or the Boundary Element Method (BEM), which brings to prohibitive computational times when applied to the highest tones.

Statistical methods are instead based on a stochastic energy model for the distribution of total vibration power into the various subsystems; they imply a higher accuracy degree at the largest frequencies, where modal overlap is significant.

In the Handbook of Noise and Vibration Control, Bruce et al. [63] analyze some of the most important works about the empirical prediction of sound coming from industrial machines. While the work by Miller et al. [72] is used for transformers and the one by Bies et al. [73] for generators, the authors suggest a formulation based on a US manual [74] for the computation of the A-weighted sound power level radiated by electric motors.

Gearbox noise

In the context of General Aviation, another possible source of noise is related to the presence of a gearbox for power transmission from the engine to the propeller.

Gear noise prediction through theoretical and semi-empirical models basically addresses the two main sources of noise, namely whine and rattle. As for the former, it is a periodic sound occurring at the gear mesh frequency (f_m) and its harmonics, where f_m is simply the product between the number of teeth and the shaft rotational speed. Such noise is then transmitted externally through the transmission path of Figure 2.2.

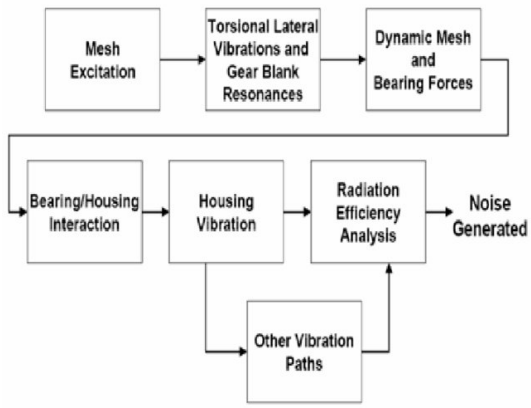

Figure 2.2: Gear noise transmission path [75]

As evidenced in the work by Singh [76], Lim and Singh made an extensive literature review on housing excitation [77] and focused on the vibration transmission through the bearings using both a Finite Element Method [78, 79, 80] and a Statistical Energy Analysis [81, 82]. Moreover, Singh et al. developed a more recent semi-empirical method for the prediction of whine noise by combining a linear model of the system with measured transfer functions of the structural paths [83].

Gear rattle is instead an impulsive sound occurring just in presence of light loadings and involving a high number of different elements such as gears, bearings, splines and clutches. Its complexity makes computer simulation not feasible, to the point that several models with a single degree of freedom have been introduced, such as the ones by Doğan [84] and Lang [85].

Concerning simple empirical formulations, even in this case Bruce et al. [63] have given an important contribution in the Handbook of Noise and Vibration Control. As happened for the electric motor, the authors prefer the manual prepared by Bolt, Beranek and Newman [74] to the book by Bies et al. [73] for the estimation of gear noise. According to the suggested formulation, the sound power level is computed from the rotational speed of the slower shaft, from the transmitted power and from the dimensions of the bounding box.

2.1.2 Noise prediction procedures

All the main actors belonging to the aeronautical sector are involved in the estimation of aircraft noise as a result of the global effort in minimizing the acoustic pollution deriving from aircraft operations.

The European airports covered by the EU Directive 2002/49/EC [86] should produce noise emission maps and prepare action plans for a noise-oriented land-use planning and flight-operation management. The results of the analysis must be submitted to the policymakers, who exploit them as a basis for future improvement regulations.

Moreover, according to the EU Directive 2009/12/EC [87], airport managing bodies are allowed to make charges to all airlines failing to comply with some specific standards. As a result, the issue of noise estimation even extends to the airline companies and to aircraft manufacturers as well, since they need to grant the airplane compliance with the more and more restrictive acoustic requirements.

As pointed out by Filippone [11], all techniques for aircraft noise prediction can be subdivided into the theoretical and the best-practice methods. While the former are based on physical models for noise generation and propagation, best-practice approaches essentially rely on a database of sound levels recorded through experiments.

Theoretical methods

Currently, the level of complexity relative to theoretical procedures is so high that some input models and data are still derived from experimental procedures. Nevertheless, a great number of approaches has been introduced since the early 1970's with the *ANOPP* code proposed by NASA [88, 89]. In this program, semi-empirical models are implemented for noise generation and propagation, which is capable of handling spherical spreading, atmospheric attenuation and ground reflection.

An upgrade has been achieved with the *ANOPP2* program [90], which is particularly suitable for the preliminary design of new aircraft thanks to its large number of input parameters.

NASA's latest projects have however been analyzed through the *FOOTPR* and *RADIUS* codes [91]: these two models are particularly suitable in relation to high-speed jets as they take into account the effects of engine geometry and flow interaction.

Another interesting tool is *PANAM* [92], developed by DLR as an aircraft design program that takes fan and jet noise into consideration. DLR also developed *SIMUL* [93], a midway between a theoretical and a best-practice method as it is based on both physical models and experimental databases.

Finally, Filippone developed his own software *FLIGHT* [94], a comprehensive program not only for noise prediction, but also for the aircraft description in terms of structural, mechanical, aerodynamic and propulsive characteristics.

Best-practice methods

The great majority of current best-practice methods is based on the guidelines offered by ICAO for the US [95] and ECAC in the European context [96]. Both manuals are very similar and refer to a segmentation procedure in which the entire departure or arrival flight path is split into a series of continuous segments.

Each of these trajectory portions contribute to the overall noise registered in a precise location depending on the aircraft thrust and airspeed as well as on the relative position between the segment and the ground sensor. The coefficients describing aircraft trajectory and the baseline noise of each segment are obtained from the Airfcraft Noise and Performance (ANP) database, which is hosted by EUROCONTROL in Europe and freely available [97].

One of the most important methods complying with the ECAC Report is the English $ANCON$ [98, 99], which is used for the annual generation of noise emission maps around the three major airports. An important distinguishing feature of this model is related to the continuous updating of trajectory and sound pressure levels with actual data. A drawback of this method, common to practically all empirically-based procedures, lies in the impossibility to estimate the noise coming from the single aircraft component.

Similar methods are the Swiss program $FLULA$ [100] and the two DLR codes ($SIMUL$ [93] and AzB [101]) used for noise estimation around German airports.

Besides other national prediction tools like the Norwegian $NORTIM$ or the one provided by the Dutch NLR, an important application is the French $IESTA$ [102], which combines the estimation of acoustic and atmospheric pollution.

Other programs analogous to IESTA are the EUROCONTROL $IMPACT$ [103] and the $AEDT$ [104, 105] developed by CAA. The former is one of the three codes prepared by EUROCONTROL for the SESAR project and integrates the $STAPES$ [106] and AEM [107] codes for acoustic and atmospheric pollution respectively.

Noise prediction in AEDT is instead performed thanks to the INM program [108], which has been widely used for the tracing of noise maps. This software is based on the procedure described in SAE AIR1845 [109], which relies on the closest point of approach for the computation of sound exposure. It therefore represents a further simplification of the segmentation approaches since the overall noise is computed just from the contribution of the trajectory segment closest to the sensor.

2.2 Prediction of atmospheric pollution

Although noise is "the most immediate impact of aircraft" [110] and "the most significant cause of adverse community reaction" [111], numerous studies have been performed in the field of atmospheric pollution, above all in the most recent years. The release of harmful chemical substances from the engine exhaust is not only a great concern for the people living in the vicinity of airports, but also an important driving force of climate change.

One of the most detrimental substances is carbon monoxide (CO) which is mainly produced in the flame areas characterized by fuel-rich conditions. It has proven to be related to several health diseases, ranging from headaches to memory loss and possibly heart attacks according to the level of exposure.

The incomplete combustion is also responsible for the generation of unburned hydrocarbons (UHC), derived from fuel not reacting inside the chamber. Some of these compounds like benzene

can cause eye and lung irritation and even cancers; others such as methane are greenhouse gases characterized by a tremendous global warming potential.

The main responsible for the greenhouse effect is however carbon dioxide (CO_2), which is produced in great quantities as it is a primary product of all combustion reactions of hydrocarbon fuels.

The oxides of nitrogen (NO_x) represent another important class of pollutants having significant harmful effects on both human health and the environment. They are related to various kinds of irritations and a long exposure can bring to serious diseases in the respiratory system. As for the environment instead, these compounds are responsible for the formation of photochemical smog and acid rains, which can have detrimental effects on the main biological systems [112].

Finally, a special mention must go to particulate matter (PM10 and PM2.5), for which "there is no threshold at which health effects do not occur" [113].

When dealing with atmospheric pollution in aviation, an important distinction needs to be made between the so-called Landing and Take-Off (LTO) cycle and the Climb/Cruise/Descent (CCD) phases, defined in Figure 2.3.

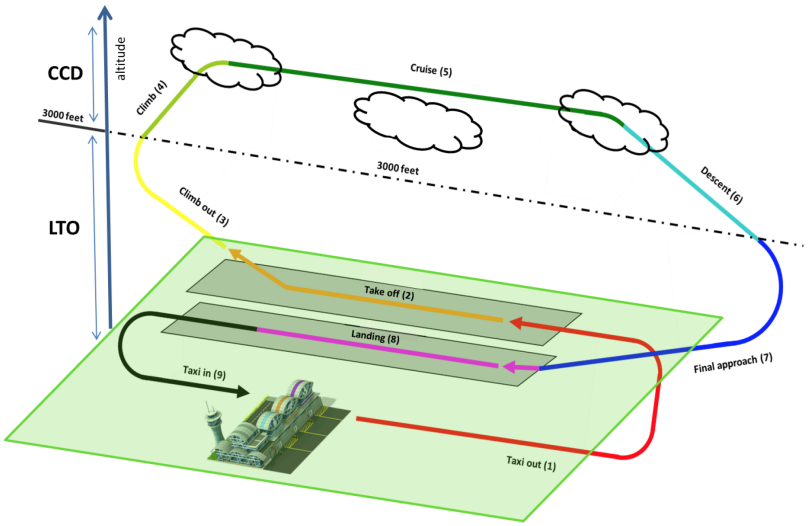

Figure 2.3: LTO cycle and CCD phases [114]

The delimitation between the two groups of flight phases is conventionally fixed at 3000 ft above ground level, which represents the average atmospheric mixing height, defined as the altitude below which the mixing of air and suspended particles occur.

According to the mixing height definition, the estimation of pollutant dispersion makes sense only for the LTO cycle since all substances emitted in the CCD phases are located in the vicinity of the aircraft route. However, even for the LTO cycle in most cases what really matters is the global amount of pollutant discharge and not the distribution in the airport area.

Concerning the problem of atmospheric pollution not only in the aeronautical world, a paramount text is the EMEP/EEA Air Pollutant Emission Inventory Guidebook. In part B, chapter 1.A.3.a of the most recent version [115], the important concept of tiers is introduced in the context of

civil aviation. They basically represent categories into which all national methods for atmospheric pollution can be subdivided according to the type of data in possession.

2.2.1 Tier 1 methods

The first category refers to all those procedures starting from the number of LTO cycles and fuel consumption for both domestic and international flights. In particular, domestic aviation refers to all flights departing and arriving in the country under consideration, while international flights are directed towards a foreign airport. Generally, the information necessary for pollution computation can easily be obtained from national statistics.

Starting from a general knowledge about the fleet, a single representative aircraft is chosen for the entire national-based analysis. The amount of fuel consumed in a unique LTO cycle (m_F) is estimated through the LTO emissions calculator, a spreadsheet provided in the Guidebook which exploits the formula

$$m_F = N_e \sum_{j=1}^{5} \dot{m}_{F_j} t_j. \tag{2.1}$$

For each of the N_e engines, the summation is performed for the five movements of the LTO cycle, namely taxi-out, take-off, climb-out, approach and taxi-in. Each of these flight phases is characterized by the thrust levels and times (t_j) reported in Table 2.1, which refers to the standard LTO cycle defined in ICAO in Annex 16, Volume II [116].

	Taxi-out	**Take-off**	**Climb-out**	**Approach**	**Taxi-in**
Thrust Level [%]	7	100	85	30	7
Time in mode [s]	1 140	42	132	240	420

Table 2.1: ICAO standard LTO cycle [116]

The actual t_j values used in the spreadsheet are the same as the standards except for taxi-in and taxi-out times, for which specific airport-dependent data are used. The fuel flow values of each phase ($\dot{m}_{F_j}$) are instead obtained from a database contained in the spreadsheet itself.

The very same program provides similar calculation for the emission of carbon monoxide, unburned hydrocarbons and the oxides of nitrogen according to the expression

$$m_k = N_e \sum_{j=1}^{5} I_{j,k} \dot{m}_{F_j} t_j. \tag{2.2}$$

Focusing on the single engine, the emission of the k-th substance in the j-th phase is computed by multiplying the fuel flow ($\dot{m}_{F_j}$), the time in the j-th mode (t_j) and a pollutant-specific emission factor ($I_{j,k}$).

The sum of the five LTO contributions, multiplied by the number of engines (N_e), gives the total mass of pollutant (m_k) produced per flight below the limit altitude of 3000 ft.

The only exception to equation 2.2 is represented by carbon dioxide, which is proportional to fuel consumption according to a coefficient equal to 3.15 $\mathrm{kg}_{CO_2}/\mathrm{kg}_F$ for jet fuel, to 3.067 $\mathrm{kg}_{CO_2}/\mathrm{kg}_F$ for aviation gasoline.

In the following step, the total fuel consumption in domestic LTOs can be estimated through a simple multiplication between the number of domestic LTOs and the fuel used in each of them.

Then, the difference between the overall amount of domestic fuel and the one used in domestic LTO cycles gives the total fuel consumption of domestic flights in the CCD phases.

Similarly to fuel consumption, the overall mass of pollutant discharged in domestic LTOs is computed by multiplying the corresponding LTO emission with the total number of domestic cycles.

As for CCD emissions instead, the ratio between LTO's k-th pollutant mass and fuel is multiplied by the total amount of fuel used in the CCD phases. This allows for a rough estimation of the overall emissions of the k-th pollutant above the limit altitude of 3000 ft AGL.

Finally, the entire procedure needs to be repeated for the international movements.

This kind of methods is not so common in studies about atmospheric pollution since pollutant emissions are computed on the basis of a single representative aircraft. As highlighted in the Guidebook, it is even difficult to estimate a level of uncertainty, which is quantified between 20% and 30% for LTO emission factors, in the range from 20% to 45% for the CCD ones.

2.2.2 Tier 2 methods

The great novelty introduced with Tier 2 procedures concerns the additional information on the number of national LTO cycles per aircraft type. This allows for a more accurate estimation of atmospheric pollution, based on the real national fleet and not on a representative airplane. However, no data about the duration of the CCD phases is available in these methods, even for domestic flights.

As for LTO computation, the same procedure typical of Tier 1 methods is applied considering the real national fleet in lieu of the representative aircraft.

Consequently, the first step is represented by the estimation of fuel consumption below the limit altitude of 3000 ft, performed thanks to the EMEP/EEA spreadsheet. In this way, the overall fuel burnt in domestic and international LTOs is computed from the sum of the consumption values typical of all airplanes falling inside each category.

The CCD fuel is simply the difference between the total domestic or international fuel and the corresponding LTO overall consumption.

Focusing on domestic aviation for convenience, the mass of each pollutant per aircraft type is computed again through the LTO emissions calculator. The single contribution sums to the emissions of the other airplanes to give the overall pollutant mass released in domestic LTOs.

The emissions of each aircraft in the CCD phases are instead computed from the overall CCD fuel in the same way as for Tier 1 approaches; even in this case, the overall amount results from the sum of the different aircraft values. Naturally, the very same procedure needs to be repeated for international flights.

Although information about actual fleet leads to a larger accuracy, the number of methods complying with Tier 2 is still poor above all for what concerns the CCD emissions. The estimation of atmospheric pollution above 3000 ft AGL still relies on the same rough proportionality relationship taken from Tier 1 approaches.

2.2.3 Tier 3 methods

The most advanced class of prediction methods belongs to Tier 3 approaches, which are based on the actual data about every national and international flight. The peculiar feature of these procedures

is related to the knowledge about the origin and destination of each flight. This information can be obtained from different sources, such as national statistical offices or ministries, ATC records, airport transcriptions or air carrier schedules.

In any case, this allows for a better estimation of pollutant emissions even in the CCD phases. The higher level of detail translates into an accuracy ranging from 5% to 10% for LTO emission factors, from 15% to 40% for CCD values.

All Tier 3 procedures are in turn split into two categories, namely the Tier 3A and the more sophisticated Tier 3B models.

Tier 3A methods

Tier 3A approaches are centred on the knowledge of the number of LTO cycles and of the distance flown by each airplane in the period under consideration. This represents the starting point for the subsequent calculations, which are performed by means of another spreadsheet called Master emission calculator.

This program allows for the computation of fuel consumption and pollutant emissions in both ICAO's LTO cycle and in the CCD phases. As for the latter, the code is also capable of performing a linear interpolation between the different predefined lengths in order to consider the actual distance between the origin and destination airports. The procedure is repeated for all domestic and international flights in order to provide the total fuel consumption and the global amount of pollutants emitted.

However, the use of Master Calculator is not a must in this kind of procedures also because it has been introduced only in 2016 with the most recent version of the Guidebook.

An interesting method has been developed by NETCEN [117], an operating division of a private English company (AEA Technology plc) providing environmental consulting services. In this procedure, the mass of carbon monoxide, oxides of nitrogen and unburned hydrocarbons is computed using equation 2.2 for each LTO cycle.

The fuel flow and emission factors appearing in the equation are obtained from the ICAO Aircraft Engine Emission Databank (AEED) [118], which also provides information about the Smoke Number (SN). This in turn allows for the computation of the PM10 emission factor thanks to a procedure defined in another NETCEN study [119].

Furthermore, the transit time in each phase does not correspond to ICAO's default value, but is directly taken from individual airport studies.

As for CCD phases instead, the fuel consumption and the emissions of CO, NO_x and UHC are computed through the EMEP/CORINAIR Emission Inventory Guidebook 1996 [120].

Finally, CO_2 and SO_2 emissions are supposed to be proportional to fuel consumption through a coefficient depending on the average carbon and sulphur content of the fuel.

Tier 3B methods

The most refined and complex approaches for pollutant estimation belong to Tier 3B category, which relies on full flight trajectory information for a more accurate estimation of the transit times.

In some Tier 3B programs, even pollutant dispersion in the aerodrome area is computed by means of sophisticated diffusion models. Despite granting the highest level of accuracy, they are not always the most suitable method for atmospheric pollution calculations above all in preliminary studies, when a faster, though less accurate, procedure is more advisable.

Examples of Tier 3B methods include programs used also for noise estimation, like the French software IESTA, the EUROCONTROL IMPACT and AEDT, which includes the high fidelity code *SAGE* [121] for pollutant emissions.

Other important tools are *AEM* [107] and *Open-ALAQS* [122], which have been developed by EUROCONTROL in the context of the SESAR program.

As for the first, LTO emissions are computed on the basis of the standard ICAO cycle and the data provided in the AEED for turbofans, in the FOCA database for piston-engine aircraft. In the CCD phases instead, fuel consumption is estimated thanks to EUROCONTROL Base of Aircraft Data (BADA) [123], while the emission factors are obtained thorugh a linear interpolation of the AEED values, adapted to the actual altitude through the Boeing Fuel Flow Method 2 (BFFM2) [124].

Open-ALAQS is instead an open-source application capable of estimating the mass and the distribution of pollutants emitted from airplanes and non-aircraft sources inside the airport area. It therefore relies on a dispersion model provided by *AUSTAL2000* and on a tool (*QGIS*) for the definition of the main airport elements. In the latest version of the software, flight trajectory is computed according to the ANP database provided by EUROCONTROL, while the emission factors are obtained from the AEED or FOCA and corrected with the BFFM2.

Chapter 3

Modelling of acoustic pollution

The problem of aircraft noise has become more and more important in the evaluation of aviation environmental impact, favoured by an increasing awareness of its effects on human health. Unlike atmospheric pollution, which extends in all flight phases, the noise issues are essentially confined to the aerodrome region, where the low distances limit sound spreading effects.

The increasing importance of noise in the evaluation of aircraft performances is marked by the continuous noise decrement imposed by ICAO [125] to subsonic jet airplanes, as evidenced in Figure 3.1.

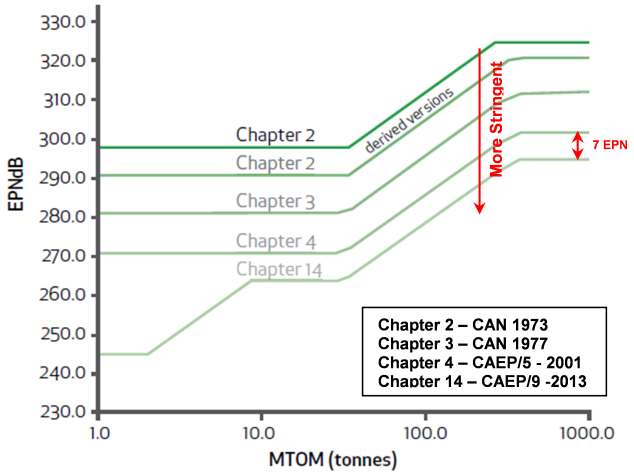

Figure 3.1: Progression of ICAO noise standards [126]

In a certification procedure, acoustic requirements are expressed in terms of effective perceived noise (EPN), a peculiar unit of measurement specifically defined by ICAO in this context. It essentially derives from the instantaneous perceived noise level (PNL), which is in turn computed from the spectral SPL contributions.

In particular, the certification of subsonic jet airplanes passes through the computation of EPN

in the approach, lateral and flyover points. In the y axis, the sum of the three limit values is reported, while the x axis refers to the aircraft maximum take-off mass.

Looking at the figure, it is evident that the limit in the sum of the three noise levels has become more and more stringent over the years. A 15 dB decrement was introduced by Chapter 3 in 1977, followed by a further 10 dB reduction in Chapter 4 and a final 7 dB decrease imposed with the most recent Chapter 14.

Although the focus of the current work is more on light propeller-driven airplanes than subsonic jets, such noise certification history marks the current tendency towards less noisy aviation. This in turn justifies the interest in comparing a conventional and a hybrid-electric aircraft from the acoustic point of view.

3.1 The method suggested by ECAC

The continuous efforts in reducing aircraft noise together with an increasing awareness of its harmful effects have led to the development of several models for the generation of noise emission maps around airports.

In the European context, an important milestone is represented by the Regulation (EU) No 598/2014 [127], based "on the establishment of rules and procedures with regard to the introduction of noise-related operating restrictions at Union airports within a Balanced Approach".

According to this document, each Member State has to designate one or more competent authorities in order to periodically monitor sound exposure at the main national airports and suggest new operating restrictions for acoustic pollution mitigation.

In addition, the Regulation establishes that noise computation shall be made in accordance with the directives imposed by the ECAC Report Doc. 29 [128, 96, 129]. In its most recent version, the guidance is subdivided into three separate volumes destined to the different subjects involved.

The first one [128] is a more general document describing the main concepts of noise estimation and is specific to both practitioners and end-users. The former basically define the working scenario and plan the analysis, while the latter are essentially concerned with the model output in terms of noise contours and population exposure to the highest sound levels.

The other two parts of the guidance are instead suited to the modeller, the specialist in aircraft noise designated to build up the program. In particular, the second volume [96] is highly technical as it contains all equations and guidelines for programming, while Volume 3 [129] presents a set of reference cases for model check and verification.

3.1.1 The concept of segmentation

As stated in the Applications Guide [128], all estimation procedures can essentially be split into the Closest Point of Approach (CPA), the segmentation and the simulation methods in increasing order of complexity.

As the acronym suggests, noise computation in CPA algorithms is based only on the sound emissions at the shortest distance between the aircraft and the receiver. Therefore, these models are particularly indicated for the estimation of the maximum sound pressure level related to a single flight movement (L_m). They instead give poor results for time-integrated metrics like the single event sound exposure level (L_E).

Segmentation procedures represent an important development of CPA methods since the focus is not on the closest point of approach, but on the entire aircraft movement. Several aspects have

been inherited from CPA algorithms like the flight path description as a series of straight segments: differently from CPA techniques, even turns are described as a sequence of chords, leading to a complete trajectory segmentation.

The sound contribution of each segment is computed and then combined to the others in order to obtain the event noise level, which refers to the entire aircraft movement. As for maximum sound pressure level, the event noise level (L_m) is simply the greatest of the segment values ($L_{m,j}$), namely

$$L_m = \max(L_{m,j}). \tag{3.1}$$

Considering sound exposure instead, the contribution of the j-th among the N_s segments ($L_{E,j}$) is summed on an energetic basis in order to obtain the single event sound exposure level (L_E) as follows

$$L_E = 10 \log_{10} \left(\sum_{j=1}^{N_s} 10^{\frac{L_{E,j}}{10}} \right). \tag{3.2}$$

The more sophisticated procedures belong to the class of simulation approaches, which model the aircraft flight path through a series of consecutive points. The noise contribution from each point is calculated in order to obtain the sound time history at any specific observer position. These techniques lead to the most accurate results, but at the same time imply large computational costs and require highly-accurate acoustic input data for noise computation.

For this reason, segmentation algorithms still represent the most widespread techniques used for noise modelling since they combine a simple estimation procedure with an acceptable degree of accuracy. The guidelines and equations provided in the second volume of ECAC Doc. 29 [96] indeed refer to a segmentation procedure.

3.1.2 The ANP database

Besides the calculation program, any noise estimation method needs to rely on a database for the storage of aircraft performance and acoustic characteristics. In particular, the segmentation procedure outlined in the second volume of ECAC Doc. 29 refers to the information inside the ANP database, an international data resource compliant with the directives of ICAO Doc. 9911 as well.

Such database is hosted by EUROCONTROL, is completely free and available after a registration form in the official ANP webpage [97]. Data is provided for a great number of aircraft currently in use and even a substitution table is offered for those jets and heavy propeller-driven airplanes not covered by the database.

As the acronym suggests, the data storage inside ANP mainly refers to three macro-categories related to the Aircraft, Noise and Performance characteristics. As for the first, a general description is provided for each aircraft inside the database in order to identify the basic features of the airplane and of its propulsion system.

Noise information essentially consists in a couple of tables useful for acoustic computation. The most important one refers to the NPD data, a set of noise levels at ten slant distances as a function of engine power; the *Spectral classes* table is instead useful for the NPD adjustment due to non-reference atmospheric conditions.

Finally, the ANP database contains all engine and aerodynamic inputs for flight-profile definition in terms of altitude, airspeed and thrust at each segment end.

3.1.3 Trajectory definition

In implementing a method complying with ECAC Doc. 29, the first step is represented by flight path modelling through a sequence of straight lines. In accordance to the segmentation concept, the main purpose of this phase is the description of each segment end in terms of 3-D spatial coordinates, true airspeed, power and bank angle.

A first possibility to define aircraft trajectory is based on the analysis of radar data describing the airplane position in space and its local velocity; if no power information is available, thrust is estimated from the altitude and speed change. Clearly, a simulation based on actual data gives the most accurate results, but at the same time access to external proprietary data is difficult. Moreover, this trajectory reconstruction lacks generality as it is confined to specific airport procedures.

A more feasible alternative is represented by flight path synthesis from the standard departure or arrival routes and from the performance information provided in ANP. Generally speaking, an aircraft trajectory is defined by the superposition of two different 2-D motions, which are supposed to be independent from each other.

Ground track corresponds to the flight path projection onto the ground surface and is constituted by a sequence of straight segments and circular arcs mirroring aircraft turns. In Tables 3.1 and 3.2, the departure and arrival tracks are provided for Runway 18 at Milan Bresso airport, a General Aviation aerodrome already studied in a previous project [7].

Type	**Length [ft]**	**Radius [ft]**	**Heading change [°]**	**Heading change at transitions [°]**	**Turn direction**
Straight	8 050				
Turn		1 190	90	5	Right
Straight	2 530				
Turn		1 140	90	5	Right
Straight	7 370				
Turn		1 160	90	5	Left

Table 3.1: Departure ground track at Milan Bresso airport - Runway 18

Type	**Length [ft]**	**Radius [ft]**	**Heading change [°]**	**Heading change at transitions [°]**	**Turn direction**
Straight	10 000				
Turn		1 320	40	2	Left
Straight	13 770				
Turn		1 140	90	5	Right
Straight	2 580				
Turn		1 140	90	5	Right
Straight	5 770				

Table 3.2: Arrival ground track at Milan Bresso airport - Runway 18

While straight segments are defined just in terms of length, turns are modelled considering their radius, their direction and the heading change.

As stated in Section 3.1.1, segmentation procedures prevent from the use of circular arcs: therefore, turns have to be modelled through a series of chords so that the heading change along each of them is lower than 10 degrees. Moreover, two additional segments are inserted at the two ends for a more realistic modelling of the initial and final portions; their amplitude is left to the modeller as an input variable.

The ECAC document suggests a reference fixed at the point of brake release, with the x-axis aligned to the runway and the z coordinate describing aircraft's altitude. Ground track is therefore described by a sequence of straight segments in the xy plane, as can be seen in Figures 3.2 and 3.3.

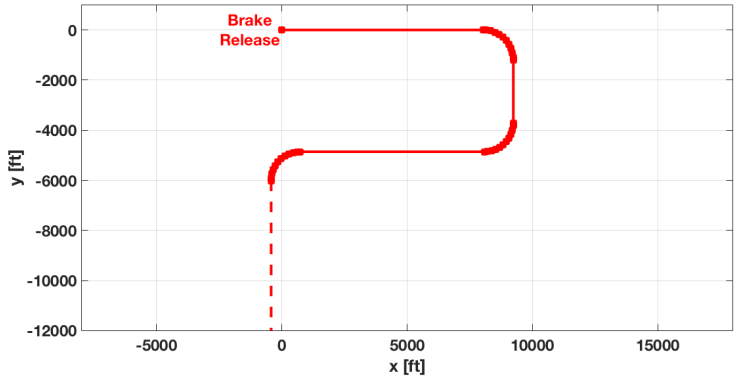

Figure 3.2: Departure ground track at Milan Bresso airport - Runway 18

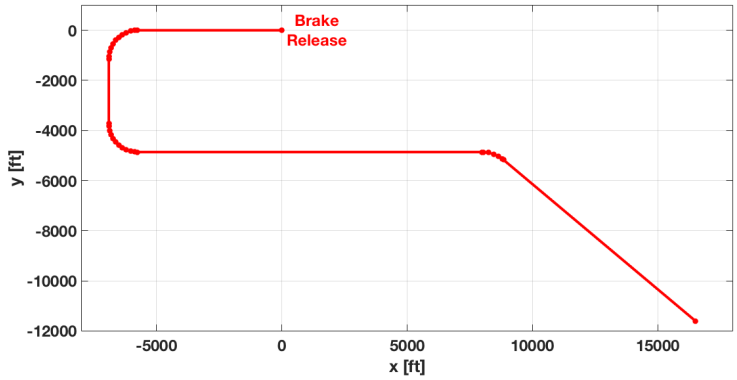

Figure 3.3: Arrival ground track at Milan Bresso airport - Runway 18

The other component needed for a complete trajectory synthesis is represented by flight profile, a description of aircraft motion in the vertical plane in terms of altitude, speed, power and bank angle. The flight profile determination is quite straightforward and essentially relies on the default departure and arrival procedures defined in the ANP database.

In some cases, the vertical motion of the aircraft is directly described by some fixed points characterized by precise altitude, speed and thrust values as a function of the ground distance from brake release.

A more refined description is achieved when procedural steps are defined in place of points since the flight profile computation refers to the actual operating conditions in terms of airplane weight and headwind speed among others.

Considering a classical departure case, the entire procedure is described by a sequence of three different steps, namely take-off, acceleration and climb at constant calibrated airspeed; the arrival movements instead include the descent, level, landing approach, touchdown and deceleration phases.

The second volume of ECAC Doc. 29 [96] provides all equations for the computation of the initial and final point of each segment as well as for the further subsegmentation. Each segment can indeed be split into a finite number of parts in order to have more realistic results: additional profile points are introduced when power setting is modified, at some predefined altitudes or in the case of speed changes larger than 10 m/s.

As an example, Figures 3.4 and 3.5 provide an altitude flight profile description for a departure and arrival procedure of a Cessna 172R Skyhawk at Milan Bresso airport.

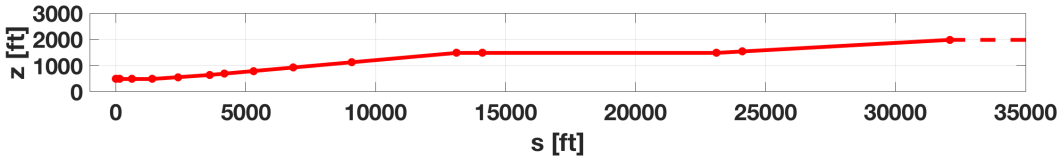

Figure 3.4: Departure altitude profile of a Cessna 172R Skyhawk at Milan Bresso airport

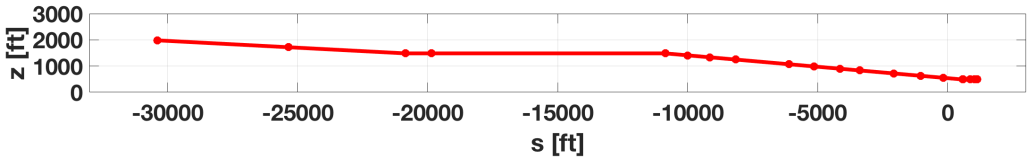

Figure 3.5: Arrival altitude profile of a Cessna 172R Skyhawk at Milan Bresso airport

The last step for a complete flight path definition consists in the coupling of ground track and flight profile points. The former are described in terms of x and y coordinates in the ground plane, the latter in terms of altitude (z), speed (V) and thrust (P). The link between the two is represented by the distance along the ground track (s), which is common to both motions.

Considering a ground track segment, the classical linear interpolation formulas

$$\begin{aligned} x &= x_1 + \frac{s - s_1}{s_2 - s_1}(x_2 - x_1) \\ y &= y_1 + \frac{s - s_1}{s_2 - s_1}(y_2 - y_1) \end{aligned} \tag{3.3}$$

are exploited for the computation of the x and y coordinates of a flight-profile point inside it; the subscripts 1 and 2 are used to indicate the quantities belonging to the initial and final segment point respectively.

In the case of flight profile segments instead, the expressions

$$z = z_1 + \frac{s - s_1}{s_2 - s_1}(z_2 - z_1)$$
$$V = \sqrt{V_1^2 + \frac{s - s_1}{s_2 - s_1}(V_2^2 - V_1^2)} \tag{3.4}$$
$$P = \sqrt{P_1^2 + \frac{s - s_1}{s_2 - s_1}(P_2^2 - P_1^2)}$$

are adopted for the altitude (z), speed (V) and thrust (P) of ground-track points located inside the segment. While linear interpolation is assumed for altitude, the other two quantities are supposed to linearly vary with time and a second-order interpolation is performed according to the values at the two segment ends, indicated again with subscripts 1 and 2.

Moreover, the matching of the two motions is essential for the bank angle (ε) computation in each turn point starting from the groundspeed (V_g), the turn radius (r) and the gravity acceleration (g), according to equation

$$\varepsilon = \tan^{-1}\left(\frac{V_g^2}{rg}\right). \tag{3.5}$$

The final result of the ground track coupling with flight profile is evidenced in Figures 3.6 and 3.7, referred to the departure and arrival trajectories of a Cessna 172R Skyhawk at Bresso airport.

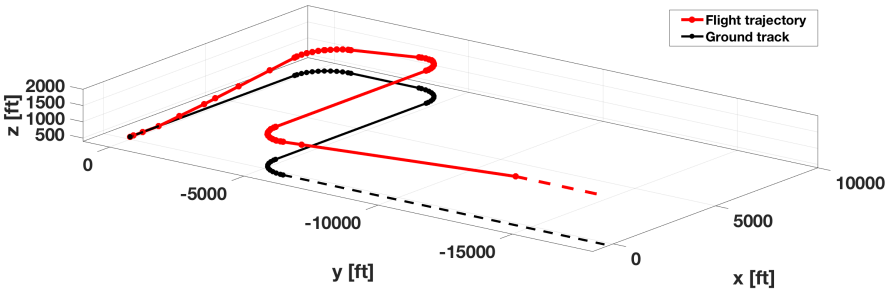

Figure 3.6: Departure trajectory of a Cessna 172R Skyhawk at Milan Bresso airport - Runway 18

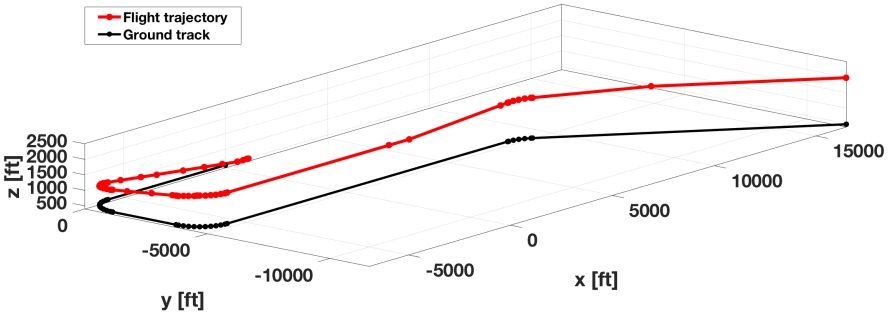

Figure 3.7: Arrival trajectory of a Cessna 172R Skyhawk at Milan Bresso airport - Runway 18

3.1.4 Noise emission computation

According to the segmentation concept, the noise related to an entire departure or arrival movement is computed from the corresponding segment values through equations 3.1 and 3.2.

As for the single segment, the second volume of ECAC Doc. 29 points out the basic expressions

$$\begin{aligned} L_{m,j} &= L_m(P,d) + \Delta_I(\varphi) - \Lambda(\beta,l) + \Delta_S \\ L_{E,j} &= L_E(P,d) + \Delta_V + \Delta_I(\varphi) - \Lambda(\beta,l) + \Delta_F + \Delta_S \end{aligned} \tag{3.6}$$

for noise estimation in terms of maximum sound pressure level ($L_{m,j}$) and sound exposure level ($L_{E,j}$).

As can be seen, the segment noise level is simply given by a baseline noise term obtained from the NPD data ($L_m(P,d)$, $L_E(P,d)$), which is corrected in order to consider the effects related to sound absorption and attenuation.

In particular, Δ_V refers to the adjustment for event duration, $\Delta_I(\varphi)$ takes engine installation into account, $\Lambda(\beta,l)$ considers lateral attenuation, while Δ_F and Δ_S are related to the finite segment and the start-of-roll corrections respectively.

The relative position between the segment end points and the ground observer is essential for the power (P) and distance (d) inputs for the obtainment of the baseline term. Since the NPD noise levels are provided for a discrete number of power settings and distances, the following interpolation formulas

$$\begin{aligned} L(P) &= L(P_I) + \frac{P - P_I}{P_{II} - P_I}[L(P_{II}) - L(P_I)] \\ L(d) &= L(d_I) + \frac{\log_{10}(d) - \log_{10}(d_I)}{\log_{10}(d_{II}) - \log_{10}(d_I)}[L(d_{II}) - L(d_I)] \end{aligned} \tag{3.7}$$

need to be exploited for the computation of the baseline noise levels related to the actual power ($L(P)$) and distance ($L(d)$) values. In particular, subscripts I and II refer to the quantities relative to the lower and upper interpolation point respectively.

The very same formulas can be applied in case of inward extrapolation from the first two values or outward from the penultimate and last noise levels.

Before the interpolation or extrapolation, an adjustment is applied to the standard noise levels in order to mirror the actual atmospheric conditions at the aerodrome in terms of density (ρ) and sound speed (c). Expressed according to the International System of Units, the corrective term is given by the formula

$$\Delta_i = 10 \log_{10}\left(\frac{\rho c}{409.81}\right). \tag{3.8}$$

Differently from this adjustment, the other correction terms are applied after the estimation of the baseline noise level and their effect is usually much more evident than that of acoustic impedance adjustment (Δ_i).

The duration correction (Δ_V) is applied just to sound exposure as it accounts for the effects of aircraft velocity on the duration of the event. It depends on the ratio between the segment airspeed and the reference velocity of 160 kt, to which the exposure NPD data relate.

The effects of engine installation (Δ_I) consider the reflection, refraction and scattering of engine sound due to the interaction with the surrounding solid surfaces. In jets, this corrective term

depends on engine position and on the angle between the wing plane and the propagation path (φ); no adjustment is instead expected for propeller-driven aircraft.

Another important correction, applied to both maximum- and exposure-level metrics, is linked to lateral attenuation (Λ), accounting for the interaction between the direct radiated sound waves and the ones reflected by the terrain. It therefore depends on the lateral displacement of the observer from ground track (l) and from the elevation angle (β) between the direct sound propagation path and the ground.

Figure 3.8 helps in identifying such quantities as well as the depression angle (φ) previously cited for engine installation effects.

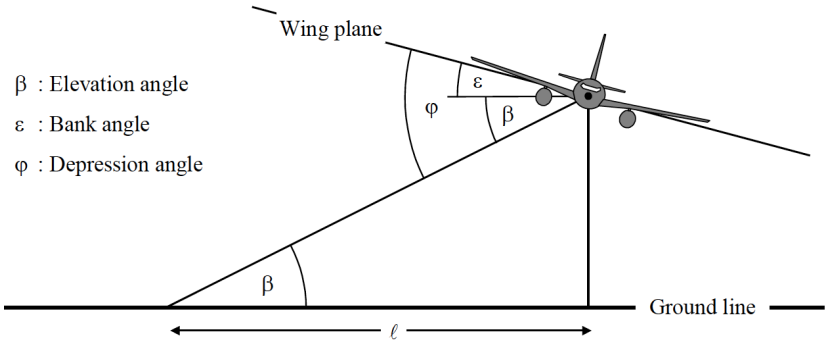

Figure 3.8: Geometric parameters for engine installation and lateral attenuation corrections [96]

The finite segment correction (Δ_F) is applied just to exposure levels since the NPD data essentially refer to an aircraft in level flight, covering a virtually infinite flight path. This does not have any influence on maximum-level metrics as they do not account for the duration of the event; instead, sound exposure results need to be corrected in order to consider the actual segment length and time exposure.

Finally, the start-of-roll directivity function (Δ_S) accounts for the large directionality of jet exhaust noise in presence of low airspeeds and high jet velocities. It therefore applies just to sensor locations behind each individual take-off segment and no adjustment is expected for piston-engine aircraft. This correction basically depends on the radial distance between the observer and the aircraft (d_{SOR}) and on the azimuth angle (ψ) between this distance and the runway axis.

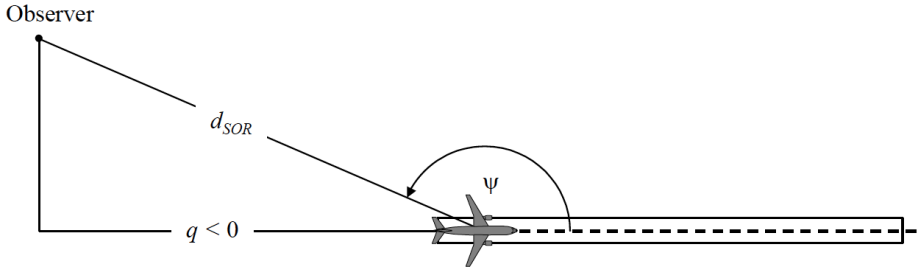

Figure 3.9: Geometric parameters for start-of-roll correction [96]

3.1.5 Model implementation and validation

All guidelines provided in the second volume of ECAC Doc. 29 have been implemented into a MATLAB® program for noise calculation, which is organized into two different modules.

The first refers to trajectory segmentation and basically consists in the definition of each segment end in terms of spatial coordinates, true airspeed, power and bank angle. On one side, ground track points are defined through a specific subroutine, exploiting route data similar to that presented in Tables 3.1 and 3.2. Flight profile is instead computed on the basis of the information provided in the ANP database; a subroutine is introduced for the definition of each flight phase as well as for the further subsegmentation of the different trajectory portions. Ground track and flight profile points are then coupled in the main trajectory program according to equations 3.3 and 3.4.

The second module basically deals with the computation of acoustic emissions according to equation 3.6. An important MATLAB® function is built for the definition of the main geometric parameters connected to the relative position between the segment and the ground sensor. This represents the common source of input data for the estimation of the baseline level and of the adjustment terms, which is performed according to separate subroutines.

The implemented prediction method has subsequently been validated thanks to the third volume of ECAC Doc. 29, which is specifically devoted to the verification of the model compliance with the directives inside Volume 2.

Three different hypothetical aircraft are considered, namely a turbofan with fuselage-mounted engines (JETF), another one with underwing engines (JETW) and a propeller-driven airplane (PROP). Each of this aircraft is assigned a straight and a curved ground track for both departure and arrival operations, leading to a total of twelve different reference cases.

Eighteen receptors are established in precise ground locations in order to perform a preliminary model check. A map showing the position of the sensors in relation to the departure and arrival routes is provided in Figure 3.10, where the origin corresponds to the point of brake release.

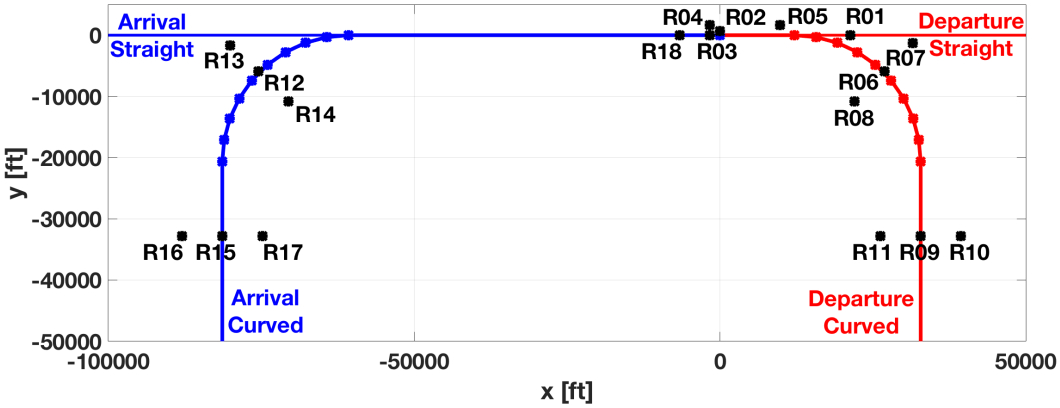

Figure 3.10: Ground tracks and receptors for validation

The validation procedure defined in Volume 3 of ECAC Doc. 29 essentially passes through three different steps for each of the twelve movements. A free workbook [130] provides all target results for the three validation stages together with the information about the airplanes, the receptors, the routes and the airport characteristics.

The first set of reference cases refers to the SEL results, which refer to the sound exposure levels computed for each of the twelve procedures at the most relevant receptors. The comparison with the target values is not just qualitative since no maximum limit is imposed to the deviation between the model output and the reference sound exposures. This check is therefore useful just for a preliminary estimation of model goodness and for the identification of the most critical methodological aspects.

The subsequent step goes into the details of the modelling procedure since it describes each trajectory segment in terms of geometry, thrust, baseline SEL and noise adjustments. Although the set of receptors is identical to the previous case, this phase represents an important step towards a more accurate noise model. It is indeed possible to check the subdivision of the entire aircraft trajectory and all the noise-related issues concerning each segment.

However, a quantitative assessment of model goodness is performed just in the third validation phase concerning reference grid results. As the name suggests, the set of receptors is replaced by an extremely dense grid of sensors covering a vast area around the airport.

In order to simplify the analysis and reduce the computational effort, grid results are only provided for the points away from the runway in which noise exposure is greater than or equal to 80 dB.

The error (δ_{RMS}) is estimated through the root mean square of the differences between the model output (L_i) and the corresponding reference grid result ($\bar{L}_i$) for all the N_S sensors under consideration, namely

$$\delta_{RMS} = \sqrt{\frac{\sum_{i=1}^{N_S}(\overline{L_i} - L_i)^2}{N_S}}. \tag{3.9}$$

The ECAC report imposes a δ_{RMS} limit in the order of 0.01 dB, which is fully satisfied for each of the twelve reference cases, as evidenced in Table 3.3.

	Departure Straight	**Departure Curved**	**Arrival Straight**	**Arrival Curved**
JETF	$2.99 \cdot 10^{-3}$	$3.11 \cdot 10^{-3}$	$2.84 \cdot 10^{-3}$	$2.89 \cdot 10^{-3}$
JETW	$2.99 \cdot 10^{-3}$	$3.04 \cdot 10^{-3}$	$2.98 \cdot 10^{-3}$	$2.97 \cdot 10^{-3}$
PROP	$3.00 \cdot 10^{-3}$	$3.19 \cdot 10^{-3}$	$2.83 \cdot 10^{-3}$	$2.85 \cdot 10^{-3}$

Table 3.3: Validation results of the ECAC method

It is possible to see that the validation results are well below the limit of 0.01 dB and are very close to each other: this means that the model is unaffected by systematic errors about the aircraft type, the procedure and the ground track.

3.2 The source-based method

The validation of the prediction procedure complying with the ECAC document has proven to be extremely successful, as evidenced by the sound exposure errors of Table 3.3. However, this model is useful just for the computation of noise levels related to existing aircraft since the NPD data refers to actual sound measurements.

The TRL of hybrid-electric aircraft is still too low to establish a standard departure or arrival procedure and to execute accurate sound measurements forming the NPD baseline noise levels. For this reason, a new approach based on the sound contribution of the most significant sources needs to be considered for the noise of hybrid-electric airplanes.

The first step of the new prediction method consists in the identification of the sources mostly affecting the overall aircraft noise: focusing on the typical General Aviation aircraft and the application to hybrid-electric power-trains, the five sources of Section 2.1.1 are considered.

The sound emission produced by each source is computed through highly-specific models and the different contributions are summed on an energetic basis to obtain a simple estimation of the overall aircraft noise. This constitutes the fundamental idea of the new prediction procedure named source-based method.

Actually, the estimation of sound emitted by a complex system from the contribution of its constituents does not represent a complete novelty in noise prediction methods. As an example, Fink's formulation for airframe noise combines the contributions of the wing, the leading-edge flaps and slats, the trailing-edge flaps and the landing gear.

Another important study was performed by Kumasaka et al. [131] in the context of the NASA *AST* noise reduction program. In this project, specifically devoted to jet airplanes, the acoustic contribution of the single airframe and engine source was computed thanks to a Boeing proprietary program and a common adjustment was applied to all sound levels in order to match the overall aircraft noise with the certification value.

The nature of the source-based method makes it particularly suitable in all those situations where sound measurements are not available, as in the case of new configurations or prototypes. Similarly to the current work, Synodinos et al. [132] predicted the NPD curves relative to new aircraft designs by combining the sound contributions of the different sources. However, their attention was focused on large jet airplanes and the estimation formulas for noise prediction are still based on too specific inputs for the application to hybrid-electric aircraft.

3.2.1 Model selection

A crucial part in the source-based method lies in the choice of the model describing the noise contribution of the single acoustic source. Section 2.1.1 provides a complete overview of the most well-known methods for the prediction of sound coming from each relevant source. The focus is on piston-engine aircraft and the contribution of the electric motor has been introduced for hybrid-electric airplanes.

All methods can essentially be split into the more-sophisticated theoretical procedures and the simpler best-practice models based on graphs or algebraic equations derived from acoustic measurements.

In this analysis, the second approach is preferable mainly because the theoretical procedures often require a great amount of highly-specific inputs, which are unavailable for a hybrid-electric aircraft.

Moreover, the general larger level of accuracy typical of theoretical methods is not a great deal in a comparative analysis, when the same model is applied to both a conventional and a hybrid-electric aircraft.

At some point in the future, when electric propulsion will be more mature, a more sophisticated theoretical procedure may be required for a higher level of sophistication and accuracy.

Propeller noise

Historically, propeller noise has gained considerable attention since the early years of aviation for the interest in silencing the aircraft as much as possible, above all in the military field. For this reason, a great amount of empirical procedures has been introduced for the estimation of propeller noise from flight speed and the main propeller parameters.

Among the most recent works, an important study was performed by Smith [30], who provided his own empirical equation and compared it to SAE AIR1407 [29] and to Rathgeber's formulation [31]. The results of Smith's work prove to be comparable to SAE AIR1407, while Rathgeber's equation is generally characterized by a lower level of accuracy.

In the present work, SAE AIR1407 is chosen since Smith's formulation just refers to flyover noise measurements and does not consider the relative position between the aircraft and the ground sensor. Moreover, Smith's equation requires the data about propeller thickness-to-chord ratio at the 95% station, and twist at the blade tip, two rarely available inputs.

A more recent alternative to SAE AIR1407 is represented by ESDU 11005 [32], which however requires a full description of the blade radial characteristics from the geometric and aerodynamic points of view.

Airframe noise

The prediction of airframe noise is an extremely complex task for the interaction between the different sources and sound-generation mechanisms. This reflects into a limited number of empirical expressions for the prediction of sound generated by the interaction between the airplane surfaces and the external airflow.

A first formulation was provided by Fink [34, 35], who estimated the overall airframe noise starting from the contribution of the wings, the flaps, the slats and the landing gear. The author supplies simple empirical expressions for each noise source based on his own theoretical formulas for far-field acoustic pressure.

Fink's works are used as a reference for the present work since the computer program provided by ESDU 90023 "is not suitable for use on propeller-driven aeroplanes" [46]. The reason is that such prediction method has been built on turbofan aircraft, which are characterized by different interaction and installation effects with respect to propeller-driven airplanes.

Internal combustion engine noise

Simple formulas for the estimation of piston-engine noise are provided in the Handbook of Noise and Vibration Control, which however focuses on industrial [63] and automotive [48] applications. These equations can not be transferred to the aeronautical field where the internal combustion engines are built according to a completely different philosophy. Most of the innovations introduced in the industrial and automotive field are indeed not applied in aviation unless they prove to grant a sufficiently-high level of reliability.

Focusing on the aeronautical sector, one of the first works was performed by Thurston [64], whose estimation formula is extremely simple as it is based just on shaft power. The more recent formulation provided by Dobrzynski [65] and reported by Tada [66] is preferable as it takes into account a larger number of engine parameters, such as the actual and the maximum rotational speed.

Lately, an empirical expression for aeronautical piston engine sound has been introduced by Moshkov et al. [67], but is unsuitable for a general noise prediction: it indeed contains engine-specific coefficients, which are provided just for a few motors.

Electric motor noise

As stated in Section 2.1.1, the study by Bruce et al. [63] refers to basically three works on the estimation of sound emission from electronic equipment.

As for electric motors, the authors rely on a US manual and make an important distinction between the more widespread Totally Enclosed Fan Cooled (TEFC) motors and the open drip-proof machines. The basic difference between the two lies in the enclosure type since the former have a closed off chamber and require the use of an external fan, while the latter are characterized by open vents.

The overall sound power level (L_W) as well as the octave-band spectrum is estimated for both machines starting from the rotational speed, the power output and the dimensions of the motor itself.

Consistency with the other noise measurements requires the conversion to sound pressure level (L_P) on the basis of the distance between the source and the sensor (r). Assuming the electric motor as a point source, the conversion formula is expressed according to equation

$$L_P = L_W + 10 \log_{10} \left(\frac{Q}{4\pi r^2} \right). \tag{3.10}$$

In this expression, the directivity factor Q determines the ratio between the surface sphere of radius r and the actual area in which spreading occurs: it is therefore equal to one for pure spherical diffusion, while it equals two in case of semi-spherical spreading.

Gearbox noise

The work by Bruce et al. [63] focuses on gearbox noise as well and suggests the use of the same US manual even in this application: according to this study, gearbox noise is estimated through the expressions

$$\begin{aligned} L_W &= 86 + 3 \log_{10} N + 4 \log_{10} P_W + 10 \log_{10} S \\ S &= LW + 2H(L + W) + \pi[L + W + 2(H + 1)]. \end{aligned} \tag{3.11}$$

The A-weighted sound power level (L_W) therefore depends on the rotational speed of the slower shaft (N), on the transmitted power (P_W) and on the conformal surface area at one meter from the gearbox (S). This is in turn computed from the length (L), width (W) and height (H) of the reference box surrounding the equipment.

As happens for electric motors, simple corrective adjustments need to be applied to L_W values if octave-band spectrum is required. In either case, the acoustic power is converted to pressure through equation 3.10 on the basis of the actual distance between the ground sensor and the gearbox.

3.2.2 Application of the ECAC method

Though originally developed for conventional aircraft, the method based on ECAC Doc. 29 [96] represents a solid basis even for the evaluation of the acoustic impact of radically new airplanes.

The development of the new source-based model is indeed formulated in the attempt to exploit the most numerous and relevant aspects belonging to the ECAC method.

The greatest advantage of this approach essentially lies in the possibility to treat the most peculiar and complex noise-related issues in exactly the same way as a validated model which constitutes the basis of all EU regulations on noise estimation.

The first distinguishing point inherited from the ECAC procedure is connected to flight trajectory segmentation according to the inputs provided in the ANP database. Since the hybrid-electric power-train is still an immature technology, very few tests have been performed on this kind of airplane and a default flight path has not been defined yet.

Accordingly, an alternative flight profile description needs to be provided for the hybrid-electric, while the ground-track definition is common to any conventional aircraft as it depends just on the airport under consideration.

As for flight profile, the only practical solution consists in making the hybrid-electric trajectory coincident with the one of a conventional airplane characterized by similar design and performance features. The most reasonable option consists in selecting the aircraft contained in the ANP database with which the acoustic comparison is made.

Although such trajectory match could appear a brute force approach to the problem, the flight profile discrepancies between the different airplanes are not relevant when the same aircraft category is considered; moreover, departure or arrival operations in General Aviation aerodromes need to comply with strict altitude limits, as it occurs at Milan Bresso airport.

Considering for example a Cessna 172R Skyhawk and a Piper PA-28-161 Warrior, the flight profile variation is minimum, as evidenced in Figure 3.11.

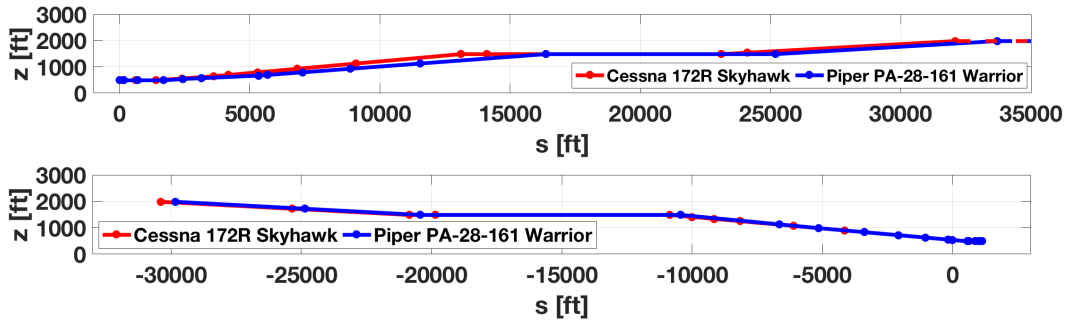

Figure 3.11: Flight profile comparison between Cessna 172R Skyhawk and Piper PA-28-161 Warrior

Looking at the two departure profiles, it is possible to notice that Cessna 172R Skyhawk generally climbs at a higher rate since it is capable of reaching the limit altitudes in a slightly shorter distance with respect to Piper PA-28-161 Warrior. The differences are however extremely small, particularly when examining the arrival paths, which are practically overlapping as a result of the 5° glide angle.

The other important aspect inherited from the ECAC approach concerns noise estimation, which is performed according to equations 3.1 and 3.2.

In both formulas, the noise of each segment is estimated from a baseline sound level, which is obtained from the NPD data inside the ANP database. The resulting noise value is then corrected with terms dependent on the segment length, on true airspeed and on the relative position between the segment and the sensor.

The identification of the hybrid-electric flight profile with the one of a similar conventional aircraft makes the additional corrective terms practically coincident for the two airplanes since the airspeed and all geometrical parameters are the same. As a result, all noise-related issues concerning sound attenuation, installation and duration effects are treated in the same manner as the ECAC procedure, resulting into a more accurate modelling of such second-order aspects.

What is instead different in the new sound estimation method is the baseline noise level, which is deeply aircraft-specific. The main idea behind the new prediction approach is therefore centred on the attempt to generate a new set of NPD data through the combination of the sound pressure levels relative to the most significant noise sources.

This very same procedure must be applied not only to the hybrid-electric, but also to a similar conventional airplane in order to have a more meaningful and fairer acoustic comparison, which is the primary objective of the entire work.

3.2.3 Mixing noise sources: theoretical aspects and issues

As its name suggests, the basic concept behind the source-based method essentially lies in a combination of the sound pressure levels relative to the most relevant acoustic sources in order to obtain a simple estimation of the overall aircraft noise.

Since the focus is on hybrid-electric airplanes for General Aviation, the five noise sources listed in Sections 2.1.1 and 3.2.1 have been considered. For the sake of a less heavy notation, the aircraft quantities are indicated with the subscript A, the airframe with the lowercase a, the propeller with p, the engine with e, the electric motor with m and the gearbox with g.

According to the simplest formulation, as in the case of Fink's airframe model, the different sources are assumed to be independent and the individual noise contribution is computed with no regard to the others. Consequently, the sound power emitted by the entire aircraft is simply given by the sum of the single contributions in order to satisfy energy conservation.

Since the propagation surface is the same for the noise of the aircraft and its components, the power equivalence can alternatively be written in terms of sound intensity (I), which depends on the root-mean-square acoustic pressure (P) according to the formula

$$I = \frac{P^2}{\rho c}. \tag{3.12}$$

Since the air density (ρ) and speed of sound (c) are the same for the noise of the airplane and the sources, the intensity equivalence between the aircraft and the sum of its components leads to a conservation equation, written in terms of root-mean-square acoustic pressure as

$$P_A^2 = P_a^2 + P_p^2 + P_e^2 + P_m^2 + P_g^2. \tag{3.13}$$

This conservation equation shows that an interesting RSS relationship links the aircraft sound pressure (P_A) with the contributions coming from the airframe (P_a), the propeller (P_p), the engine (P_e), the electric motor (P_m) and the gearbox (P_g).

The signal corresponding to acoustic pressure variation in time is then passed through Fourier transformation and converted into its spectral contributions. Focusing on the n-th frequency band, the sound pressure level of the entire aircraft (L_{A_n}), related to the reference pressure (P_0) of 20 micropascals, is computed from the corresponding spectral contributions of its constituents according to the formula

$$
\begin{aligned}
L_{A_n} &= 10\log_{10}\left(\frac{P_{A_n}^2}{P_0^2}\right) = 10\log_{10}\left(\frac{P_{a_n}^2}{P_0^2}+\frac{P_{p_n}^2}{P_0^2}+\frac{P_{e_n}^2}{P_0^2}+\frac{P_{m_n}^2}{P_0^2}+\frac{P_{g_n}^2}{P_0^2}\right) = \\
&= 10\log_{10}\left(10^{\frac{L_{a_n}}{10}}+10^{\frac{L_{p_n}}{10}}+10^{\frac{L_{e_n}}{10}}+10^{\frac{L_{m_n}}{10}}+10^{\frac{L_{g_n}}{10}}\right).
\end{aligned}
\tag{3.14}
$$

Another important step consists in the addition of the spectral term given by the A-weighting curve (A_n), which is transferred from the overall aircraft to the single sources as follows

$$
\begin{aligned}
L_{A_n,A} &= L_{A_n} + A_n = \\
&= 10\log_{10}\left(10^{\frac{L_{a_n}}{10}}+10^{\frac{L_{p_n}}{10}}+10^{\frac{L_{e_n}}{10}}+10^{\frac{L_{m_n}}{10}}+10^{\frac{L_{g_n}}{10}}\right)+10\log_{10}\left(10^{\frac{A_n}{10}}\right) = \\
&= 10\log_{10}\left[10^{\frac{A_n}{10}}\left(10^{\frac{L_{a_n}}{10}}+10^{\frac{L_{p_n}}{10}}+10^{\frac{L_{e_n}}{10}}+10^{\frac{L_{m_n}}{10}}+10^{\frac{L_{g_n}}{10}}\right)\right] = \\
&= 10\log_{10}\left(10^{\frac{L_{a_n,A}}{10}}+10^{\frac{L_{p_n,A}}{10}}+10^{\frac{L_{e_n,A}}{10}}+10^{\frac{L_{m_n,A}}{10}}+10^{\frac{L_{g_n,A}}{10}}\right).
\end{aligned}
\tag{3.15}
$$

Finally, the frequency domain contributions are integrated as

$$
\begin{aligned}
L_A &= 10\log_{10}\left(\int 10^{\frac{L_{A_n,A}}{10}}df\right) = \\
&= 10\log_{10}\left(\int 10^{\frac{L_{a_n,A}}{10}}df+\int 10^{\frac{L_{p_n,A}}{10}}df+\int 10^{\frac{L_{e_n,A}}{10}}df+\int 10^{\frac{L_{m_n,A}}{10}}df+\int 10^{\frac{L_{g_n,A}}{10}}df\right)
\end{aligned}
\tag{3.16}
$$

in order to obtain the overall sound pressure level relative to the entire aircraft (L_A) from the contributions of the airframe ($L_{a_n,A}$), of the propeller ($L_{p_n,A}$), of the engine ($L_{e_n,A}$), of the electric motor ($L_{m_n,A}$) and of the gearbox ($L_{g_n,A}$).

According to some models, the estimation formula for the single component refers to the spectral contributions, which later have to be A-weighted and integrated in the frequency domain; in others, the overall A-weighted sound pressure level is directly modelled.

3.2.4 Effects of atmospheric attenuation

As stated in Section 3.1.2, the NPD data essentially consists in a series of sound levels provided at ten slant distances for a restricted number of departure and arrival power settings. The noise dependence on distance therefore plays a crucial role in the development of new NPD data according to the source-based method.

The main contribution to noise decay with distance is represented by sound spreading, whose effects are clearly visible in equation 3.10. As its name suggests, this phenomenon is essentially related to the fact that the power of the sound pressure wave is applied to a progressively larger surface as soon as propagation advances. This results into a pressure decrement with the square of the distance between the aircraft and the observer.

Their extreme importance in sound pressure level computation makes spreading effects explicitly appear in the noise estimation formulas for the airframe, propeller and piston engine. This is not the case for gearbox and electric motor since their noise is expressed in terms of sound power and equation 3.10 is required.

However, the propagation of acoustic waves is responsible for another minor physical behaviour affecting noise decay with distance. Such phenomenon goes under the name of sound absorption

and basically refers to an energy transfer from the acoustic wave to the non-idealized medium in which it propagates.

Considering the case of sound travel in air, atmospheric absorption is the result of heat dissipation due to air shear viscosity and thermal conductivity, combined with the relaxation of nitrogen, oxygen and water vapor particles caused by the excitation of molecular internal degrees of freedom.

Atmospheric absorption therefore results into a sound power attenuation which depends on the wave frequency, on the distance between the source and the sensor, and on the local meteorological conditions in terms of pressure, temperature and relative humidity.

The second volume of ECAC Doc. 29 clearly states that the NPD levels inside ANP have all been normalized according to the standard attenuation rates defined in SAE AIR1845 [109] and revised in CAN/7-WP/59 [133].

According to this method, the the corrected sound pressure level relative to the n-th frequency band ($L_{P_n,\alpha}$) is obtained from the uncorrected value (L_{P_n}) through a simple corrective term that is directly proportional to the distance (d) through a frequency-dependent attenuation coefficient (α_n), namely

$$L_{P_n,\alpha} = L_{P_n} - \alpha_n d. \tag{3.17}$$

Apart from wing noise, which however plays a minor role with respect to flaps and landing gear, Fink's model does not include a relationship for atmospheric absorption. Since the airframe prediction formulas refer to the spectral contributions, SAE AIR1845 is directly applied for the simulation of atmospheric attenuation effects.

Instead, the SAE AIR1407 for the estimation of propeller noise already includes the absorption effects in the graph for the sound pressure dependence on distance.

Unfortunately, the model for engine noise does not take atmospheric absorption into account and is expressed in terms of overall sound pressure level. No information about its spectral content is indeed provided in Dobrzynski's formula and therefore SAE AIR1845 can not be applied. Tada [66] suggested a 0.1 dB decrement of the overall sound pressure level every 100 m, but this value is suitable just for ground tests as it is valid for a temperature range between 10°C and 40°C.

Another solution has been found on the basis of what ECAC Doc. 29 suggests for the recalculation of NPD data through a new absorption model. The procedure starts from the reference noise spectra provided in the *Spectral classes* table for all aircraft covered in the ANP database; as for the hybrid-electric, it is sufficient to consider the values of a similar conventional airplane since this data is just function of the aircraft size.

In the *Spectral classes* folder, two different sets of spectral pressure levels are provided depending on whether they relate to a departure or arrival procedure. They refer to a slant distance of 1000 ft and have already been corrected according to SAE AIR1845.

As a result, the first step consists in inverting equation 3.17 in order to remove the absorption correction and obtain the unattenuated spectrum at the reference distance ($\bar{d}$) equal to 1000 ft.

Considering the n-th frequency band, the corresponding sound pressure level ($L_{P_n}(\bar{d})$) is then adjusted to each NPD slant distance (d_i) on the basis of the expression

$$L_{P_n,\alpha}(d_i) = L_{P_n}(\bar{d}) - 20\log_{10}\left(\frac{d_i}{\bar{d}}\right) - \alpha_n d_i. \tag{3.18}$$

On one side, equation 3.18 is fully exploited in order to include the effects of atmospheric absorption, modelled according to SAE AIR1845 and resulting into the spectral levels $L_{P_n,\alpha}(d_i)$;

on the other, an unattenuated spectrum $L_{P_n}(d_i)$ is developed from just the first two terms related to sound spreading.

The spectra are later A-weighted and decibel-summed in order to obtain the A-weighted overall sound pressure levels, which are subtracted for the estimation of noise reduction $\Delta L_P(d_i)$ as

$$\Delta L_P(d_i) = 10\log_{10}\left(\sum 10^{\frac{L_{P_n,\alpha}(d_i)+A_n}{10}}\right) - 10\log_{10}\left(\sum 10^{\frac{L_{P_n}(d_i)+A_n}{10}}\right). \tag{3.19}$$

In this way, two different sound decrements are obtained for each NPD distance (d_i), one for departure and another for arrival. Finally, this term is added to the uncorrected engine noise levels in order to simulate the effects of atmospheric absorption.

The very same procedure is applied to the electric motor and the gearbox since their estimation formulas do not account for atmospheric sound absorption and refer to the overall sound pressure level.

3.2.5 Recalculation of NPD exposure data

Once the source-based method is formulated and the attenuation effects included into the prediction models, it is possible to compute the aircraft sound pressure level thanks to equation 3.16.

In the evaluation of acoustic effects, the most significant and widely accepted metric is the A-weighted sound exposure level ($L_{E,A}$), which is defined as

$$L_{E,A} = 10\log_{10}\left(\int_{t_1}^{t_2} 10^{\frac{L_A(t)}{10}}\,dt\right). \tag{3.20}$$

In the definition of sound exposure, the instantaneous A-weighted SPL ($L_A(t)$) is converted in energetic terms and subsequently integrated in time. Technically speaking, the time interval between t_1 and t_2 should correspond to the duration of the entire sound event, namely to the entire departure or arrival movement. However, the sound exposure levels contained in ANP refer to the so-called 10dB-down time, defined as the period in which the A-weighted sound pressure level is within 10 dB of the maximum. In general, sound exposure is preferable to the maximum sound pressure level as it accounts for both the intensity and the duration of the entire aircraft movement.

An important estimation of source-model goodness is obtained through the comparison between the actual sound exposure levels contained in ANP and the corresponding values generated by means of the new estimation procedure.

Besides introducing a new atmospheric absorption model and a CPA algorithm, SAE AIR1845 [109] clearly defines the conditions in which ANP data has been obtained, which are schematically represented in Figure 3.12.

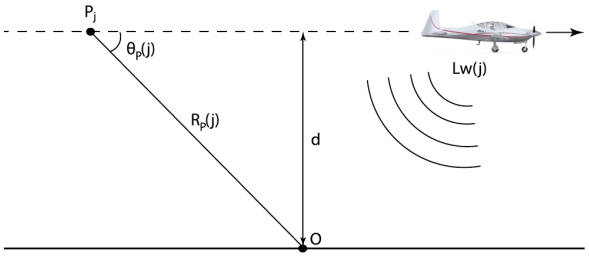

Figure 3.12: Flyover test for the obtainment of NPD data [132]

The noise values inside ANP therefore refer to a series of flyover tests with the aircraft in steady level flight at a speed of 160 kt. The spectral pressure contributions are measured every 0.5 seconds and subsequently manipulated through A-weighting, frequency and time integration in order to obtain the A-weighted sound exposure level. Normally, noise measurements are available just for a single slant distance (d) between and 100 and 800 m; extrapolation is therefore required for the adjustment to the other default distances. Moreover, the sound exposure levels contained in ANP are provided for at least a couple of power settings for departure and for arrival movements.

Although the testing procedure is perfectly known and can be simulated for each of the ten NPD slant distances, users are provided just with the information about aircraft power setting during the flyover test. The FAA Aviation Sustainability Center (ASCENT) recently emphasizes the need for a NPD re-evaluation including all data about aircraft configuration [134]. According to the authors, this would allow for a more precise investigation of configuration effects on the tracing of noise contours. In the current thesis instead, the knowledge of aircraft configuration would imply a more precise modelling of the testing procedures, resulting into a more accurate comparison between the NPD values inside ANP and the ones generated through the new source-based method.

Some important hypotheses are therefore needed for the definition of aircraft configuration at each flyover test. In order to mimic take-off and landing, the noise contribution of a retractable landing gear is taken into account just for the arrival at the lowest power setting and for the departure at the highest regime. When present, analogous considerations apply to the leading-edge flaps and slats, while the other main contribution to airframe noise is related to trailing-edge flaps.

In all those cases when flight profile is defined in terms of procedural steps, users are provided with the typical flap angles in departure and arrival. The take-off deflection is assigned to the largest departure setting, while the landing flap angle is selected for the least powerful arrival case; as for the intermediate ratings, the typical climb and approach configurations are chosen for departure and arrival settings respectively.

When flight profile is expressed through fixed points instead, the pilot's operating handbook is consulted for typical take-off and landing configurations: the former is chosen for the departure at the highest power, while the latter is considered at the lowest arrival regime. In analogy with the procedural case, typical climb and approach flap deflections are used for the low-power departure cases and the high-speed arrival settings respectively.

Besides aircraft configuration, other important assumptions concern the knowledge of the power and rotational speed inputs for the evaluation of propeller and engine noise in particular. The NPD sound levels contained in ANP are indeed given as a function of a single power parameter, either the shaft rotational speed or the corrected net thrust.

The latter can in turn be expressed in absolute or relative terms with respect to the maximum static value. Since the maximum power setting is always fixed at the 100% of static thrust, the absolute corrected net thrust values are all normalized with respect to the maximum in order to be consistent with the formulation in relative terms. As a result, in both cases the power parameter corresponds to thrust fraction, which in turn translates into power fraction for sound exposure computation; the airspeed is indeed fixed at 160 kt and the propeller efficiency variation is neglected in the range of settings under consideration.

Anyway, the extremely wide operational variability typical of an aircraft piston engine makes it impossible to establish a single correlation for power estimation from rotational speed or viceversa. This is confirmed by the engine performance curves, showing that the relationship between engine power and shaft speed depends on manifold air pressure. Such parameter is not known by the user as it is connected to the way the pilot decides to operate on the throttle and mixture levers.

An interesting and simple way to overcome this problem is provided with the ACRP Research Report 164 by Yacovitch et al. [135]. In this work, the authors collected the results obtained through a series of ground tests on the most common General Aviation engines. Some pilots were asked to operate the aircraft at the same power settings effectively used in seven flight phases, namely take-off, climb, cruise, approach, final approach, taxi and idle. The main propulsive and emission parameters are annotated for each aircraft in the seven different conditions.

In this way, a rough correlation between engine power and rotational speed can be introduced as "the fuel flow measure is expected to be most linear with thrust" [135]. Accordingly, when NPD power rating is expressed in terms of shaft rotational speed, the percentage of maximum fuel flow allows for the estimation of thrust fraction. This in turn translates into a power percentage since the airspeed is fixed at 160 kt and the propeller efficiency is assumed constant. The opposite situation occurs when the NPD levels refer to thrust fraction and rotational speed needs to be estimated.

Focusing on the current work, the final approach fuel flow or rpm fraction is assigned to the lowest power setting, the take-off to the highest; in the intermediate cases, the climb, cruise or approach values are selected according to the intensity of the power setting with respect to the maximum. Moreover, readers are provided not only with the results of single tests, but also with the average values obtained from all engines belonging to the same family. In this way, if the exact version of the aircraft engine was tested by ACRP, the corresponding rpm or power value is taken from the table of the single engines, possibly averaged in case of test repetitions; otherwise, the value of the family to which the engine belongs is used.

Under the aforementioned hypotheses, the application of the source-based method leads to a set of NPD sound exposures for each of the power settings under consideration. In particular, Figure 3.13 refers to a Cessna 172R Skyhawk and compares the new NPD values with those inside ANP.

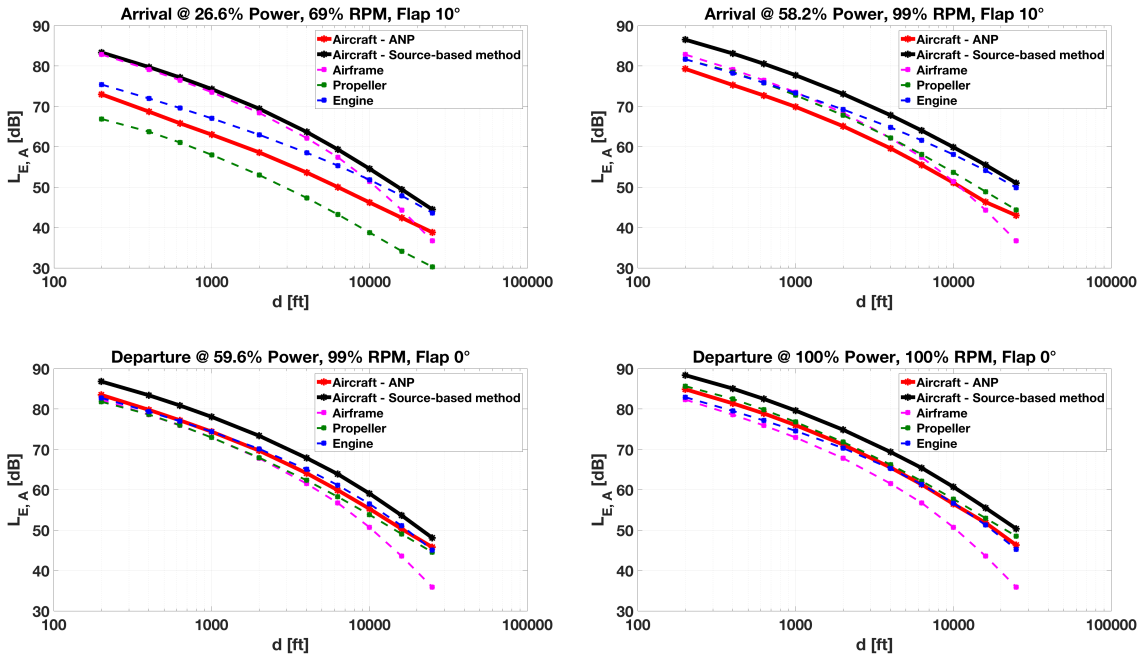

Figure 3.13: Comparison of NPD data for Cessna 172R Skyhawk

It is possible to see that the ANP sound exposures and the corresponding source-based values are very distant from each other, above all in the two arrival movements.

The average discrepancy between the points belonging to the black and red curve is indeed equal to 9.5 dB for the arrival at the 26.6% power, to 5.1 dB for the 58.2% case. When departure is considered instead, the values get closed and the average distance between the curves reduces to 3.5 dB for the 59.6% power, to 3.8 dB for the full take-off regime.

Focusing on the single figures, the overall noise at the 26.6% power is governed by the airframe contribution at the lowest distances, while the engine sound dominates from 10000 ft onwards. Apart from the exposure at the largest distance, both contributions are higher than the ANP data, while propeller noise correctly lies below the red line of the target levels.

As for the arrival at the largest power, each of the three noise contributions is higher than the reference ANP values apart from the two airframe levels at the largest distances. This results into an overestimation of the overall sound exposure, whose trend is very similar to the target red line.

In the two departure cases, the sound exposure relative to the airframe is constantly lower than the ANP aircraft value. The two lines corresponding to propeller and engine contributions are very close to the reference sound exposure levels and the acoustic summation of the three sources still results into an overestimation of aircraft noise.

In conclusion, the application of the source-based method leads to a general overvaluation of the real sound exposures and a modified version needs to be implemented. Besides the general overestimation, in three of the four cases the sound emitted from at least one source overcomes the actual ANP aircraft value.

3.2.6 The source blending method

The application of the source-based method through equations 3.16 and 3.20 has given extremely poor results when comparing the model output to the NPD values contained in the ANP database.

Such discrepancy in sound exposure is basically related to multiple reasons, starting from all the hypotheses on aircraft configuration and power setting listed in the previous section.

Moreover, the database provided by Yacovitch et al. is not exhaustive as it does not include all piston engines used in General Aviation and can not cover the infinite possible ways in which such machines can be operated.

Another important aspect is represented by the accuracy of the models implemented for the estimation of sound emitted by the different sources. The use of a single prediction formula representative of all aircraft is a possibility when no acoustic data is available, but does not perfectly match the actual sound emission from an existing airplane.

Furthermore, any method for airframe noise prediction can be formulated just through in-flight tests, when all acoustic sources act at the same time; a further problem therefore arises from the difficulty in isolating the airframe contribution from the others.

A final important issue concerns the models for atmospheric attenuation since the SAE AIR1845 used in the extrapolation of the target ANP values is exploited just for airframe noise prediction.

Since all contributions coming from the different sources are affected by some error, an innovative expression for sound exposure level ($L_{E,A}$) is formulated on the basis of equation 3.20 as

$$L_{E,A} = 10 \log_{10} \left(\int_{t_1}^{t_2} 10^{x_1 \frac{L_a(t)}{10}} + 10^{x_2 \frac{L_p(t)}{10}} + 10^{x_3 \frac{L_e(t)}{10}} + 10^{x_4 \frac{L_m(t)}{10}} 10^{x_5 \frac{L_g(t)}{10}} dt \right), \tag{3.21}$$

remembering that $L(t)$ is the instantaneous sound pressure level and that subscript a refers to the airframe, p to the propeller, e to the engine, m to the electric motor and g to the gearbox.

The great novelty introduced in equation 3.21 concerns the sound emitted by the single source as it passes through a multiplicative factor (x_i) quantifying the degree of uncertainty intrinsic in the noise prediction formula for the i-th source. In particular, the x_1 coefficient is related to the airframe, x_2 to the propeller, x_3 to the engine, x_4 to the electric motor and x_5 to the gearbox.

Retracing the procedure in Section 3.2.3 back, energy conservation is still satisfied in the new formulation since the acoustic power of the entire aircraft results from the sum of the different contributions.

Considering an existing airplane covered in the ANP database, the x_i coefficients are estimated for each of the power settings to which the NPD data relates. In particular, the numerical minimization of the objective function

$$J = \frac{\sum_{j=1}^{10}(\overline{L_{E,A,j}} - L_{E,A,j})^2}{10} + (x_1 - 1)^2 + (x_2 - 1)^2 + (x_3 - 1)^2 + (x_4 - 1)^2 + (x_5 - 1)^2 \quad (3.22)$$

is exploited for the obtainment of the blending coefficients (x_i) from the ten target ANP values ($\overline{L_{E,A,j}}$) and the corresponding sound exposures computed according to equation 3.21 ($L_{E,A,j}$).

The first term of the objective function corresponds to the average quadratic error over the ten default NPD distances, but other additional terms have to be introduced for a more physical minimization.

When just the first term in equation 3.22 is considered, in many cases the solver finds the optimal solution by suppressing some coefficients to extremely low values; though being the optimal solution in mathematical terms, the suppression of blending coefficients is not an acceptable procedure from a physical point of view.

In the ideal case, the estimation formulas for the different noise sources would be unaffected by any error if the blending factors were equal to unity. The application of unit coefficients to Cessna 172R Skyhawk has given poor results, but at the same time the higher the distance from unity, the lower is the accuracy degree of the prediction formulas. As an example, a practically null value of x_i would imply a 100% error in noise prediction and no acoustic contribution coming from the i-th source.

For this reason, the objective function is increased with other additional terms related to the distance of each coefficient to one, a sort of 'elastic' contribution balancing the pure mathematical minimization with a physically based correction.

3.2.7 Design of blending coefficients

The introduction of blending coefficients in the estimation of sound exposure brings to a better fit with the actual noise levels contained in the ANP database. The minimization procedure for the obtainment of the blending factors gives birth to a set of coefficients for each of the power settings to which the ANP noise data relates. In this way, it is possible to provide a rough estimation of the average accuracy degree of the prediction models over the ten default NPD distances.

However, the meaning of these coefficients is still extremely poor from a predictive point of view as they can be computed just for those airplanes inside the ANP database. Moreover, these coefficients are strictly related to the target ANP levels and are therefore typical of the aircraft and power setting under consideration.

The research for a generic prediction tool applicable to any airplane starts from the investigation of the blending coefficients obtained for the eight piston-engine aircraft contained in ANP, which are presented in Table 3.4.

Aircraft name	**Nickname**	**Number of engines**	**MTOW [lb]**
Piper PA-28-161 Warrior	PA-28	1	2 325
Cessna 172R Skyhawk	C172R	1	2 450
Cessna 182H Skylane	C182H	1	2 800
Cessna 206H Stationair	C206H	1	3 600
Cessna T206H Stationair	T206H	1	3 600
Piper PA-30 Twin Comanche	PA-30	2	3 600
Beechcraft Baron 58P	BB 58	2	6 100
Piper PA-31-350 Navajo Chieftain	PA-31	2	7 000

Table 3.4: General Aviation aircraft inside the ANP database

Each aircraft is given a nickname in order to ease its citation all over the work and is characterized by distinguishing features connected to its size, its wing configuration and the number and type of engines. Since neither the gearbox nor the electric motor is present in all these airplanes, it is evident that the analysis focuses just on x_1, x_2 and x_3, the factors relative to the airframe, to propeller and to engine noise respectively.

Focusing on the single aircraft, the triplets relative to the different power settings are split into the departure and arrival values, and a simple statistical analysis is performed for all x_i coefficients falling inside each category.

At first, the mean ($\bar{x}_i$) and standard deviation (σ_i) are computed for the N departure or arrival movements as follows

$$\begin{aligned} \overline{x_i} &= \frac{\sum_{i=1}^{N} x_i}{N} \\ \sigma_i &= \sqrt{\frac{\sum_{i=1}^{N} (x_i - \overline{x_i})^2}{N-1}}. \end{aligned} \tag{3.23}$$

Other important statistical parameters are the lower ($x_{i,-2\sigma}$) and upper ($x_{i,+2\sigma}$) limits of the 2σ bilateral confidence interval of the mean, computed from Student's t-parameter ($t_{N-1,97.7\%}$) as

$$\begin{aligned} x_{i,-2\sigma} &= \overline{x_i} - t_{N-1,97.7\%} \frac{\sigma_i}{\sqrt{N}} \\ x_{i,+2\sigma} &= \overline{x_i} + t_{N-1,97.7\%} \frac{\sigma_i}{\sqrt{N}}. \end{aligned} \tag{3.24}$$

The same statistical analysis is performed considering the eight airplanes together and including the 3σ bilateral confidence interval of the mean. Figures 3.14, 3.15 and 3.16 graphically present a comparison between the different departure and arrival results for each of the three coefficients.

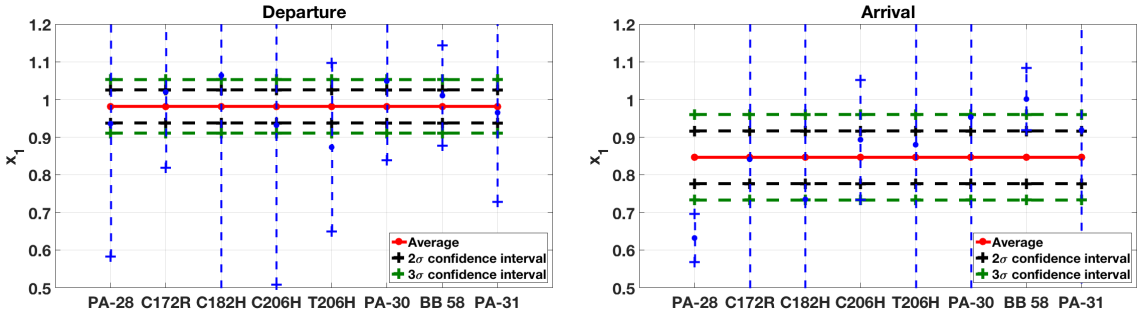

Figure 3.14: Statistical results on airframe coefficient

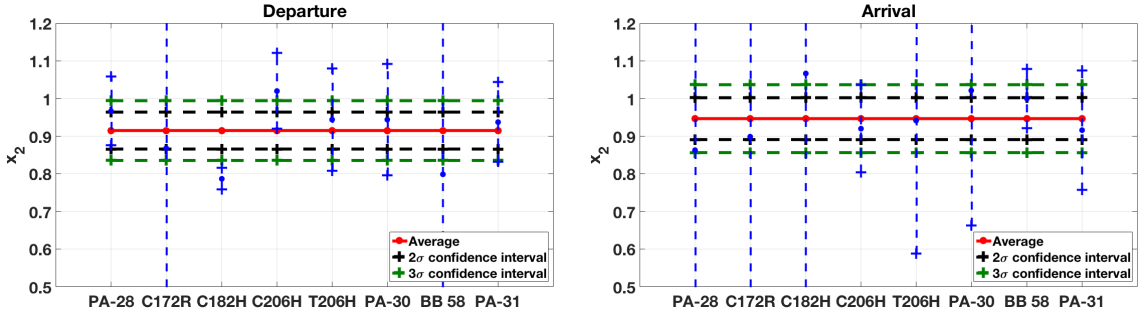

Figure 3.15: Statistical results on propeller coefficient

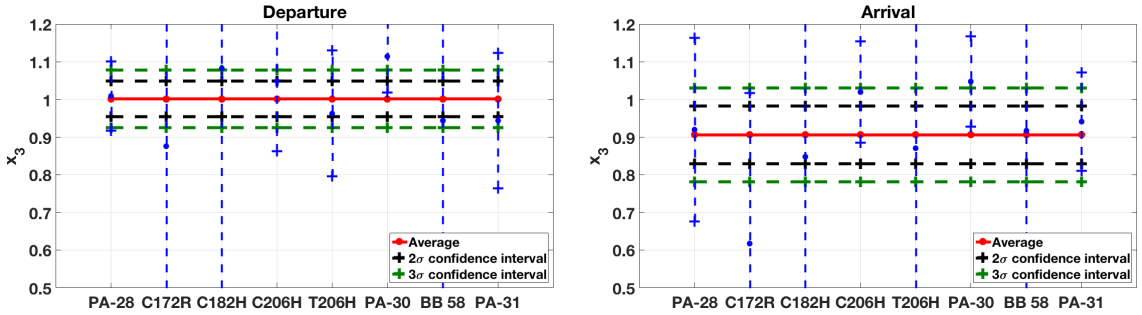

Figure 3.16: Statistical results on engine coefficient

Looking at the plots in a general perspective, it is possible to notice that the blue dashed lines, representing the 2σ bilateral confidence of the mean relative the single aircraft, often goes beyond the limits imposed at 0.5 and 1.2. This behavior basically results from the combination of a large standard deviation with a poor number of x_i values, leading to high deviations of the 2σ limits from the mean.

Moreover, in most cases the 2σ bilateral confidence band relative to each aircraft comprises the average value of the overall analysis, meaning that the identification of the single average airplane

coefficient with the overall value is within the 95% bilateral confidence interval.

Considering the analysis on all eight airplanes, the statistical results can be summarized in the Tables 3.5 and 3.6, relative to departure and arrival operations respectively.

	3σ lower limit	**2σ lower limit**	**Average**	**2σ upper limit**	**3σ upper limit**
$\boldsymbol{x}_1$	0.91	0.94	0.98	1.03	1.05
$\boldsymbol{x}_2$	0.84	0.87	0.91	0.96	0.99
$\boldsymbol{x}_3$	0.93	0.95	1.00	1.05	1.08

Table 3.5: Statistical results for departure coefficients

	3σ lower limit	**2σ lower limit**	**Average**	**2σ upper limit**	**3σ upper limit**
$\boldsymbol{x}_1$	0.73	0.78	0.85	0.92	0.96
$\boldsymbol{x}_2$	0.86	0.89	0.95	1.00	1.04
$\boldsymbol{x}_3$	0.78	0.83	0.91	0.98	1.03

Table 3.6: Statistical results for arrival coefficients

It is interesting to see that the prediction models imply a general overestimation of the actual noise level since the average coefficients are all lower or equal to unity. Moreover, the average lowest value is relative to arrival for x_1 and x_3, while the propeller blending factor shows the opposite trend.

Considering the confidence limits instead, the span of the departure bands are the same for the three coefficients: in particular, the 2σ bilateral confidence interval is 0.09 broad, while a 0.15 width is registered for the 3σ limits. Looking at equation 3.24, the coincidence between the three spans is evidently the result of the same standard deviation value since the number of movements is necessarily identical for the three factors.

Arrival confidence bands are characterized by much larger expansion with respect to departure. In particular, the width of the confidence bands for x_1 and x_3 is approximately the same, while a lower span characterizes the confidence intervals of propeller coefficient. Considering the 3σ band for instance, its expansion is fixed at 0.18 for x_2, while the width of the x_1 and x_3 bands is equal to 0.23 and 0.25 respectively. The same previous considerations apply for the linear dependence of confidence limits on standard deviation.

The analysis of the different plots shows that the error committed in using a single triplet of coefficients for all aircraft is not so relevant, particularly when departure and arrival operations are clearly distinguished since they are characterized by different mean values. Accordingly, a single triplet composed of the average results is defined for departure, another one for arrival; according to the type of procedure, each of them is exploited in equation 3.21 and used to generate the new set of baseline sound exposure levels.

The application of such coefficients in the estimation of sound exposure and the comparison with real NPD data are provided in Appendix A for two radically different airplanes, namely Cessna T206H Stationair and Piper PA-31-350 Navajo Chieftain.

The use of generic coefficients even allows for noise estimation in relation to the two main versions of Pipistrel Panthera, namely the conventional and the hybrid-electric.

In developing the NPD curves for these airplanes, five power settings are considered in order to mirror the flight phases defined in the database by Yacovitch et al.. Take-off is assigned the 100% thrust, climb the 80%, cruise the 60%, while approach and final approach are given the 40% and 20% of maximum static thrust respectively. The first three phases are relative to departure operations, while approach and final approach come under the arrival mode.

Focusing on the aircraft configuration in each of the five cases, the landing gear is assumed to be extended at the maximum and minimum thrust fraction, while the cockpit images show three possible flap settings: the maximum value of 45° is assigned to the 20% thrust, a null flap angle is assumed for the three intermediate cases, while a deflection of 15° is considered for take-off.

Moreover, Panthera Hybrid features the two additional noise contributions coming from the electric motor and the gearbox, which have not been considered so far as they are not mounted on the eight airplanes covered by ANP.

As for the electric motor, its contribution in terms of sound power is compared to the propeller one for each of the five thrust settings, as evidenced in Table 3.7.

	Propeller [dB]	**Electric motor [dB]**	**Difference [dB]**
200 kW, 2 400 rpm	130.6	102.7	27.9
160 kW, 1 920 rpm	123.5	100.3	23.2
120 kW, 1 440 rpm	115.7	97.1	18.6
80 kW, 960 rpm	106.9	92.7	14.2
40 kW, 480 rpm	96.1	85.2	10.9

Table 3.7: Sound power comparison between propeller and electric motor

In the computation of sound power levels and in the obtainment of the new NPD data, the electric power delivered to the propeller is assumed to be proportional to the rotational speed, a simplification of the characteristic curve for a brushless electric motor.

Naturally, the sound power relative to both sources is extremely dependent on the rotational speed and power output, particularly for what concerns propeller noise: the sound power difference between the propeller and the electric motor indeed increases with power, but even in the worst case it is higher than 10 dB. This implies that the noise coming from the electric motor can safely be neglected as it just represents a small part of the propeller contribution to the overall noise.

As for gearbox instead, it is integrated directly inside the casing of Rotax 914 in order to slow down the output shaft to acceptable rotational speeds for propeller motion. As a result, the sound power comparison is made with engine noise, as evidenced in Table 3.8.

	Engine [dB]	**Gearbox [dB]**	**Difference [dB]**
115 hp, 5 800 rpm	123.0	113.3	9.7
92 hp, 5 800 rpm	123.0	112.9	10.1
69 hp, 5 220 rpm	121.2	112.3	8.9
46 hp, 3 828 rpm	115.8	111.2	4.6
23 hp, 3 828 rpm	115.8	110.0	5.8

Table 3.8: Sound power comparison between engine and gearbox

The database provided by Yacovitch et al. highlights that the rotational speed is the same for take-off and climb as well as for approach and final approach. As a result, the engine sound power level is the same in the first and last two cases since Dobrzynski's model does not take the real output power into consideration. Gearbox noise instead depends on both the transmitted power and the shaft speed, resulting into progressively lower values for decreasing power settings.

Moreover, it is interesting to see that engine noise is at least 4.6 dB higher than the gearbox, and a difference of 9.7 dB is expected at maximum power. For this reason it is possible to neglect the gearbox contribution or at least assume that it is already included in engine sound.

In Chapter 5 applicative examples of the source blending method will be presented on the basis of two different analyses centred on a traffic pattern at Milan Bresso airport.

The first investigation will show the acoustic effects related to power management, while the second analysis will focus on the comparison between a Cessna 172R Skyhawk and the two Panthera versions, namely the conventional and the hybrid-electric one.

Chapter 4

Modelling of atmospheric pollution

Historically, the quantification of the harmful chemical substances released by aircraft engines has been treated with much minor emphasis with respect to noise issues. Such lower attention is even reflected in the certification standards for aircraft engine emissions, defined by ICAO ten years later than the acoustic requirements. Furthermore, the prescriptions in terms of atmospheric pollution, imposed with Annex 16, Volume II [116], are confined to turbojets and turbofans, while no attention is given to piston-engine airplanes.

However, in the most recent years the discharge of air pollutants has become so important that in 2017 ICAO published a third volume of Annex 16 specifically devoted to the emission of carbon dioxide [136]. Another important challenge in current engine design is represented by the release of the oxides of nitrogen, as evidenced in Figure 4.1: it refers to the certification requirements imposed by ICAO on subsonic jets above 89 kN thrust.

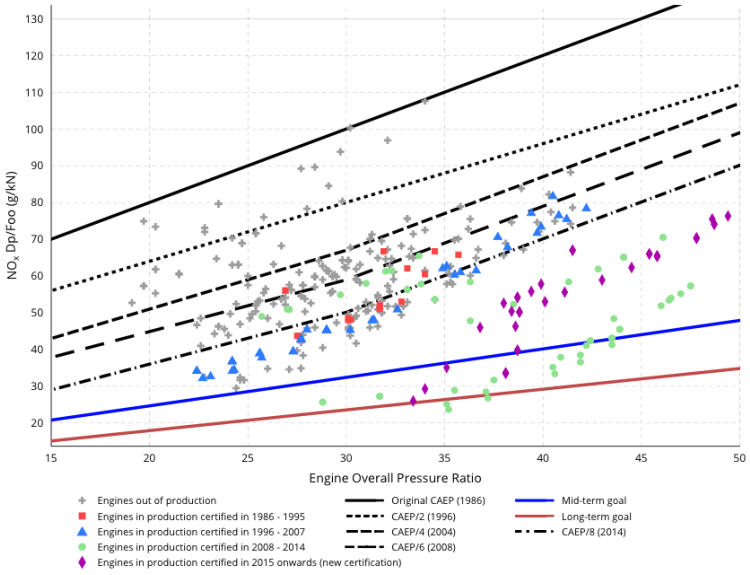

Figure 4.1: Progression of ICAO standard on NO_x emissions [137]

The limit imposed to NO_x emissions, expressed in terms of mass per rated thrust, shows a linear increment with the reference pressure ratio, defined by the mean total pressure at the last compressor stage with respect to the inlet value when the engine develops take-off thrust.

Moreover, Figure 4.1 shows the progressive reduction imposed by the different meetings of the Committee on Aviation Environmental Protection (CAEP). Apart from the curve relative to the 1996 assembly, the other black lines are essentially characterized by the same slope and show a constant reduction of 8 grams per kN imposed by the last two meetings. As a matter of fact, the two bottom lines corresponding to future objectives evidence a lower slope and at least a half decrement is foreseen on a long-term period.

The continuous effort in reducing NO_x emissions is not only related to their tremendous effect on human health, but is mainly dictated by engine-design issues: the natural tendency towards a more efficient thermodynamic cycle leads to progressively high temperatures in the combustion chamber, resulting into a massive production of thermal NO_x.

4.1 Choice of the estimation model

The tier subdivision proposed by the European Environment Agency [115] is in most cases used as a reference point for the prediction of atmospheric pollution connected to aircraft operations.

The great majority of all prediction methods basically relies on the concept of tiers, from the simpler models by the English NETCEN [117] or the Dutch TNO [138], to the more complex numerical analysis of the IESTA program by ONERA.

In fact, there are few exceptions as in the study about piston-engine emissions led by Markowski et al. [139]. Their model is however based on engine-dependent coefficients related to the amount of pollutant emitted per energy unit, a strange and rarely available parameter.

All procedures complying with the EEA document are essentially based on equations 2.1 and 2.2 for the estimation of fuel consumption and pollutant emissions respectively. As a result, the basic difference among all prediction methods is related to the level of detail of the input data used for pollution estimation.

Focusing on Tier 1 approaches, atmospheric pollution is predicted simply from the overall number of LTO cycles performed in a certain country and from the national fuel sales. Since no aircraft information is available, the quantification of pollutant emissions passes through the selection of a single airplane representative of the entire national fleet.

These kind of approaches are characterized by the lowest accuracy level since pollution is estimated on a national scale starting from representative emission values. Their low level of detail makes Tier 1 procedures totally unsuitable for an accurate comparison between a conventional and a hybrid-electric powertrain.

Tier 2 methods represent a slight improvement in the evaluation of pollutant emissions but they are suitable just for an approximate national estimation. The overall number of movements inside each airport per aircraft type is known, allowing for an estimation based on airplane-specific LTO emission factors.

Though characterized by larger accuracy, even Tier 2 models are limited to a national context for the estimation of pollutant emissions in cruise, which are still computed on the basis of national fuel sales. This makes Tier 2 approaches unsuitable for a complete aircraft-specific comparison extended to all flight phases.

A more detailed computation of the emissions relative to an entire airplane movement is achieved with Tier 3 methodologies as they are based on the use of aircraft-specific emission factors for what

concerns both the LTO cycle and the CCD phases.

Since the focus is on the amount of pollutants discharged in every flight phase, Tier 3 approaches are particularly indicated for a comparison between conventional and hybrid-electric power-trains.

The key difference between Tier 3A and Tier 3B procedures is basically linked to the way in which emissions are computed since the former are based on representative transit times, while the latter rely on full flight trajectory information and possibly implement sophisticated numerical algorithms for pollutant dispersion.

4.2 Segmentation of flight trajectory

The procedure for the modelling of flight trajectory represents the distinguishing feature for the method classification inside Tier 3A or Tier 3B category. A more refined definition of aircraft flight path implies a more accurate estimation of the transit times, leading to a more likely evaluation of pollutant emissions.

Tier 3A approaches substantially refer to the Master emission calculator, a spreadsheet provided by EEA for the estimation of LTO and cruise emissions.

As for the former, the mass of pollutants emitted in take-off, climb and approach are computed on the basis of the corresponding transit times of Table 2.1. Though taxi-in and taxi-out times are allowed to vary according to the airport of interest, the values of the other three phases correspond to the symbolic LTO cycle defined by ICAO in the Annex 16, Volume II.

Since this document focuses just on the certification of turbojet and turbofan engines, a more appropriate modelling of LTO phases needs to be considered for general aviation piston-engine airplanes.

Looking at the instruments in possession, a significant improvement in flight path definition is achieved when the same segmentation procedure outlined in ECAC Doc. 29 is applied even to the prediction of atmospheric pollution.

Similarly to the acoustic analysis, the departure and arrival trajectories are subdivided into a finite number of segments, each contributing to the overall pollutant emissions. In this way, the quantification of pollutant emissions in the LTO cycle is not limited by fixed time values, but the time spent in each flight phase varies according to the aircraft under consideration.

Going back to equation 3.4, the interpolation formulas for airspeed estimation implicitly assumes a linear dependence of velocity with time. Therefore, the hypotheses of constant acceleration can safely be adopted for the computation of the time spent in the i-th segment (t_i) through the simple formula

$$t_i = \frac{2d_i}{V_i + V_{i+1}}, \tag{4.1}$$

where d_i corresponds to the segment length, while V_i and V_{i+1} are the true airspeed values at the two segment ends.

No specific trajectories are defined for hybrid-electric aircraft, which is supposed to follow exactly the same route as the conventional airplane; in this way, pollution results are independent on the modelling of aircraft flight path.

A more accurate estimation thanks to a consolidated trajectory definition makes the prediction model perfectly compliant with Tier 3B category, to which all the most important pollution prediction methods belong. Unlike other more sophisticated Tier 3B approaches like the French

IESTA or the EUROCONTROL Open-ALAQS, this new model does not implement any equation for pollutant dispersion since the interest is just on a comparison in terms of overall emitted mass and social cost.

4.3 Choice of the emission indices

A relevant quantity in all procedures outlined by EEA is represented by the emission index ($I_{j,k}$), representing the mass of the k-th pollutant emitted per amount of fuel burnt along the j-th flight phase. Technically speaking, this parameter does not depend just on the engine model, but also on all those factors affecting the combustion reaction inside the chamber, like the engine age, the number of on/off cycles, the chamber configuration and the injectors wear.

However, pollution calculations inside the two EEA spreadsheets are not very accurate for general aviation piston-engine airplanes, which represent just a small part of the overall aeronautical operations. The emission indices and fuel flows inside these two programs are indeed obtained from a study performed by the Swiss FOCA on a restricted number of internal combustion engines.

The need for pollution data covering a wider range of engines is perfectly satisfied by the ACRP Research Report 164 by Yacovitch et al. [135], who also focused on the emission variability resulting from pilot's philosophy about fuel mixture.

The most interesting results of this database concern the values of the fuel flow and of the emission indices, which refer to carbon monoxide, unburned hydrocarbons and the oxides of nitrogen. No factor is assigned to carbon dioxide since its emissions are computed according to the carbon content of AVGAS 100 LL, for which a coefficient equal to 3.067 grams of CO_2 per gram of fuel is assumed.

Moreover, the database provided by ACRP is arranged in quite an interesting way as the results are not only provided for each of the 47 ground tests but have also been collected and averaged for each engine family. Accordingly, the table of single results is consulted if the engine of the aircraft under consideration was tested, otherwise the value of the engine family is used.

Another interesting analysis performed by the ACRP research team concerns the influence of ambient conditions on the emission indices typical of naturally aspirated piston engines. While no systematic effects were observed within the range of barometric pressures, more interesting results were obtained for the dependence on outside temperature.

In particular, the authors found a quite good agreement with the correlations

$$\begin{aligned} I_{CO}(T) &= I_{CO}(T_0) + 3.1259(T - T_0) \\ I_{UHC}(T) &= I_{UHC}(T_0) + 0.0164(T - T_0) \end{aligned} \tag{4.2}$$

introduced by FOCA in the appendix 5 of its report [140], where reference conditions are indicated with the subscript 0.

The emission indices of unburned hydrocarbons (I_{UHC}) and carbon monoxide (I_{CO}) are expected to linearly vary temperature (T) according to a coefficient which is sensibly lower for UHC. This is basically connected to the typical emission values, which are much higher for carbon monoxide than for unburned hydrocarbons.

No temperature variation is instead expected for fuel flow and the oxides of nitrogen, nor for turbocharged internal combustion engines.

In relation to flight trajectory, the temperature at each segment end can be obtained from its altitude after the application of the ISA model. The segment temperature exploited for the

correction of the emission indices is supposed to coincide with the average of the two end values, as a result of the linear dependence expressed in equation 4.2.

4.4 Definition of the flight phases

Theoretically, the modelling of flight trajectory according to the directives suggested by ECAC even results into the knowledge of thrust or rpm fraction at the two ends of each segment. The ACRP Research Report 164 by Yacovitch et al. relates each emission index to a precise rotational speed and fuel flow, which is expected to linearly vary with thrust.

Accordingly, both the emission indices and the fuel flows could in principle be corrected on the basis of the thrust or rpm value at the two segment ends for a more accurate pollution estimation.

However, a correlation for the emission index variation with respect to thrust or rotational speed is extremely difficult to be established, above all in relation to aviation piston engines. The possibility to act on the throttle and mixture levers allows these machines to provide the same thrust or run at the same rotational speed for different air/fuel ratios, resulting into distinct emission indices.

Consequently, a simpler, though less accurate, method is introduced for the assignment of the emission index and fuel flow to each segment.

It is important to recall that the database by Yacovitch et al. substantially refers to five different in-flight phases, namely take-off, climb-out, cruise, approach and final approach; the taxi and idle settings are instead related to ground operations, which are not considered in the present analysis.

Going back to trajectory definition, the power value at each segment end is computed according to the information contained in the ANP database: both the departure and arrival flight profiles can be either given as a sequence of points or computed on the basis of default procedures.

The simplest case corresponds to the departure profiles defined in terms of procedural steps since a thrust rating is assigned to each take-off, climb or acceleration segment: in all those segments where maximum thrust is applied, take-off fuel flow and emission indices are used, while climb-out values are exploited in case of maximum climb thrust.

No information on power setting is instead provided for departure profiles defined as a sequence of points, but the thrust or rpm value is known at each trajectory point: the instants when power changes are identified and take-off values are assigned to the highest rating, climb-out to the lowest.

As for arrival instead, thrust setting is defined neither for the procedural nor for the fixed-point profiles and the distinction between approach and final approach is itself not clear. For this reason, the final approach fuel flow and emission indices are selected for ground segments and the last airborne step, while the other in-flight sections fall under the approach case.

4.5 Estimation through the social cost

The procedure outlined in the previous paragraphs allows for an accurate estimation of the pollutant mass emitted in each flight segment as a result of the combustion process inside the engine.

Even without looking at the typical values, it is evident that the emissions of carbon dioxide are by far larger than the other pollutants since CO_2 is a primary product in the combustion reactions of all hydrocarbon fuels. For this reason, a comparison between the different pollutants in terms of mass is absolutely a nonsense and a different unit of merit needs to be chosen.

Moreover, the knowledge of pollutant mass is not sufficient for the estimation of the effects on human health since a kilogram of CO_2 can be less dangerous than a gram of a more harmful quantity like NO_x.

Both problems are solved when the emissions of the k-th pollutant are expressed in terms of social cost (C_k) according to the simple formula

$$C_k = €_k m_k. \tag{4.3}$$

In this way, the impact towards the population is expressed in more practical terms as it is related to a sort of cost the human beings have to pay as a result of aircraft operation. For the sake of simplicity, the social cost is shown to be proportional to the pollutant mass (m_k) according to a coefficient dependent on the chemical substance under consideration ($€_k$).

Focusing on the pollutants of the present study, these coefficients, given in Table 4.1, are obtained from a study performed by Lu on Taiwan airport [141].

Pollutant	**Social cost per unit mass [€/kg]**
CO_2	0.035
CO	0.09
UHC	4.47
NO_x	10.05

Table 4.1: Social cost coefficients per unit of pollutant mass [141]

It is evident that the lowest values belong to the least dangerous chemical substances like carbon monoxide and dioxide, while the most tremendous potential on human health is typical of unburned hydrocarbons and of the oxides of nitrogen in particular. The coefficient specific to these two classes of pollutants is at least two orders of magnitudes larger than the ones related to carbon monoxide and dioxide.

Moreover, the prices are expressed according to the value the Euro assumed in 2008 and the CPI Inflation Calculator suggests a multiplication of 1.1397 of all coefficients in order to express them in accordance with the actual Euro value.

The following chapter will exploit the method for pollutant emissions in the attempt to perform two different quantitative analyses.

In a first stage, the investigation will focus on the power management issues typical of any hybrid-electric power-train. The emissions in terms of mass and social cost will be computed for each leg of Bresso pattern and seven different operational modes will be considered.

In the second part, the prediction model will be applied for a direct emission comparison between a Cessna 172R Skyhawk, a conventional Panthera and a Panthera Hybrid.

Chapter 5

Application studies

The methods for the prediction of acoustic and atmospheric pollution are eventually applied to both hybrid-electric and conventional aircraft for a comparative analysis between the two propulsive technologies.

Environmental effects are studied with reference to Bresso airport, a General Aviation aerodrome located northwest of Milan at an altitude of 484 ft above mean sea level. In this aerodrome, most takeoffs and landings are performed along the southern direction and the proximity to Linate airport imposes strict altitude limits inside Bresso ATZ and working area. A maximum altitude of 1500 ft AMSL is prescribed for all departure procedures, while arrivals are limited to 2000 ft AMSL.

Moreover, the presence of Linate CTR east of the runway implies a western traffic pattern, which is used as a reference condition for all environmental studies. As an example, Figure 5.1 refers to the standard circuit of a Cessna 172R Skyhawk at Bresso airport, limited to a maximum altitude of 1000 ft AGL.

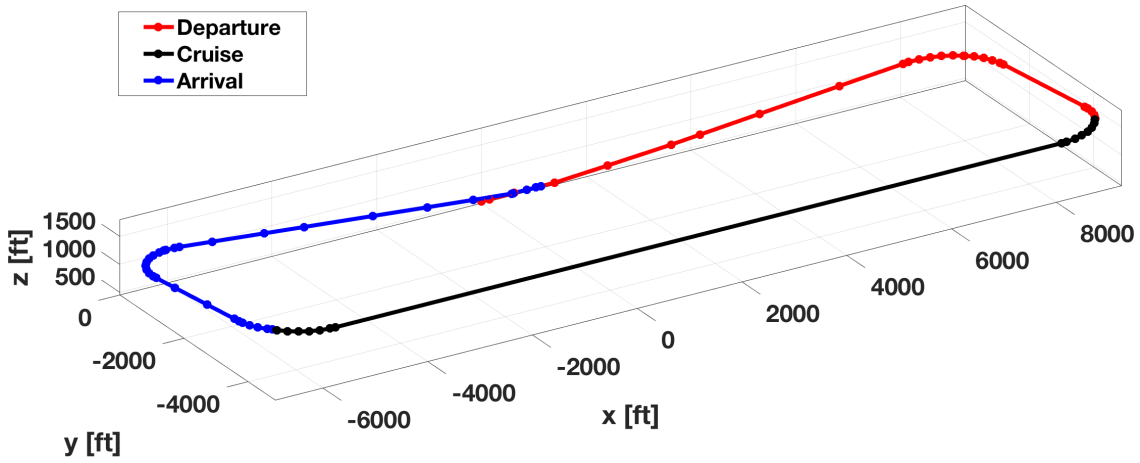

Figure 5.1: Circuit pattern of Cessna 172R Skyhawk at Milan Bresso airport

In general, each pattern is assumed to include three different movements, namely departure, cruise and arrival. As for the former, the take-off and climb phases are supposed to encompass all points going from brake release to the limit altitude of 1484 ft AMSL. The cruise part encloses all segments at maximum altitude, while arrival goes from the start of descent up to the end of ground deceleration.

Thanks to this trajectory subdivision, every flight phase is considered in the evaluation of acoustic and atmospheric effects, with the advantage of confining the study area in a small region around the airport.

The analyses on noise and pollutant emissions start from the investigation of the environmental effects connected to power management. Without looking at the real Panthera Hybrid operation, the study refers to hypothetical hybrid-electric aircraft equipped with battery packs capable of replacing the internal combustion engine in every flight phase. According to the circuit legs in which the electric mode is activated in lieu of the ICE, different effects are produced since battery contribution is evidently null in both acoustic and atmospheric terms.

The investigation of power management is applied to two radically different airplanes, namely Cessna T206H Stationair and Piper PA-31-350 Navajo Chieftain. The former is a six-seater high-wing aircraft featuring a single turbocharged engine capable of providing up to 310 horsepowers; its maximum speed is fixed at 178 kt and has a MTOW of 3600 lb. Instead, Piper PA-31-350 Navajo Chieftain is a low-wing airplane with two turbocharged piston engines rated at 350 hp each; its speed is limited to 225 kt and its maximum take-off weight is equal to 7000 lb, almost twice the T206H value.

The second part of the environmental studies is instead devoted to a more practical comparison between conventional and hybrid-electric power-trains as it refers to real airplanes and considers actual engine activation. In particular, the focus is on a comparison between a Cessna 172R Skyhawk, a conventional Panthera based on the Lycoming IO-540-V motorization, and the Panthera Hybrid at the centre of the MAHEPA project.

Cessna 172R Skyhawk has been chosen as a reference since it belongs to the most widespread family of General Aviation airplanes and has similar design characteristics with respect to Panthera. Its trajectory is modelled according to the directives of ECAC Doc. 29 and assigned even to the conventional and hybrid-electric Panthera versions.

In this way, the comparison among the three airplanes is strictly focused on their specific emission properties and not on the actual aircraft trajectory.

5.1 Analysis of acoustic emissions

In general, the investigation of noise effects essentially consists in the calculation of the sound exposure level perceived by a set or a grid of ground sensors.

Focusing on the single receptor, the acoustic emissions relative to a departure, arrival or pattern movement are computed through the combination of the different segment contributions thanks to equation 3.2.

The sound exposure relative to the single trajectory portion is then estimated on the basis of reference NPD data, computed according to the source blending method even for the aircraft covered in the ANP database. The noise comparison would have been a nonsense if the baseline noise levels were obtained through the source blending method for the hybrid-electric and from the ANP database for conventional aircraft.

As mentioned in the previous introductory part, the entire analysis is centred on the typical traffic pattern at Milan Bresso airport, distinguished into the departure, cruise and arrival phases.

As for the first and the last, the computation of sound exposure relative to each segment is quite straightforward since the NPD data are clearly distinguished into the departure and arrival values.

Acoustic estimation is instead more demanding in the cruise phase, which is usually neglected for its high altitudes. In particular, the sound exposure relative to the j-th cruise segment ($L_{E,j}$) is computed as if it were part of both the departure ($L_{E,d,j}$) or arrival ($L_{E,a,j}$) flight path. The two results are then combined through the interpolation formula

$$L_{E,j} = 10 \log_{10} \left[10^{\frac{L_{E,d,j}}{10}} + \frac{D_j}{S_c} \left(10^{\frac{L_{E,a,j}}{10}} - 10^{\frac{L_{E,d,j}}{10}} \right) \right], \tag{5.1}$$

where the length of the cruise phase (S_c) is put in relation to the distance between the segment midpoint and the departure end (D_j).

In this way, the contribution of each segment results from a balance between departure and arrival values according to the segment position inside the entire cruise stage.

5.1.1 Sound exposure dependence on the power-train operational mode

The first part of the acoustic study is specifically devoted to the influence of power management on the sound exposure level recorded by a set of ground receptors.

This analysis is based on a Cessna T206H Stationair and a Piper PA-31-350 Navajo Chieftain, two different aircraft for which the application of the source blending method has proven to be successful, as shown in Appendix A.

The accurate investigation of power management issues implies a hybrid-electric retrofit of these airplanes in which the power coming from either the batteries or the ICE is exploited by an electric motor to drive the propeller.

Besides the noise data already developed for the conventional mode, a new set of sound exposure levels is created for the all-electric operation, simply by excluding the noise coming from the internal combustion engine. No additional contribution is considered for the electric motor, whose effects can safely be neglected, as evidenced in Section 3.2.7.

The standard traffic pattern at Bresso airport is split into its five typical legs and the sound level meters are located directly on the ground track according to the arrangement outlined in Figure 5.2, which refers to the same frame of reference as the one suggested by ECAC.

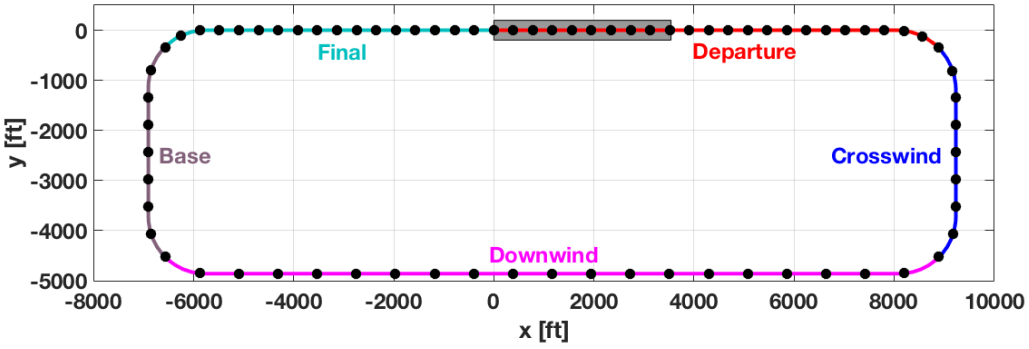

Figure 5.2: Sensor locations in the five pattern legs at Milan Bresso airport

Besides brake release, the separation of the different legs is determined by the four midpoints of each turn, where a power commutation can instantaneously occur from the conventional to the electric mode or viceversa; all on-off transients are indeed neglected since engine noise is not known in these conditions.

The sensor arrangement, which is schematically presented in Table 5.1, basically results from a compromise since a high number of receptors implies more accurate noise estimation, but at the same time leads to a dramatic increase in computational cost.

Leg	**Length [ft]**	**Number of sensors**	**Distance between sensors [ft]**
Departure	8 990	24	391
Crosswind	4 360	9	545
Downwind	15 660	21	783
Base	4 370	9	546
Final	6 670	18	392

Table 5.1: Sensor arrangement along the pattern ground track

Departure and final legs are related to the largest altitude changes and the sound exposure values are supposed to undergo substantial variation along them. For this reason, the maximum distance between two consecutive microphones is fixed at 400 ft, resulting into 24 sensors in the departure leg, 18 along the final one.

Aircraft altitude and power do not significantly vary along the crosswind and base legs, for which a maximum receptor distance of 600 ft is imposed. A limit of 800 ft is instead established for the receptors belonging to the downwind leg: no significant exposure variations are expected along this circuit portion since altitude is constrained at the limit value of 1000 ft AGL.

Besides the conventional and the all-electric operation, the analysis considers five intermediate cases corresponding to the most relevant and practical solutions for power management. For the sake of a lighter notation, each of these modes is named with a number according to Table 5.2.

Legs of ICE activation	**Identificative number**
All legs	1
Departure-crosswind	2
Departure-crosswind-downwind	3
Downwind	4
Downwind-base-final	5
Base-final	6
All-electric	7

Table 5.2: Identification of the operational modes

As it is impractical to provide the sound exposure value for each of the 76 sensors in the seven different cases, the average sound exposure along each circuit leg ($\overline{L_E}$) is introduced as

$$\overline{L_E} = 10 \log_{10} \left(\frac{\int_{s_1}^{s_2} 10^{\frac{L_E(s)}{10}} ds}{s_2 - s_1} \right). \tag{5.2}$$

Since the direct summation of sound levels can not be performed, the procedure starts from the conversion of sound exposure ($L_E(s)$) in energetic terms. A line integral of the resulting quantities is computed from s_1 to s_2, the arc lengths of the two points limiting the leg under consideration. The result is averaged on the length of the leg and then reconverted back in sound level terms.

Tables 5.3 and 5.4 refer to the average sound exposure obtained for Cessna T206H Stationair and Piper PA-31-350 Navajo Chieftain. For each of the seven operational modes, the results are provided along the five circuit legs and the entire pattern as well: for convenience, the departure leg is indicated with DP, the crosswind with CW, the downwind with DW, the base with BS and the final with FN.

ID	**DP [dB]**	**CW [dB]**	**DW [dB]**	**BS [dB]**	**FN [dB]**	**Overall [dB]**
1	93.18	83.22	78.82	76.22	88.92	88.15
2	93.15	83.02	76.44	74.39	88.68	87.99
3	93.16	83.22	78.79	74.82	88.69	88.08
4	90.22	80.45	78.48	74.79	86.21	85.43
5	90.26	80.45	78.52	76.20	86.62	85.55
6	90.26	80.06	75.97	75.89	86.61	85.38
7	90.22	80.06	75.91	74.36	86.20	85.25

Table 5.3: Average sound exposure relative to Cessna T206H Stationair

ID	**DP [dB]**	**CW [dB]**	**DW [dB]**	**BS [dB]**	**FN [dB]**	**Overall [dB]**
1	97.25	87.83	83.19	80.30	91.72	92.03
2	97.22	87.69	80.66	78.66	91.33	91.83
3	97.22	87.83	83.17	78.99	91.34	91.94
4	93.68	85.01	82.96	78.97	88.84	88.87
5	93.75	85.01	82.99	80.29	89.49	89.05
6	93.75	84.73	80.34	80.04	89.47	88.83
7	93.67	84.73	80.29	78.64	88.82	88.65

Table 5.4: Average sound exposure relative to Piper PA-31-350 Navajo Chieftain

Looking at the results in their totality, the overall sound exposure levels of T206H are in average 3.62 dB lower than the PA-31 values. This variation is basically related to the different aircraft

size, as confirmed by the two maximum take-off weights of table 3.4. The double MTOW of PA-31 reflects into larger wing and tail surfaces, into a bigger landing gear and into a double engine and propeller, all factors contributing to an increment in acoustic emissions.

Focusing on sound exposure variation along the pattern, the highest values are relative to the microphones located along the departure and final legs.

A first significant contribution is related to the low aircraft altitudes, which limit the effects of sound spreading. In addition, the high intensity of take-off power not only influences the departure average levels, but also affects the sound exposure perceived by the final-leg microphones closer to the runway.

Considering the two extreme modes in order to exclude the effects of power commutation, the average difference between departure and final values is equal to 4.14 dB for Cessna T206H Stationair and to 5.19 dB for Piper PA-31-350 Navajo Chieftain.

After departure and final legs, the highest sound exposures belong to the crosswind portion as it is characterized by intermediate altitudes and high power settings. The average exposure difference with respect to departure values is fixed at 10.06 dB for T206H, at 9.18 dB for PA-31.

The lowest sound levels are instead relative to downwind and base legs as in the former the airplane is at the maximum distance from ground, while the combination of intermediate altitudes with low power settings makes base values drop. In this case, the difference between downwind and base exposures does not depend on the aircraft but on the operational mode: an average discrepancy of 1.60 dB is found for the all-electric (7), while the all-ICE mode (1) is characterized by a 2.75 dB difference.

Going into the details of the seven activation cases, it is evident that the lowest sound exposures are relative to the all-electric mode (7), while the highest values refer to the entire circuit performed with the ICE activated (1).

As for the five intermediate cases, the average sound exposure in a certain leg practically collapses to the all-electric value when power is provided by the batteries, to the all-ICE case when piston engine is activated.

The overall results basically come from the combination of this behaviour with the average sound exposure registered in the two extreme operational modes. The ICE activation along the departure leg is therefore the key factor for the overall sound exposure since the noise levels are the highest in this circuit portion.

This is confirmed by the minimum discrepancy among the all-ICE (1), the departure-crosswind (2) and the departure-crosswind-downwind (3) modes. The same is true for the other four cases because the downwind (4) and base-final (6) exposures are extremely close to the all-electric (7) values and an average discrepancy of 0.15 dB distinguishes the downwind-base-final (5) from the downwind (4) activation.

A second different analysis attempts to expand the horizon by looking at what happens across a grid of receptors surrounding Milan Bresso airport. In this way, the map of sound exposure in the aerodrome area can be traced for each of the seven different modes in order to investigate the noise effects on a broader scale.

Considering the same frame of reference as the previous analysis, the domain of interest includes the x values going from -15000 ft to 15000 ft and expands from -10000 ft to 5000 ft along the y direction. Naturally, sensor resolution can not be the same as the previous study as it would imply a too large computational cost: accordingly, a sound level meter is placed every 1000 ft in both directions for an overall number of 496 receptors.

The computation of sound exposure in each of these microphones allows for the tracing of noise emission maps, which are presented in Appendix B for each of the seven activation modes.

Though being very effective from a visual point of view, the sound exposure contours around an airport are not very useful, particularly when a comparison between different cases is meant to be performed.

An important way to describe noise contours in quantitative terms results from the computation of the area enclosed by the most significant emission lines. Tables 5.5 and 5.6 provide the values of the area internal to the k-th sound exposure contour, indicated with the notation A_k and expressed in ft^2.

ID	$\mathbf{A}_{70}$	$\mathbf{A}_{75}$	$\mathbf{A}_{80}$	$\mathbf{A}_{85}$	$\mathbf{A}_{90}$	$\mathbf{A}_{95}$	$\mathbf{A}_{100}$
1	$2.1 \cdot 10^8$	$1.2 \cdot 10^8$	$4.4 \cdot 10^7$	$9.8 \cdot 10^6$	$2.8 \cdot 10^6$	$7.4 \cdot 10^5$	$8.8 \cdot 10^4$
2	$1.8 \cdot 10^8$	$8.9 \cdot 10^7$	$3.8 \cdot 10^7$	$9.6 \cdot 10^6$	$2.7 \cdot 10^6$	$7.2 \cdot 10^5$	$8.4 \cdot 10^4$
3	$2.0 \cdot 10^8$	$1.1 \cdot 10^8$	$4.3 \cdot 10^7$	$9.7 \cdot 10^6$	$2.7 \cdot 10^6$	$7.2 \cdot 10^5$	$8.5 \cdot 10^4$
4	$1.8 \cdot 10^8$	$9.4 \cdot 10^7$	$2.4 \cdot 10^7$	$4.7 \cdot 10^6$	$1.4 \cdot 10^6$	$2.6 \cdot 10^5$	
5	$1.9 \cdot 10^8$	$1.0 \cdot 10^8$	$2.5 \cdot 10^7$	$4.7 \cdot 10^6$	$1.4 \cdot 10^6$	$2.7 \cdot 10^5$	
6	$1.7 \cdot 10^8$	$7.6 \cdot 10^7$	$2.1 \cdot 10^7$	$4.7 \cdot 10^6$	$1.4 \cdot 10^6$	$2.7 \cdot 10^5$	
7	$1.6 \cdot 10^8$	$7.0 \cdot 10^7$	$2.0 \cdot 10^7$	$4.6 \cdot 10^6$	$1.4 \cdot 10^6$	$2.5 \cdot 10^5$	

Table 5.5: Sound exposure areas relative to Cessna T206H Stationair

ID	$\mathbf{A}_{70}$	$\mathbf{A}_{75}$	$\mathbf{A}_{80}$	$\mathbf{A}_{85}$	$\mathbf{A}_{90}$	$\mathbf{A}_{95}$	$\mathbf{A}_{100}$	$\mathbf{A}_{105}$
1	$2.6 \cdot 10^8$	$1.8 \cdot 10^8$	$9.4 \cdot 10^7$	$2.6 \cdot 10^7$	$7.8 \cdot 10^6$	$2.4 \cdot 10^6$	$3.2 \cdot 10^5$	$3.6 \cdot 10^2$
2	$2.3 \cdot 10^8$	$1.6 \cdot 10^8$	$6.0 \cdot 10^7$	$2.4 \cdot 10^7$	$7.7 \cdot 10^6$	$2.3 \cdot 10^6$	$3.0 \cdot 10^5$	$1.9 \cdot 10^2$
3	$2.5 \cdot 10^8$	$1.7 \cdot 10^8$	$8.8 \cdot 10^7$	$2.6 \cdot 10^7$	$7.7 \cdot 10^6$	$2.4 \cdot 10^6$	$3.0 \cdot 10^5$	$2.0 \cdot 10^2$
4	$2.3 \cdot 10^8$	$1.6 \cdot 10^8$	$7.4 \cdot 10^7$	$1.3 \cdot 10^7$	$3.7 \cdot 10^6$	$6.1 \cdot 10^5$	$3.2 \cdot 10^4$	
5	$2.4 \cdot 10^8$	$1.7 \cdot 10^8$	$7.9 \cdot 10^7$	$1.4 \cdot 10^7$	$3.8 \cdot 10^6$	$6.6 \cdot 10^5$	$3.8 \cdot 10^4$	
6	$2.1 \cdot 10^8$	$1.4 \cdot 10^8$	$4.9 \cdot 10^7$	$1.3 \cdot 10^7$	$3.8 \cdot 10^6$	$6.6 \cdot 10^5$	$3.7 \cdot 10^4$	
7	$2.1 \cdot 10^8$	$1.4 \cdot 10^8$	$4.5 \cdot 10^7$	$1.2 \cdot 10^7$	$3.7 \cdot 10^6$	$6.1 \cdot 10^5$	$3.2 \cdot 10^4$	

Table 5.6: Sound exposure areas relative to Piper PA-31-350 Navajo Chieftain

The comparison between the two airplanes evidences that the lines corresponding to the largest exposures are 5 dB higher for PA-31 with respect to T206H.

This can be explained by looking at the maximum sound exposures, which are presented in Table 5.7 for the seven operational modes.

ID	**T206H [dB]**	**PA-31 [dB]**	**Δ [dB]**
1	102.91	105.17	2.26
2	102.89	105.13	2.24
3	102.89	105.13	2.24
4	99.90	101.58	1.68
5	99.95	101.68	1.73
6	99.94	101.68	1.74
7	99.90	101.58	1.68

Table 5.7: Maximum sound exposures

The average 3.62 dB difference outlined in the previous analysis is significantly reduced when maximum sound exposures are considered: an average discrepancy of 2.25 dB is indeed registered for the modes characterized by the largest levels, while a 1.71 dB deviation holds for the four least noisy cases.

Though not very high, such discrepancies are sufficient for a 5 dB step of the maximum exposure lines. Looking at the first three modes, the maximum of PA-31 emissions is just above 105 dB and the area enclosed by the 105 dB line is indeed very limited; since the T206H values are 2.25 dB lower, the line corresponding to maximum sound exposure is fixed at 100 dB for this airplane.

The opposite situation occurs in the last four cases where the T206H values are just 0.1 dB lower than 100 dB; the addition of the 1.71 dB difference makes PA-31 maximum exposures fall inside the range between 100 and 105 dB.

Focusing on the single aircraft, the largest enclosed areas naturally belong to the all-ICE mode (1), followed by the case where the engine is activated in the departure, crosswind and downwind legs (3).

An interesting behaviour affects the departure-crosswind mode (2) as it is the other situation in which maximum exposure overcomes 100 and 105 dB, but the enclosed region is not always larger than the value of the four least noisy cases.

Looking at the T206H results, the areas enclosed by the 80 dB line onwards are all larger than the values of the least noisy activations. However, the region surrounded by the 75 dB contour becomes smaller than the values corresponding to downwind (4) and downwind-base-final (5) activations; as for the 70 dB region instead, the area of the departure-crosswind mode is less extended than just the downwind-base-final (5) value.

As for PA-31, trend separation occurs at the 85 dB line, below which the enclosed region relative to the departure-crosswind case (2) is constantly lower than the downwind-base-final (5) area; as for the 80 dB line, the value of the departure-crosswind mode (2) is even lower than the one corresponding to downwind activation (4).

In both airplanes, such behaviour is strictly connected to what happens to the four modes relative to the lowest maximum exposures, for which an analogous inversion can be noticed.

The minimum areas are naturally relative to the all-electric mode (7), while the largest among the four cases belong to the downwind-base-final activation (5). As for the other two modes, in the A_{70}, A_{75} and A_{80} cases the larger areas constantly belong to the downwind activation (4), while the opposite situation occurs at the highest exposures.

5.1.2 Comparison of acoustic emissions for different aircraft

After the investigation of power management effects, a more practical acoustic comparison is performed on the basis of three similar airplanes currently under production, namely Cessna 172R Skyhawk, conventional Panthera and Panthera Hybrid.

Since the influence of ICE activation in the different pattern legs is not meant to be studied, it is possible to neglect the sensor arrangement along the ground track, outlined in Figure 5.2.

The sound pressure level is instead computed for the same grid of receptors considered in the second part of the previous analysis: the region around Milan Bresso airport is therefore subdivided into squares of side 1000 ft, with a sensor placed at each of the four vertices.

In general, the computation of sound exposure deriving from an aircraft movement is based on the definition of a segmented aircraft trajectory and on the creation of a set of NPD data according to the source blending method.

As for the former, the flight path definition in terms of airspeed, power and spatial coordinates is computed thanks to the directives of ECAC Doc. 29 and to the airplane performance characteristics given in ANP.

Since the two Panthera versions are not included in this database, their trajectory is assumed to coincide with the one of Cessna 172R Skyhawk. The three airplanes are characterized by similar design characteristics and the presence of limit altitudes at Bresso is likely to make the real trajectory differences negligible.

Moreover, the flight path coincidence among the three aircraft allows for an acoustic comparison based just on the noise-related issues and unaffected by trajectory differences.

The other important aspect is represented by the definition of a new set of NPD data on the basis of the average departure and arrival blending coefficients obtained according to the procedure outlined in Section 3.2.7.

A single set of sound exposure levels is produced for Cessna 172R Skyhawk and conventional Panthera, while the hybrid-electric version needs to consider the all-ICE and all-electric operations.

The series architecture of Panthera Hybrid implies that the propeller is always driven by the brushless Siemens e-Motor *SP150D*. The power trend with respect to rotational speed is assumed linear for this kind of machines, resulting into the coincidence between power and rpm fraction.

This aspect needs to be considered in the calculation of both sets of sound exposure levels, which therefore differ just by the activation of the internal combustion engine.

Since the real operating conditions are considered, the acoustic contribution of piston engine always needs to be considered for Cessna 172R Skyhawk and conventional Panthera; as for Panthera Hybrid instead, the Rotax 914 is activated just in cruise and designed to run always at maximum rpm.

A first important result of noise computation is represented by the emission maps, which are presented Figures 5.3, 5.4 and 5.5 for the three airplanes under consideration.

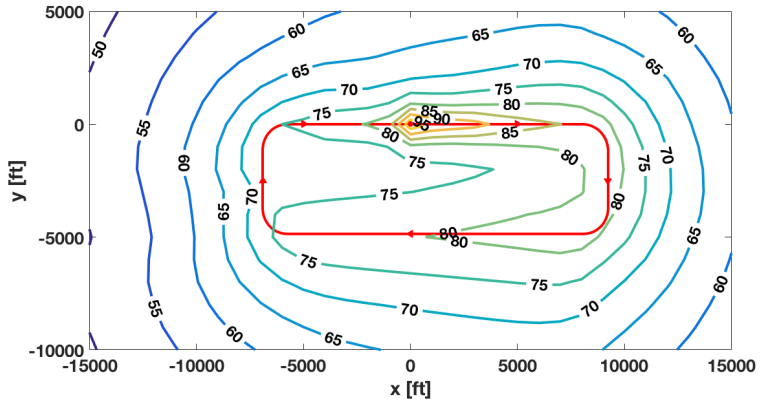

Figure 5.3: Sound exposure map relative to Cessna 172R Skyhawk

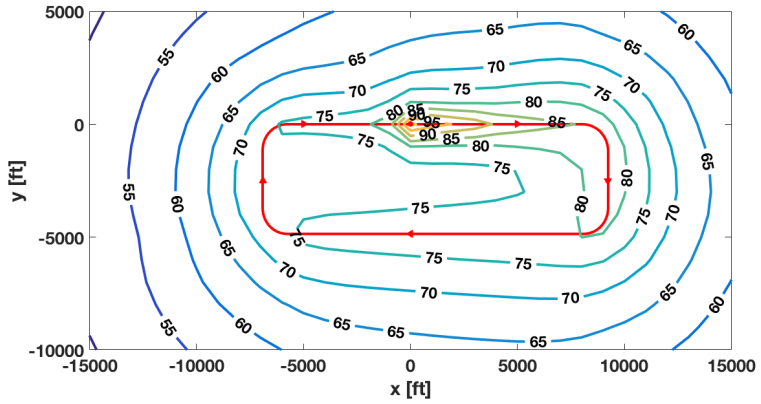

Figure 5.4: Sound exposure map relative to conventional Panthera

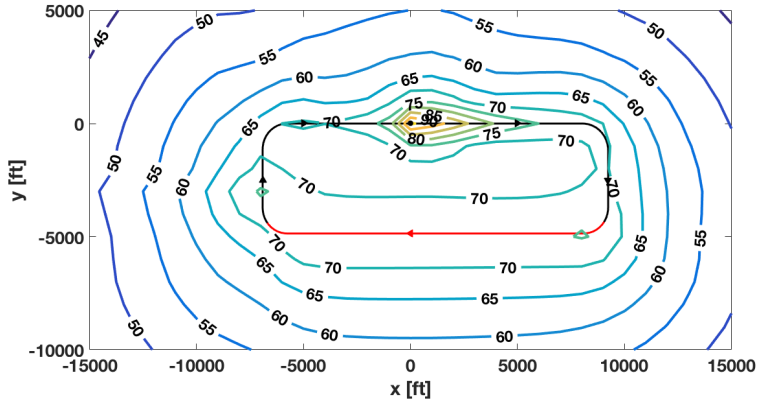

Figure 5.5: Sound exposure map relative to Panthera Hybrid

The three figures show the typical and natural stretch of the contour lines along the runway direction as a result of the rapid change in sound exposure occurring along the final and departure circuit legs.

As evidenced in the previous section, the largest sound exposures are relative to the departure leg since it is characterized by the highest power settings and the lowest distances between the aircraft and the ground.

Though featuring lower powers, even the sensors in the final leg are affected by high sound exposures, which are not so much related to the low aircraft altitude in approach, but rather depend on the vicinity to take-off segments.

In the crosswind leg, the aircraft is more distant to ground sensors, but power demand still keeps very high. On one side, the larger distances bring to lower sound exposures with respect to the values near the departure leg. On the other side, the high power demand reflects in larger exposures with respect to the values surrounding the initial part of the final leg, the one more distant to the runway.

Finally, the large distances typical of the downwind phase and the low powers of the base leg make these two circuit portions the least noisy ones.

Looking at the figures more in detail, no significant differences can be noticed in the departure and final legs between Cessna 172R Skyhawk and the conventional Panthera version. However, the different emission lines below 80 dB are much less expanded for conventional Panthera, which is a less noisy aircraft in the majority of domain points.

The most significant differences concern the sensors located near the downwind leg and the microphones inside the circuit, as evidenced by the 80 dB and the 75 dB lines.

As for the points surrounding the circuit, the sound exposure values external to the downwind leg are lower for conventional Panthera with respect to Cessna 172R Skyhawk; no great discrepancy is instead visible in the area outside the other four circuit portions.

The sound exposure levels relative to Panthera Hybrid are much lower than those of the two conventional aircraft, particularly for what concerns high-power legs.

Even in the hybrid-electric case, departure sensors are characterized by large exposures connected to the high power delivered to the propeller; however, the absence of piston engine noise is still responsible for a 5 dB decrement near the runway.

Moreover, it is interesting to notice that the sound exposure variation along the departure leg is more intense for Panthera Hybrid than for the other airplanes. This means that the absence of piston engine is not just responsible for a general noise decrement, but also affects the sound exposure rate of decay.

Furthermore, the activation of the internal combustion engine at maximum regime leads to the creation of a 70 dB band parallel to the downwind leg, which contrasts with the noise decay registered for the two conventional airplanes.

Another relevant aspect concerns the presence of two tiny regions near the points of engine start and shutdown, characterized by a sound exposure between 75 and 80 dB.

Looking at the area external to the circuit, Panthera Hybrid brings about an exposure decrement of at least 5 dB and a modification in the shape of noise contours, particularly on the side of the runway and of the 70 dB downwind band.

As previously done for the analysis on power management, Table 5.8 refers to the areas enclosed by the most significant emission lines for each of the three aircraft under consideration.

Aircraft	$\mathbf{A}_{70}$	$\mathbf{A}_{75}$	$\mathbf{A}_{80}$	$\mathbf{A}_{85}$	$\mathbf{A}_{90}$	$\mathbf{A}_{95}$	$\mathbf{A}_{100}$
Cessna 172R	$1.9 \cdot 10^8$	$1.1 \cdot 10^8$	$3.4 \cdot 10^7$	$6.2 \cdot 10^6$	$1.9 \cdot 10^6$	$2.5 \cdot 10^5$	
Panthera Conv.	$1.8 \cdot 10^8$	$9.0 \cdot 10^7$	$2.8 \cdot 10^7$	$7.4 \cdot 10^6$	$2.6 \cdot 10^6$	$6.0 \cdot 10^5$	$1.6 \cdot 10^4$
Panthera Hybr.	$7.9 \cdot 10^7$	$8.3 \cdot 10^6$	$4.1 \cdot 10^6$	$1.9 \cdot 10^6$	$5.5 \cdot 10^5$	$9.0 \cdot 10^3$	

Table 5.8: Comparison in sound exposure area

One of the most striking aspects is connected to the presence of sound exposures higher than 100 dB for conventional Panthera, which is also characterized by the largest enclosed areas from the 85 dB contour onwards. Looking at the emission maps, such discrepancy must be related to the take-off phase since exposures higher than 85 dB are registered just near the departure leg.

The main reason is linked to Dobrzynski's model for piston engine noise as it accounts just for maximum power and not for its actual value. The conventional Panthera version is equipped with a 260-hp Lycoming IO-540-V, which is much more powerful than the Lycoming IO-360-L2A mounted on Cessna 172R Skyhawk. This results into higher engine noise and larger exposure for conventional Panthera during take-off and climb, two phases in which engine contribution is relevant.

The areas relative to the lowest sound exposures are instead higher for Cessna 172R Skyhawk with respect to conventional Panthera, especially considering the 80 dB and the 75 dB lines, for which the same area ratio of 1.2 is registered. Looking at the emission maps, this discrepancy essentially concerns the first part of the downwind leg and must be related to the landing gear contribution to the overall aircraft noise.

Since engine power is not at its maximum value in cruise, the engine and propeller noise become comparable to the airframe contribution, which is mainly related to landing gear since wing noise is generally not high and flap deflection is assumed null. As for Panthera, landing gear retraction has been assumed in the generation of the NPD data used in this flight phase, while Cessna 172R Skyhawk is equipped with a fixed landing gear contributing to the difference in overall aircraft noise.

Focusing on Panthera Hybrid instead, the areas enclosed by the different emission contours are sensibly lower than the values of the two conventional airplanes.

There are still points at which sound exposure overcomes 95 dB, but the area they surround is two orders of magnitude smaller than the corresponding value of Cessna 172R Skyhawk and conventional Panthera.

The region inside the 90 dB and the 85 dB contours is three-times smaller for Panthera Hybrid with respect to Cessna 172R Skyhawk as a result of the different rate of decay in the departure leg. The area enclosed by the 85 dB line relative to Panthera Hybrid even equals the 90 dB value of Cessna 172R Skyhawk.

The comparison at the lowest exposures is instead performed with respect to the conventional Panthera version as it is characterized by lower values with respect to Cessna 172R Skyhawk.

Focusing on the 75 dB and the 80 dB contours, the enclosed region is one order of magnitude larger for conventional Panthera with respect to the hybrid-electric version. Since the aerodynamic and structural characteristics are evidently the same for the two aircraft, such behaviour is connected to the electric motor activation by means of batteries.

Finally, the 70 dB area relative to Panthera Hybrid is just 2.2 times smaller than the value of the conventional version as a result of the large 70 dB band on both sides of the downwind leg.

5.2 Analysis of atmospheric emissions

The second part of the application studies is specifically devoted to a comparative analysis on pollutant emissions thanks to the Tier 3B procedure outlined in Chapter 4. According to this method, the flight trajectory of any departure, arrival or circuit movement is subdivided into a finite number of segments, each contributing to the overall amount of pollutant discharge.

In particular, the mass of CO, UHC and NO_x produced in each segment is computed thanks to equation 2.2, while the emission of carbon dioxide is simply 3.067 times the fuel consumption.

The mass of each pollutant is finally converted into social cost in order to compare the different substances according to their effect on human health.

Unlike other more sophisticated computer programs, the prediction method introduced in the current work does not implement any diffusion model as it would imply a too large degree of complexity for a preliminary study. Moreover, what is mostly important in the prediction of atmospheric pollution is an estimation of the overall mass emitted per each species rather than the dispersion in the aerodrome area.

The scenario in which atmospheric analyses are performed is identical to the one chosen for noise investigation as it refers to a traffic pattern at Milan Bresso airport.

Differently from the acoustic study, pollution estimation in cruise is the most straightforward since the ACRP Research Report 164 provides the fuel flow values and the emission indices specifically related to this flight phase.

As for departure instead, the distinction between take-off and climb-out setting relies on the considerations made in Section 4.4, which are also exploited for the subdivision between approach and final approach conditions.

5.2.1 Pollutant mass dependence on the power-train operational mode

In parallel with the previous acoustic analysis, the first investigation is centred on the evaluation of the effects related to power management. Even in this phase, the study refers to a Cessna T206H Stationair and a Piper PA-31-350 Navajo Chieftain in order to extend the analysis to both single- and twin-engine propeller-driven aircraft.

Both airplanes are assumed to be retrofitted with a series hybrid-electric power-train in which battery packs are capable of perfectly replacing the ICE in all flight phases. Consequently, each of the five legs forming the traffic pattern at Milan Bresso airport is performed thanks to the power coming from either the emission-free batteries or the internal combustion engine.

The interest in quantifying the emitted mass rather than estimating its dispersion leads to an important modelling difference with respect to noise calculation.

In the acoustic analysis, the contribution of each trajectory portion is strictly dependent on the relative position between the segment and the microphone.

Since diffusion effects are not taken into consideration for atmospheric pollution, no ground sensors are considered, no distance issues hold and the pollution contribution coming from the single segment is fixed.

In particular, Tables 5.9 and 5.10 refer to the mass and cost emissions in each leg in case of ICE activation; results are provided per engine in order to have more meaningful comparative results between the two aircraft.

Leg	Mass [g]				Cost [€]			
	CO_2	CO	UHC	NO_x	CO_2	CO	UHC	NO_x
DP	3 884.7	1 320.1	35.5	6.8	0.155	0.135	0.181	0.078
CW	1 065.0	178.5	10.3	10.4	0.042	0.018	0.052	0.119
DW	3 714.4	622.5	36.0	36.3	0.148	0.064	0.183	0.416
BS	783.9	212.4	9.4	3.3	0.031	0.022	0.048	0.038
FN	1 578.2	467.6	19.3	4.3	0.063	0.048	0.098	0.049

Table 5.9: Single engine emissions relative to Cessna T206H Stationair

Leg	Mass [g]				Cost [€]			
	CO_2	CO	UHC	NO_x	CO_2	CO	UHC	NO_x
DP	3 330.6	1 168.5	30.3	4.1	0.133	0.120	0.154	0.047
CW	1 134.7	398.1	10.3	1.4	0.045	0.041	0.052	0.016
DW	2 566.6	445.6	24.8	24.4	0.102	0.046	0.126	0.279
BS	524.7	142.7	6.3	2.2	0.021	0.015	0.032	0.025
FN	1 196.2	354.3	14.6	3.2	0.048	0.036	0.074	0.037

Table 5.10: Single engine emissions relative to Piper PA-31-350 Navajo Chieftain

A general look at the departure, downwind, base and final legs shows that the emissions relative to T206H are higher than the corresponding PA-31 values. Apparently, this could show that the combustion reaction in T206H is less efficient than PA-31, resulting into a larger amount of pollutants produced per engine.

However, the two engines belong to the same family and are therefore characterized by identical fuel flow and emission index values. Consequently, the discrepancy in terms of emissions per engine must be related to the time spent by the aircraft in each of the four legs.

Both airplanes perform the very same pattern, but PA-31 is more powerful and the average velocity over the entire circuit is therefore higher than the T206H value; this implies average lower times, which eventually result into smaller emission values.

As for crosswind instead, different results are obtained since the T206H emissions are lower for what concerns CO_2, CO and UHC, while NO_x production is even 7.4 times larger. This behaviour is essentially related to the different aircraft trajectories as T206H reaches the maximum altitude before the beginning of the crosswind leg, while PA-31 is still climbing in this portion of the circuit.

Crosswind emission indices and fuel flows are therefore computed from the cruise values for T206H, from the climb-out ones for PA-31. In particular, the fuel flow and emission indices of CO and UHC are lower in cruise than in climb-out, while the NO_x index is maximum in the cruise phase.

Such peculiar trend is not seen in the other legs because the flight phase is the same for both airplanes along these circuit portions: departure leg is indeed performed at maximum power,

downwind is related to cruise phase, while approach and final approach conditions in the two terminal legs are characterized by similar values.

Naturally, the comparison between the two engines in terms of cost is not significant because the conversion factors of Table 4.1 are independent on the airplane.

Focusing on the single aircraft, the overall results depend on the three factors appearing in equation 2.2 and are therefore related to the time spent in each leg, to the fuel flow and to the emission index. It is important to remind that the fuel flows and emission indices are obtained from the ACRP Research Report 164, which refers to the take-off, climb-out, cruise, approach and final approach power settings.

Departure results are related to the largest fuel flow, which is responsible for a high CO_2 production and for a general increment in pollutant emissions. The large mass of CO as well as the low NO_x discharge are strictly connected to the take-off emission index, which is maximum for the former and minimum for the latter.

As for unburned hydrocarbons instead, the combination between a large fuel flow and a high emission index brings to significant UHC discharge. Moreover, their social cost is the highest one, while the lowest economic impact belongs to the oxides of nitrogen as they are produced in extremely small quantity.

No general considerations can be made for the crosswind phase since it is in one case more similar to the cruise downwind conditions, while it is more affected by the take-off indices and fuel flows for PA-31.

Cruise values are applied to both aircraft in the downwind leg, which is characterized by the highest time exposure as it is the longest portion of the pattern. Though fuel flow is lower in cruise than in take-off, the large time spent in the downwind leg leads to comparable CO_2 mass with respect to departure and brings about a significant discharge of carbon monoxide as well.

The combination of a high duration with the peak in the NO_x emission index implies a massive production of the oxides of nitrogen, which are almost six-times the departure value. The high discharge coupled with the largest social cost per unit mass brings to the highest economic impact among all pollutants and circuit portions.

As for the base and final legs, the fuel flow and emission indices are pretty much the same for the two phases since the typical values in approach and final approach are very close to each other. Therefore, the difference in terms of mass production are just related to the minor time spent in the base leg with respect to the final.

Fuel consumption in these two legs is extremely low, but in some cases the larger time spent in the final segment leads to higher emissions with respect to the peculiar crosswind values.

For each of the seven operational modes of the acoustic analysis, the mass of each pollutant is computed simply by summing the contributions relative to the legs where piston engine is activated since the other portions of the circuit are evidently emission-free.

As the focus is not on the single engine but on the airplane, the effective number of engines is considered and the results in terms of mass and social cost are presented in Tables 5.11 and 5.12; for a lighter notation, the same IDs of Table 5.2 are considered.

ID	CO_2 [g]	CO [g]	UHC [g]	NO_x [g]	Overall cost [€]
1	11 026.2	2 801.1	110.5	61.1	1.990
2	4 949.7	1 498.6	45.8	17.2	0.781
3	8 664.1	2 121.1	81.8	53.5	1.593
4	3 714.4	622.5	36.0	36.3	0.811
5	6 076.5	1 302.5	64.7	43.9	1.208
6	2 362.1	680.0	28.7	7.6	0.397
7	0.0	0.0	0.0	0.0	0.000

Table 5.11: Atmospheric pollution relative to Cessna T206H Stationair

ID	CO_2 [g]	CO [g]	UHC [g]	NO_x [g]	Overall cost [€]
1	17 505.6	5 018.4	172.6	70.6	2.901
2	8 930.6	3 133.2	81.2	11.0	1.217
3	14 063.8	4 024.4	130.8	59.8	2.325
4	5 133.2	891.2	49.6	48.8	1.108
5	8 575,0	1 885.2	91.4	59.6	1.684
6	3 441.8	994.0	41.8	10.8	0.576
7	0.0	0.0	0.0	0.0	0.000

Table 5.12: Atmospheric pollution relative to Piper PA-31-350 Navajo Chieftain

Apart from the all-electric mode, which is emission-free, the tables evidence that PA-31 is characterized by highest emissions with respect to T206H as a consequence of the double number of engines.

The only exception is represented by the NO_x emission in the departure-crosswind case, which is essentially related to the peculiar crosswind trend previously evidenced.

The largest amount of pollutants discharged by PA-31 implies higher overall costs per flight even in the departure-crosswind case: though characterized by the largest social cost per unit mass, the 6.2 g difference in NO_x emissions is not sufficient to determine a higher social cost for T206H.

Focusing on the seven different modes, it is clear that the conventional power-train configuration corresponds to the most harmful condition.

One of the most significant results is relative to the downwind phase (4) as it is characterized by very low CO_2, CO and UHC emissions, while it is the most dominant contributor to the overall NO_x production in conventional mode (1). The average contribution to the overall pollutant emissions is indeed equal to 20% for CO, to 30% for CO_2 and UHC, while the 65% of NO_x production is relative to the downwind leg.

Since the oxides of nitrogen have the most tremendous potential on human health, the social cost of the downwind mode is so high to be the main contributor to the cost of all-ICE operation.

A confirmation of this lies in the large social cost related to the other two operational modes featuring the engine activation in the downwind leg: the departure-crosswind-downwind sequence (3) implies a higher social cost with respect to the downwind-base-final case (5) since the larger power settings of the former bring to a more massive amount of pollutants, which in turn translates into higher social costs.

The peculiar behaviour in the crosswind leg leads to two different results in terms of overall cost since the departure-crosswind activation (2) is more harmful than the downwind (4) for PA-31, while the opposite situation is encountered for T206H.

Apart from the all-electric mode, the least severe condition corresponds to the activation of the internal combustion engine in the base and final legs (6), whose overall cost is half of the least harmful among the other five operational sequences.

5.2.2 Comparison of atmospheric emissions for different aircraft

The second part of the acoustic and environmental analyses compares a real hybrid-electric aircraft with two conventional airplanes.

In analogy with the acoustic study, the inquiry is centred on Panthera Hybrid, the airplane at the basis of the MAHEPA project. It features a series power-train architecture where the propeller is driven by an electric motor, powered by either the batteries, the piston engine or any combination of the two.

The development of this airplane has been based on a conventional version, representing one of the two aircraft with which Panthera Hybrid is compared.

Since trajectory definition needs to consider an existing airplane covered in the ANP database, Cessna 172R Skyhawk is selected because it has approximately the same size as the two Panthera versions and allows for a comparison between Panthera and the most common family of General Aviation airplanes.

Compliance with the acoustic analysis even implies the reference to an identical scenario, represented by the standard traffic pattern at Milan Bresso airport.

The first important step for the computation of atmospheric emissions is related to aircraft trajectory, which is segmented according to the equations and guidelines provided in ECAC Doc. 29.

Since the two Panthera versions are not included in ANP, their flight-profile is assumed to coincide with the one of Cessna 172R Skyhawk. No alternative solutions exist but trajectory coincidence at least allows for a pollution estimation depending just on engine characteristics and power management.

The computation of the overall emissions deriving from a complete circuit movement is quite straightforward for the two conventional airplanes since the engine contribution is present in all trajectory segments.

As for Panthera Hybrid instead, the internal combustion engine is activated just in the cruise phase, which basically coincides with the downwind leg, as evidenced in Figure 5.1.

When piston engine is activated, take-off emission indices and fuel flows are considered since full engine power is exploited for propeller motion and possibly battery recharge.

The departure and arrival phases are instead performed in all-electric mode and therefore are totally emission-free.

The overall amount of pollutants emitted during a standard traffic pattern is computed for each of the three aircraft, whose emissions are compared in Figure 5.6; since the mass comparison between the different pollutants is useless, a diagram is considered for each of the four species.

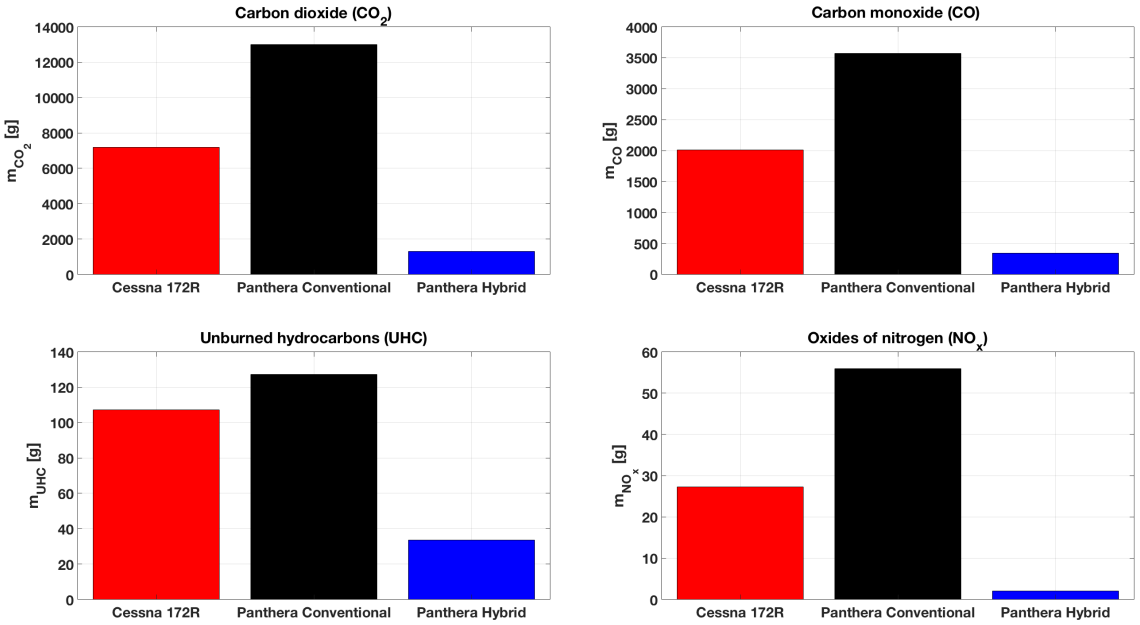

Figure 5.6: Emission comparison in terms of mass

All diagrams clearly evidence the dramatic reduction in pollutant emissions thanks to the adoption of hybrid-electric propulsion.

On one side, this relevant benefit derives from all-electric departure and arrival operations, resulting from piston engine activation just in the cruise phase.

Moreover, a hybrid-electric power-train with an emission-free take-off allows for the installation of a less powerful engine, which is characterized by lower fuel flow values and consequently lower emissions.

The fuel flow and emission dependence on power is also responsible for the discrepancy between Cessna 172R Skyhawk and conventional Panthera: the former is indeed equipped with a 160-hp engine, while the latter features a Lycoming IO-540-V capable of providing up to 260 horsepowers.

The fuel flow differences between the three airplanes are particularly visible in the first subfigure, connected to the production of carbon dioxide: since the emission index is fixed at 3.067 g_{CO_2}/g_F and the transit times are the same because of trajectory coincidence, CO_2 discharge becomes proportional to fuel consumption.

The mass of CO_2 released by conventional Panthera is ten times larger than the hybrid-electric version, while CO_2 emissions of Cessna 172R Skyhawk are the 55% of the conventional Panthera value.

As for carbon monoxide, practically the same ratios hold in relation to the emissions of the three airplanes: the analogy with fuel flow fractions suggests that the three engines do not evidence great differences in terms of CO emission index.

Looking at UHC values instead, the ratios between the different masses have changed, as evidenced by the comparable values relative to Cessna 172R Skyhawk and conventional Panthera.

The mass ratio between the two conventional aircraft increases at the 84%, while the amount of UHC produced by Rotax 914 is one-fourth of the conventional Panthera value. The increment in both percentages with respect to CO_2 results is related to a lower UHC emission index for Lycoming IO-540 with respect to the engines of Cessna 172R Skyhawk and Panthera Hybrid.

Exactly the opposite behaviour is registered for the oxides of nitrogen since the percentage reduces to the 48% for Cessna 172R Skyhawk, while an extremely poor 4% relates the emissions of the two Panthera versions.

Moreover, the previous diagrams highlight that the four chemical species are characterized by radically different emissions since CO_2 production is even 3.067 times larger than fuel consumption. Another pollutant produced in quite large quantity is carbon monoxide, while the emissions of unburned hydrocarbons and the oxides of nitrogen are at least one order of magnitude lower.

In order to compare the results relative to the different species, emissions are expressed in terms of social cost and the results are visible in Figure 5.7.

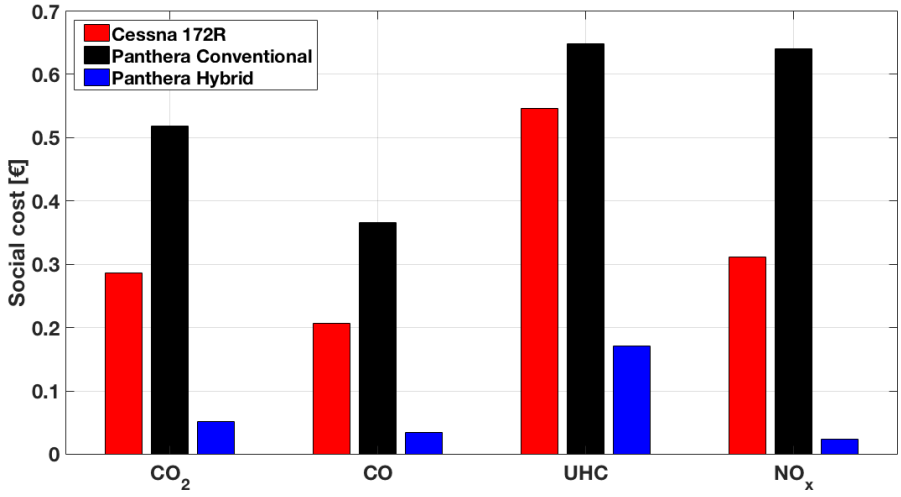

Figure 5.7: Emission comparison in terms of social cost

Considering the single chemical substance at first, the results relative to the three airplanes follow exactly the same ratios previously evidenced since the mass values are simply multiplied by a pollutant-specific factor which is independent on the aircraft.

Consequently, similar considerations apply for the comparison between the three airplanes, showing that the highest cost is relative to conventional Panthera, followed by Cessna 172R Skyhawk and Panthera Hybrid.

A more meaningful analysis is performed when the four substances are compared with each other since the social cost coefficient is higher for the species produced in minor quantities and viceversa. Consequently, the social cost relative to the single chemical species results from the trade-off between mass and cost factor, which eventually leads to comparable outcomes for the four pollutants.

Focusing on the two conventional airplanes, the lowest economic impact is related to carbon monoxide as it is produced in quite large quantities, but its social cost per unit mass is poor.

An even lower cost coefficient is specific to carbon dioxide, which is nevertheless responsible for a larger social cost with respect to CO because of its high mass production.

Since the mass ratios of both CO and CO_2 are very similar, the costs relative to these species are proportional to each other when the single aircraft is considered: in particular, the cost related to CO_2 emissions is in average 1.4 times larger than the CO value.

The highest economic impact instead belongs to the release of unburned hydrocarbons for all airplanes since this class of pollutants is produced in quite large quantity and is characterized by a high cost factor.

The previous analysis has shown that the UHC mass ratios of Cessna 172R Skyhawk and Panthera Hybrid are much higher with respect to CO_2 percentages. This is responsible for the great cost increase of unburned hydrocarbons with respect to CO_2 for these two airplanes, while the increment is much less evident when conventional Panthera is considered.

The influence of mass ratios is particularly evident when looking at the NO_x bars since the oxides of nitrogen produced by Panthera Hybrid are just the 4% of those connected to conventional Panthera. As mass ratios become cost ratios when a single substance is considered, this justifies the extremely low NO_x cost reached by Panthera Hybrid, and at the same time is at the basis of the high value relative to conventional Panthera.

Chapter 6

Conclusions

The environmental effects related to hybrid-electric propulsion have been analysed through a comparison with conventional power-trains, aimed at providing a first important idea of the pollution differences between the two propulsive technologies.

The lack of experimental pollution measurements relative to hybrid-electric aircraft implies the need to develop two generic methodologies for the estimation of noise and pollutant emissions.

The initial part of the analysis has therefore been devoted to the investigation of models currently in use for the prediction of the environmental effects deriving from aircraft operation.

Research has been made on an extremely wide perspective, going from the simplest methods to the most sophisticated numerical approaches, and has allowed to establish an important basis for the development of two prediction procedures.

6.1 An innovative modelling approach

In the current study, the prediction of noise and atmospheric pollution has been carried out thanks to two innovative methods, which are applicable to existing aircraft and new concepts as well.

Focusing on the acoustic field, the method outlined in ECAC Doc. 29 represented an important reference point for noise prediction as it is the standard for the tracing of noise emission maps around the main European airports.

At first, a procedure complying with the guidelines provided by ECAC has been implemented and validated with good results. However, the segmentation of aircraft trajectory as well as the baseline sound levels for noise computation are obtained from the ANP database, which refers only to conventional aircraft.

Therefore, a new prediction method has been introduced with the idea to inherit the greatest number of modelling aspects from the ECAC model. Accordingly, the flight trajectory followed by the hybrid-electric has been assumed to coincide with the one of a similar conventional airplane, and the acoustic corrective terms have been applied exactly in the same way as ECAC suggests.

What is instead extremely aircraft-specific is the baseline noise level, which has been computed thanks to a source-based method. The airframe, propeller and engine sound contributions have been estimated through simple models and then summed on an energetic basis in order to derive the overall aircraft noise. However, the application of this procedure to existing aircraft has given extremely poor results.

Consequently, a new formulation has been introduced on the basis of three multiplicative factors, obtained from the minimization of the error with respect to real sound data.

The application of the minimization formula to the eight conventional airplanes covered in the ANP database has brought to several triplets of blending coefficients, which have been averaged over all departure and arrival movements.

In this way, the baseline noise levels have become more similar to those provided in ANP thanks to the introduction of these average factors, which have been applied to both existing and hybrid-electric aircraft.

Things are much less complex for the prediction of atmospheric pollution since it has historically been based on a simpler formulation and has not focused on the investigation of pollutant dispersion in the aerodrome region. What really matters in a preliminary phase is indeed the estimation of the overall mass emitted rather than the complicated knowledge of its distribution in the airport area.

The very same trajectory segmentation used in noise analysis has been exploited even in this study,as it allows for a more accurate estimation of the time spent by the aircraft in each flight phase. The values of the fuel flow and of the emission indices have instead been obtained from the ACRP Research Report 164, which refers to tests made on a great number of General Aviation piston engines.

In order to compare the emissions of the different pollutants, the mass results have finally been converted into social cost by means of a coefficient related to the effects of each pollutant on human health.

6.2 Summary of results

The computation of sound exposure according to the source blending method passes through three different coefficients multiplying the sound pressure level relative to each source: in particular, the x_1 coefficient is relative to airframe noise, while x_2 and x_3 refer to propeller and engine respectively.

The triplets related to the eight piston-engine airplanes inside ANP have been averaged over all departure and arrival movements and the results are visible in Table 6.1.

	$\boldsymbol{x}_1$	$\boldsymbol{x}_2$	$\boldsymbol{x}_3$
Departure	0.98	0.91	1.00
Arrival	0.85	0.95	0.91

Table 6.1: Average departure and arrival blending coefficients

Since the ideal case corresponds to a unit x_i coefficient, the estimation formulas for airframe and engine noise have evidenced a high level of accuracy in the departure case, where the error is limited at the 2% for the former and is practically null for the latter.

The prediction of propeller noise implies a constant overestimation of the real sound exposure since the multiplicative factors are lower than unity: in particular, a 9% error has been obtained for departure, a 5% error for arrivals.

Differently from x_2, the other two blending coefficients have proven to be lower at arrival, when the estimation formulas imply a 15% error for airframe noise and a 9% error for the engine contribution.

The last part of the report has been devoted to the application of the estimation methods to two different comparative analyses relative to a complete traffic pattern at Milan Bresso airport.

The first study has been based on a typical issue affecting all power-train designs since it has dealt with the environmental effects of power management.

The circuit has therefore been subdivided into the five characteristic legs, each of which could either be performed in all-electric or conventional mode. Seven different cases have been considered for this analysis, which has taken two radically different airplanes into account, namely Cessna T206H Stationair and Piper PA-31-350 Navajo Chieftain.

For each of the two aircraft, the results in terms of average sound exposure along the circuit track and social cost have been collected in Table 6.2, which recalls the ID numbers of Table 5.2 for the definition of the seven operational modes.

	T206H		**PA-31**	
ID	**Average sound exposure [dB]**	**Social cost [€]**	**Average sound exposure [dB]**	**Social cost [€]**
1	88.15	1.990	92.03	2.901
2	87.99	0.781	91.83	1.217
3	88.08	1.593	91.94	2.325
4	85.43	0.811	88.87	1.108
5	85.55	1.208	89.05	1.684
6	85.38	0.397	88.83	0.576
7	85.25	0.000	88.65	0.000

Table 6.2: Acoustic and atmospheric effects related to the operational mode

The smaller size of Cessna T206H Stationair implies much lower social costs and is responsible for an average decrement of 3.62 dB in sound exposure with respect to Piper PA-31-350 Navajo Chieftain. This is not so surprising since a heavier airplane is expected to produce larger acoustic and atmospheric emissions as a result of the higher power demand.

Focusing on the different modes, it is evident that the lowest emissions are obtained in all-electric mode (7), while the largest values refer to the activation of piston engine in all circuit legs (1).

Looking at the five intermediate cases, the most promising results are obtained when the ICE is exploited in the base and final legs (6), while the highest emissions are related to the departure-crosswind-downwind activation (3).

This double effect is basically related to the different power demand since a high engine speed implies large propeller and engine noise and increases the cost relative to pollutant emissions.

As for the other three modes, the highest sound exposure is related to the departure-crosswind sequence (2), while the largest social cost is obtained in the downwind-base-final case (5) as a result of the high amount of NO_x discharged in cruise.

The final part of the acoustic and environmental analyses has taken Panthera Hybrid into consideration, by comparing it with the conventional Panthera version and with Cessna 172R Skyhawk.

The real operational mode has been considered for the three airplanes, with the ICE activation in every flight phase for the two conventional aircraft, in just the cruise portion for Panthera Hybrid.

The analysis on noise contours has shown that the region enclosed by the lines at the highest sound exposure is slightly more extended for conventional Panthera than for Cessna 172R Skyhawk, while the opposite trend has been registered for values lower or equal to 80 decibels.

Panthera Hybrid is instead characterized by the least sound exposure levels and, apart from the region inside the 85 dB line, the values of the enclosed area are at least one order of magnitude lower than those related to the two conventional airplanes.

As for pollutant emissions instead, the social cost specific to each substance is presented in Table 6.3 together with the overall value.

Aircraft	**CO_2 [€]**	**CO [€]**	**UHC [€]**	**NO_x [€]**	**Overall [€]**
Cessna 172R Skyhawk	0.287	0.207	0.546	0.312	1.352
Panthera Conventional	0.518	0.366	0.649	0.641	2.174
Panthera Hybrid	0.052	0.035	0.171	0.023	0.281

Table 6.3: Social cost of pollutant emissions

The highest economic impact is related to the production of unburned hydrocarbons for the three aircraft, while the lowest is linked to the oxides of nitrogen for Panthera Hybrid, to carbon monoxide for the two conventional airplanes.

The largest emissions in massive terms are relative to carbon dioxide, whose social cost per unit mass is very poor: the combination of large mass production with low specific cost is sufficient for CO_2 emissions to overcome CO social cost, but not to reach the tremendous health impact of unburned hydrocarbons.

Looking at the overall results, Panthera Hybrid is shown to produce significant environmental benefits as it implies a 80% reduction in social cost with respect to Cessna 172R Skyhawk and a striking 87% decrement with respect to conventional Panthera.

6.3 Future developments

The current work has dealt with the introduction of two procedures for the estimation of noise and pollutant emissions in order to assess the environmental benefits of hybrid-electric propulsion.

The natural evolution is therefore represented by a departure from a comparative perspective for the sake of a more accurate quantification of the real sound exposure and pollutant emissions deriving from a hybrid-electric power-train. This will be possible at some future time, when hybrid-electric aircraft will reach a sufficiently high level of diffusion to allow for numerous on-field measurements.

Another important development is related to the expansion of the current study in order to consider all the movements belonging to a General Aviation airport. In this way, acoustic and

atmospheric emissions will not be referred to a single aircraft anymore, but will focus on the overall number of departures and arrivals occurring in a precise time period.

A further possible expansion of this thesis work concerns the reference to a larger airport, characterized by a higher traffic and the presence of heavier and more powerful airplanes. This will give the possibility to consider the influence of a hybrid-electric General Aviation fleet in the global environmental effects connected to all airport operations.

In the context of the MAHEPA project, an important evolution lies in the extension of the predictive methods to larger aircraft such as commuters and micro-feeders. A comparative analysis similar to the one presented in this thesis can be performed considering these new applications.

Finally, an interesting source for future development consists in exploiting the estimation models presented in the current work in a program for aircraft design. A possible algorithm could be implemented in order to consider pollution effects in the figure of merit for the overall airplane project.

Bibliography and Links

[1] EUROCONTROL. European aviation in 2040 - Challenges of growth - Annex 1: flight forecast to 2040. 2018. Available at: https://www.eurocontrol.int/publications/flight-forecast-2040-challenges-growth-annex-1. Accessed 12/01, 2018.

[2] Gaspari F, Trainelli L, Rolando ALM, Perkon I. D1.1: concept of modular architecture for hybrid electric propulsion of aircraft. 2018. Available at: https://mahepa.eu/wp-content/uploads/2017/12/D1.1-Concept-of-Modular-Architecture-fro-Hybrid-Electric-Propulsion-of-Aircraft.pdf.Accessed 10/03, 2018.

[3] Poiana G. Hybrid-electric aircraft powertrain modellind and simulation. Milan: Politecnico di Milano; 2018.

[4] Rossi N. Conceptual design of hybrid-electric aircraft. Milan: Politecnico di Milano; 2018.

[5] Riboldi CED. An optimal approach to the preliminary design of small hybrid-electric aircraft. Aerospace Science and Technology 2018; 81: 14-31.

[6] Riboldi CED, Gualdoni F, Trainelli L Preliminary weight sizing of light pure-electric and hybrid-electric aircraft. Transportation Research Procedia 2018; 29: 376-89.

[7] Bigoni F. Impact of hybrid-electric aircraft operations. Milan: Politecnico di Milano; 2018.

[8] Coates M. Pipistrel Panthera 4 seater aircraft. 2012. Available at: https://youtu.be/0gApX-cAYMs. Accessed 12/03, 2018.

[9] Pipistrel. Images of beauty. 2012. Available at: https://www.panthera-aircraft.com/gallery. Accessed 12/03, 2018.

[10] HY4. HY4: Delivering the future. 2016. Available at: http://hy4.org. Accessed 12/10, 2018.

[11] Filippone A. Aircraft noise prediction. Progress in Aerospace Sciences 2014; 68: 27-63.

[12] Metzger BF. A review of propeller noise prediction methodology 1919-1994. 1995. NASA Contractor Report CR-198156.

[13] Lynam FJH, Webb HA. The emission of sound by airscrews. 1919. Technical Reports and Memoranda No. 624: 792-801.

[14] Lighthill MJ. On sound generated aerodynamically - I. General theory. Proceedings of the Royal Society A 1952; 211(1507): 564-87.

[15] Ffowcs Williams JE, Hawkings DL. Sound generation by turbulence and surfaces in arbitrary motion. Philosophical Transactions of the Royal Society A 1969; 264(1151): 321-42.

[16] Farassat F, Succi GP. A review of propeller discrete frequency noise prediction technology with emphasis on two current methods for time domain calculations. Journal of Sound and Vibration 1980; 71(3): 399-419.

[17] Hanson DB. Shielding of prop-fan cabin noise by the fuselage boundary layer. Journal of Sound and Vibration 1984; 92(4): 591-8.

[18] Hanson DB. Noise of counter-rotation propellers. Journal of Aircraft 1985; 22(7): 609-17.

[19] Hanson DB, Parzych DJ. Theory for noise of propellers in angular inflow with parametric studies and experimental verification. 1993. NASA Contractor Report CR-4499.

[20] Goldstein ME. Aeroacoustics. New York: McGraw-Hill International Book Company; 1976.

[21] Obata J, Morita S, Yosida Y. Studies on the sounds emitted by revolving airscrews - Part I. Aeronautical Research Institute of Tokyo Imperial University 1932; 79(13).

[22] Obata J, Yosida Y, Morita S. Studies on the sounds emitted by revolving airscrews - Part II. Experiments with model airscrews. Aeronautical Research Institute of Tokyo Imperial University 1932; 80(14).

[23] Ffowcs Williams JE, Hall LH. Aerodynamic sound generation by turbulent flow in the vicinity of a scattering half plane. Journal of Fluid Mechanics 1970; 40(4): 657-70.

[24] Curle N. The influence of solid boundaries upon aerodynamic sound. Proceedings of The Royal Society A 1955; 231(1187): 505-14.

[25] Chase DM. Sound radiated by turbulent flow off a rigid half-plane as obtained from a wavevector spectrum of hydrodynamic pressure. The Journal of the Acoustical Society of America 1972; 52(3B): 1011-23.

[26] Franken PA, Kerwin Jr EM. Methods of flight vehicle noise prediction. 1958. WADC Technical Report TR 58-343.

[27] Marte JE, Kurtz DW. A review of aerodynamic noise from propellers, rotors, and lift fans. 1970. NASA Contractor Report CR-107568.

[28] Dunn DG, Peart NA. Aircraft noise source and contour estimation. 1973. NASA Contractor Report CR-114649.

[29] SAE Aerospace. Prediction procedure for near-field and far-field propeller noise. 1977. SAE Aerospace Information Report AIR1407.

[30] Smith MH. A prediction procedure for propeller aircraft flyover noise based on empirical data. SAE Transactions 1981; 90(2): 2114-24.

[31] Rathgeber RK. The development of a flyover noise prediction technique using multiple linear regression analysis. 1981. SAE Technical Paper Series 810588.

[32] Royal Aeronautical Society. Prediction of near-field and far-field harmonic noise from subsonic propellers with non-axial inflow. 2011. IHS ESDU 11005.

[33] Munson AG. A modeling approach to nonpropulsive noise. In: 3rd AIAA Aeroacoustics Conference, AIAA Paper 76-525; Palo Alto; 1976 July 20-23.

[34] Fink MR. Airframe noise prediction method. 1977. FAA Technical Report FAA-RD-77-29.

[35] Fink MR. Noise component method for airframe noise. Journal of Aircraft 1979; 16(10): 659-65.

[36] Yamamoto KJ, Donelson MJ, Huang SC, Joshi MC. Airframe noise prediction evaluation. 1995. NASA Contractor Report CR-4695.

[37] Amiet RK. Noise due to turbulent flow past a trailing edge. Journal of Sound and Vibration 1976; 47(3): 387-93.

[38] Howe MS. A review of the theory of trailing edge noise. Journal of Sound and Vibration 1978; 61(3): 437-65.

[39] Guo YP, Yamamoto KJ, Stoker RW. Component-based empirical model for high-lift system noise prediction. Journal of Aircraft 2003; 40(5): 914-22.

[40] Guo YP. Aircraft flap side edge noise modeling and prediction. In: 17th AIAA/CEAS Aeroacoustics Conference, AIAA 2011-2731; Portland; 2011 June 5-8.

[41] Guo YP. Flap side edge noise modeling and prediction. Journal of Sound and Vibration 2013; 332(5): 3846-68.

[42] Brooks TF, Humphreys WM. Flap-edge aeroacoustic measurements and predictions. Journal of Sound and Vibration 2003; 261(1): 31-74.

[43] Dobrzynski W, Pott-Pollenske M. Slat noise source studies for farfield noise prediction. In: 7th AIAA/CEAS Aeroacoustics Conference, AIAA 2001-2158; Maastricht; 2001 May 28-30.

[44] Guo YP. Slat noise modeling and prediction. Journal of Sound and Vibration 2013; 331(15): 3567-86.

[45] Guo YP. A statistical model for landing gear noise prediction. Journal of Sound and Vibration 2005; 282(1-2): 61-87.

[46] Royal Aeronautical Society. Airframe noise prediction. 1990. IHS ESDU 90023.

[47] Yao J, Xiang Y, Qian S, Wang S. Radiation noise separation of internal combustion engine based on Gammatone-RobustICA method. Shock and Vibration 2017; 2017: 1-14.

[48] Reinhart TE. Internal combustion engine noise prediction and control - Diesel and gasoline engines. In: Crocker MJ. Handbook of noise and vibration control. Hoboken: John Wiley and Sons, Inc.; 2007. 1024-33.

[49] Royal Aeronautical Society. Aircraft noise prediction. 2009. IHS ESDU 09009.

[50] Davies POAL, Holland KR. IC engine intake and exhaust noise assessment. Journal of Sound and Vibration 1999; 223(3): 425-44.

[51] Bodén H. Recent advances in IC-engine acoustic source characterisation. In: 14th International Congress on Sound and Vibration, ICSV14; Cairns; 2007 July 9-12.

[52] Russell GA, Hjerpe ED. On the analogy between the one-dimensional acoustic waveguide and the electrical transmission line. The Journal of the Acoustical Society of America 1993; 94(1): 583-4.

[53] Mutyala BRC, Soedel W. A mathematical model of Helmholtz resonator type gas oscillation discharges of two-stroke cycle engines. Journal of Sound and Vibration 1976; 44(4): 479-91.

[54] Singh R, Soedel W. Mathematical modeling of multicylinder compressor discharge system interactions. Journal of Sound and Vibration 1979; 63(1): 125-43.

[55] Singh R, Soedel W. Interpretation of gas oscillations in multicylinder fluid machinery manifolds by using lumped parameter descriptions. Journal of Sound and Vibration 1979; 64(3): 387-402.

[56] Wang WM. Acoustical analysis of symmetrical multi-source mechanically driven fluid systems. Ann Arbor: University of Michigan; 1965.

[57] Wang WM. Matrix formulation in acoustical analysis of mechanically driven fluid systems. The Journal of the Acoustical Society of America 1967; 41(6): 1418-23.

[58] Wang WM. Acoustical analysis of a multicylinder engine air-induction system. The Journal of the Acoustical Society of America 1967; 42(6): 1244-9.

[59] Gupta VH, Munjal ML. On numerical prediction of the acoustic source characteristics of an engine exhaust system. The Journal of the Acoustical Society of America 1992; 92(5): 2716-25.

[60] Albertson F, Gilbert J. Harmonic balance method used for calculating the steady state oscillations of a simple one-cylinder cold engine. Journal of Sound and Vibration 2001; 241(4): 541-65.

[61] Davies POAL, Harrison MF. Predictive acoustic modelling applied to the control of intake/exhaust noise of IC engines. Journal of Sound and Vibration 1997; 202(2): 249-74.

[62] Takagi S, Nakamura T, Irie Y. A modeling of nonlinear wave propagation in engine exhaust systems. Proceedings of Inter-noise 84, Honolulu, 393-6.

[63] Bruce RD, Moritz CT, Bommer AS. Sound power level predictions for industrial machinery. In: Crocker MJ. Handbook of noise and vibration control. Hoboken: John Wiley and Sons, Inc.; 2007. 1001-9.

[64] Thurston DB. Design for flying. New York: McGraw-Hill; 1978.

[65] Dobrzynski W, Vogelsang BM. Emissionskennwerte von Propellerflugzeugen für Schallimmissionsrechnungen an Landeplätzen. Proceedings of DAGA 94, Dresden, 405-8.

[66] Tada H. An intermittent-combustion general aviation aircraft engine exhaust noise prediction algorithm. Daytona Beach: Embry-Riddle Aeronautical University; 1999.

[67] Moshkov PA. Integral model of noise of an engine-propeller power plant. Journal of Engineering Physics and Thermophysics 2018; 91(2): 332-8.

[68] Jordan H. Geräuscharme Elektromotoren. Essen: Girardet; 1950.

[69] Heller B, Hamata V. Harmonic field effects in induction machines. Prague: Academia; 1977.

[70] Timar PL, Fazekas A, Kiss J, Miklos A, Yang SJ. Noise and vibration of electrical machines. Amsterdam: Elsevier; 1989.

[71] Gieras JF, Wang C, Lai JC. Noise of polyphase electric motors. Boca Raton: Taylor & Francis; 2006.

[72] Miller LN, Wood EW, Hoover RM, Thompson AR, Patterson SL. Electric power plant environmental noise guide. Washington: Edison Electric Institute; 1984.

[73] Bies DA, Hansen CH. Engineering noise control. London: Spon Press; 2003.

[74] Joint Department of the Army, Air Force, and Navy. Noise and vibration control for mechanical equipment. 1980. Technical Manual TM5-805-4/AFM 88-37/NAVFAC DM-3.10.

[75] Patil CR, Kulkarni PP, Narayan Sarode N, Shinde KU. Gearbox noise & vibration prediction and control. International Research Journal of Engineering and Technology 2017; 4(11): 873-7.

[76] Singh R. Gear noise: anatomy, prediction and solutions. Proceedings of Inter-noise 09, Ottawa, 3364-93.

[77] Lim TC, Singh R. A review of gear housing dynamics and acoustics literature. 1989. NASA Contractor Report CR-185148.

[78] Lim TC, Singh R. Vibration transmission through rolling element bearings - Part I: bearing stiffness formulation. Journal of Sound and Vibration 1990; 139(2): 179-99.

[79] Lim TC, Singh R. Vibration transmission through rolling element bearings - Part II: system studies. Journal of Sound and Vibration 1990; 139(2): 201-25.

[80] Lim TC, Singh R. Vibration transmission through rolling element bearings - Part III: geared rotor system studies. Journal of Sound and Vibration 1991; 151(1): 31-54.

[81] Lim TC, Singh R. Statistical energy analysis of a gearbox with emphasis on the bearing path. Noise Control Engineering Journal 1991; 37(2): 63-9.

[82] Lim TC, Singh R. Vibration transmission through rolling element bearings - Part IV: statistical energy analysis. Journal of Sound and Vibration 1992; 153(1): 37-50.

[83] Singh R, Lake A, Asnani V, He S. Vibro-acoustic model of a geared system including friction excitation. Proceedings of Inter-noise 07, Istanbul, 2921-30.

[84] Doğan SN. Zur minimierung der losteilgeräusche von fahrzeuggetrieben. Stuttgart: Universität Stuttgart; 1999.

[85] Lang CH, Lechner G. Klappern und rasseln von fahrzeuggetrieben - Simulation der losteilschwingungen und möglichkeiten zur geräuschminimierung. VDI-Berichte 1995; 1175: 99-122.

[86] European Union. Directive 2002/49/EC of the European Parliament and of the Council of 25 June 2002 relating to the assessment and management of environmental noise. Official Journal of the European Communities 2002; 45: 12-26.

[87] European Union. Directive 2009/12/EC of the European Parliament and of the Council of 11 March 2009 on airport charges. Official Journal of the European Union 2009; 52: 11-6.

[88] Zorumski WE. Aircraft noise prediction program - Theoretical manual. 1982. NASA Technical Memorandum TM-83199, Part 1.

[89] Zorumski WE. Aircraft noise prediction program - Theoretical manual. 1982. NASA Technical Memorandum TM-83199, Part 2.

[90] Lopes LV, Burley CL. Design of the next generation aircraft noise prediction program: ANOPP2. In: 17th AIAA/CEAS Aeroacoustics Conference, AIAA 2011-2854; Portland; 2011 June 5-8.

[91] Clark BJ. Computer program to predict aircraft noise levels. 1981. NASA Technical Paper TP-1913.

[92] Bertsch L, Dobrzynski W, Guérin S. Tool development for low-noise aircraft design. Journal of Aircraft 2010; 47(2): 694-9.

[93] Isermann U, Matschat K, Müller EA. Prediction of aircraft noise around airports by a simulation procedure. Proceedings of Inter-noise 86, Cambridge, 717-22.

[94] Filippone A. Comprehensive analysis of transport aircraft flight performance. Progress in Aerospace Sciences 2008; 44(3): 192-236.

[95] ICAO. Recommended method for computing noise contours around airports. Montréal: International Civil Aviation Organization; 2008.

[96] ECAC. Report on standard method of computing noise contours around civil airports - Volume 2: technical guide. Neuilly-sur-Seine: European Civil Aviation Conference; 2016.

[97] EUROCONTROL. The Aircraft Noise and Performance (ANP) database: an international data resource for noise modellers. 2006. Available at: `https://www.aircraftnoisemodel.org`. Accessed 10/23, 2018.

[98] Ollerhead JB. The CAA aircraft noise contour model: ANCON version 1. 1992. DORA Report 9120.

[99] Ollerhead JB, Rhodes DP, Viinikainen MS, Monkman DJ, Woodley AC. The UK civil aircraft noise contour model ANCON: improvements in version 2. 1999. NATS R&D Report 9842.

[100] Pietrzko S, Bütikofer R. FLULA - Swiss aircraft noise prediction program. In: Acoustics 2002 - Innovation in Acoustics and Vibration. Annual Conference of the Australian Acoustical Society; Adelaide; 2002 November 13-15.

[101] Umweltbundesamt. Anleitung zur berechnung von lärmschutzbereichen (AzB). 2007. Available at: https://www.hlnug.de/fileadmin/dokumente/laerm/gesetze/flugverkehr/AzB_07.pdf. Accessed 04/08, 2019.

[102] Malbéqui P, Rozenberg Y, Bulté J. Aircraft noise prediction in the IESTA program. In: 3rd European Conference for AeroSpace Sciences, EUCASS 2009; Versailles; 2009 July 6-9.

[103] EUROCONTROL. IMPACT: EUROCONTROL's integrated aircraft noise and fuel burn & emission modelling platform. 2016. Available at: https://www.eurocontrol.int/publications/impact. Accessed 11/28, 2018.

[104] US DOT Volpe Center. Aviation Environmental Design Tool (AEDT) - Version 2d - User guide. 2017. US Department of Transportation Report DOT-VNTSC-FAA-17-15.

[105] US DOT Volpe Center, FAA, ATAC Corporation, CSSI, Inc., Metron Aviation. Aviation Environmental Design Tool (AEDT) - Version 2d - Technical manual. 2017. US Department of Transportation Report DOT-VNTSC-FAA-17-16.

[106] Cavadini L. STAPES final report. 2009. Available at: https://www.easa.europa.eu/sites/default/files/dfu/2009-STAPES-System%20for%20AirPort%20noise%20Exposure%20Studies-Final%20Report.pdf. Accessed 12/10, 2018.

[107] Jelinek F, Carlier S, Smith J. Advanced Emission Model (AEM3) - Validation report. 2004. EEC Report EEC/SEE/2004/004.

[108] Boeker ER, Dinges E, He B, Fleming G, Roof CJ, Gerbi PJ, Rapoza AS, Hemann J. Integrated Noise Model (INM) Version 7.0 - Technical manual. FAA Report FAA-AEE-08-01.

[109] SAE Aerospace. Procedure for the calculation of airplane noise in the vicinity of airports. 1986. SAE Aerospace Information Report AIR1845.

[110] Environmental Protection UK. Aviation pollution. 2013. Available at: https://www.environmental-protection.org.uk/policy-areas/air-quality/air-pollution-and-transport/aviation-pollution/. Accessed 12/10, 2018.

[111] ICAO Environment. Aircraft noise. 2016. Available at: https://www.icao.int/environmental-protection/pages/noise.aspx. Accessed 12/10, 2018.

[112] National Pollutant Inventory. Oxides of nitrogen. 2019. Available at: http://www.npi.gov.au/resource/oxides-nitrogen-0. Accessed 12/06, 2018.

[113] National Pollutant Inventory. Particulate matter (PM10 and PM2.5). 2019. Available at: http://www.npi.gov.au/resource/particulate-matter-pm10-and-pm25. Accessed 12/06, 2018.

[114] EUROCONTROL. EUROCONTROL method for estimating aviation fuel burnt and emissions in the framework of the EMEP/EEA air pollutant emission inventory guidebook 2016. 2016. Available at: https://www.eurocontrol.int/publications/eurocontrol-method-estimating-aviation-fuel-burnt-and-emissions. Accessed 12/10, 2018.

[115] Winther M, Rypdal K. Aviation. In: European Environment Agency. EMEP/EEA air pollutant emission inventory guidebook 2016. Luxembourg: Publications Office of the European Union; 2016.

[116] ICAO. Environmental protection - Annex 16 to the convention on international civil aviation - Volume II: aircraft engine emissions. Montréal: International Civil Aviation Organization; 2008.

[117] Watterson J, Walker C, Eggleston S. Revision to the method of estimating emissions from aircraft in the UK greenhouse gas inventory. 2004. Report to DEFRA Global Atmosphere Division NETCEN/ED47052.

[118] ICAO. ICAO aircraft engine emission databank. 2018. Available at: `https://www.easa.europa.eu/easa-and-you/environment/icao-aircraft-engine-emissions-databank`. Accessed 10/16, 2018.

[119] Döpelheuer A, Lecht M. Influence of engine performance on emission characteristics. In: RTO AVT Symposium on Gas Turbine Engine Combustion, Emissions and Alternative Fuels, RTO Paper 20; Lisbon; 1998 October 12-16.

[120] Kilde NA, Sørensen L. Air traffic. In: European Environment Agency. EMEP/CORINAIR Atmospheric Emission Inventory Guidebook. Copenhagen: European Environment Agency; 1996.

[121] US DOT Volpe Center, FAA, Massachusetts Institute of Technology, Logistics Management Institute. System for assessing Aviation's Global Emissions (SAGE) - Version 1.5 - Technical manual. 2005. US Department of Transportation Report DOT-VNTSC-FAA-05-04.

[122] EUROCONTROL. Open-ALAQS: an open-source local air quality model. 2016. Available at: `https://www.eurocontrol.int/services/open-alaqs`. Accessed 10/24, 2018.

[123] EUROCONTROL. BADA: Base of Aircraft Data (BADA) Factsheet. 2015. Available at: `https://www.eurocontrol.int/publications/base-aircraft-data-bada-factsheet`. Accessed 10/26, 2018.

[124] DuBois D, Paynter GC. "Fuel Flow Method2" for estimating aircraft emissions. 2006. SAE Technical Paper 2006-01-1987.

[125] ICAO. Environmental protection - Annex 16 to the convention on international civil aviation - Volume I: aircraft noise. Montréal: International Civil Aviation Organization; 2008.

[126] ICAO Environment. Reduction of noise at source. 2016. Available at: `https://www.icao.int/environmental-protection/pages/reduction-of-noise-at-source.aspx`. Accessed 05/07, 2019.

[127] European Union. Regulation (EU) No 598/2014 of the European Parliament and of the Council of 16 April 2014 on the establishment of rules and procedures with regard to the introduction of noise-related operating restrictions at Union airports within a Balanced Approach. Official Journal of the European Union 2014; 57: 65-78.

[128] ECAC. Report on standard method of computing noise contours around civil airports - Volume 1: appllications guide. Neuilly-sur-Seine: European Civil Aviation Conference; 2016.

[129] ECAC. Report on standard method of computing noise contours around civil airports - Volume 3, Part 1: reference cases and verification framework. Neuilly-sur-Seine: European Civil Aviation Conference; 2016.

[130] ECAC. Report on standard method of computing noise contours around civil airports - Volume 3, Part 1 (workbook). 2016. Available at: `https://www.ecac-ceac.org/ecac-docs`. Accessed 11/24, 2018.

[131] Kumasaka HA, Martinez MM, Weir DS. Definition of 1992 technology aircraft noise levels and the methodology for assessing airplane noise impact of component noise reduction concepts. 1996. NASA Contractor Report CR-198298.

[132] Synodinos AP, Self RH, Torija AJ. Framework for predicting noise-power-distance curves for novel aircraft designs. Journal of Aircraft 2018; 55(9): 781-91.

[133] ICAO. A revision to the definition of the reference atmosphere in Annex 16 to improve data quality and reliability and ease technical problems. 1983. CAN Seventh Meeting Report on Agenda Item 3 CAN/7-WP/59.

[134] ASCENT. Noise power distance re-evaluation. 2017. Available at: `https://ascent.aero/project/noise-power-distance-re-evaluation/`. Accessed 10/23, 2018.

[135] Yacovitch TI, Yu Z, Herndon SC, Miake-Lye R, Liscinsky D, Berk Knighton W, Kenney M, Schoonard C, Pringle P. Exhaust emissions from in-use general aviation aircraft. 2016. ACRP Research Report 164.

[136] ICAO. Environmental protection - Annex 16 to the convention on international civil aviation - Volume III: CO_2 certification requirement. Montréal: International Civil Aviation Organization; 2017.

[137] EASA. Aircraft engine NO_x emissions. 2016. Available at: `https://www.easa.europa.eu/eaer/topics/technology-and-design/aircraft-engine-emissions`. Accessed 06/21, 2019.

[138] Dellaert SNC, Hulskotte IJHJ. Emissions of air pollutants from civil aviation in the Netherlands. 2017. TNO report R10055.

[139] Markowski J, Pielecha J, Jasiński R. Model to assess the exhaust emissions from the engine of a small aircraft during flight. Procedia Engineering 2017; 192: 557-62.

[140] FOCA. Aircraft piston engine emissions - Appendix 5: calculation of emission factors. Bern: Federal Office of Civil Aviation; 2007.

[141] Lu C. The economic benefits and environmental costs of airport operations: Taiwan Taoyuan International Airport. Journal of Air Transport Management 2011; 17(6): 360-3.

Appendix A

Sound exposure levels for Cessna T206H and Piper PA-31-350

The source blending method for aircraft noise is centred on the introduction of three multiplicative coefficients, obtained through a statistical analysis performed on the eight piston-engine airplanes covered by the ANP database.

Average departure and arrival coefficients are defined considering the 2σ and 3σ bilateral confidence bands as well. Figure A.1 compares the ANP noise levels and the new NPD data obtained from these statistical results with regard to a Cessna T206H Stationair.

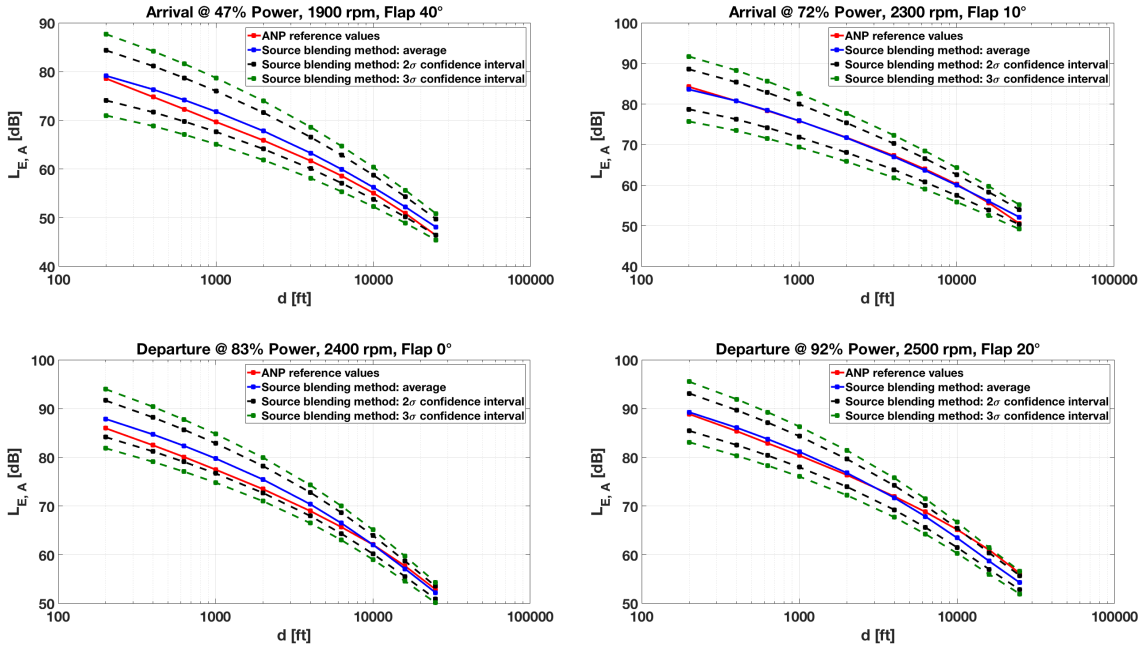

Figure A.1: Sound exposure data relative to Cessna T206H Stationair

It is possible to see that the red line corresponding to the values provided in ANP is always inside the band corresponding to the 3σ bilateral confidence interval.

The diagram of the arrival at higher power is extremely significant as it evidences a practically perfect coincidence between the ANP reference data and the sound exposure levels computed through the source blending method.

Another important airplane at the basis of noise analysis is Piper PA-31-350 Navajo Chieftain, to which Figure A.2 refers.

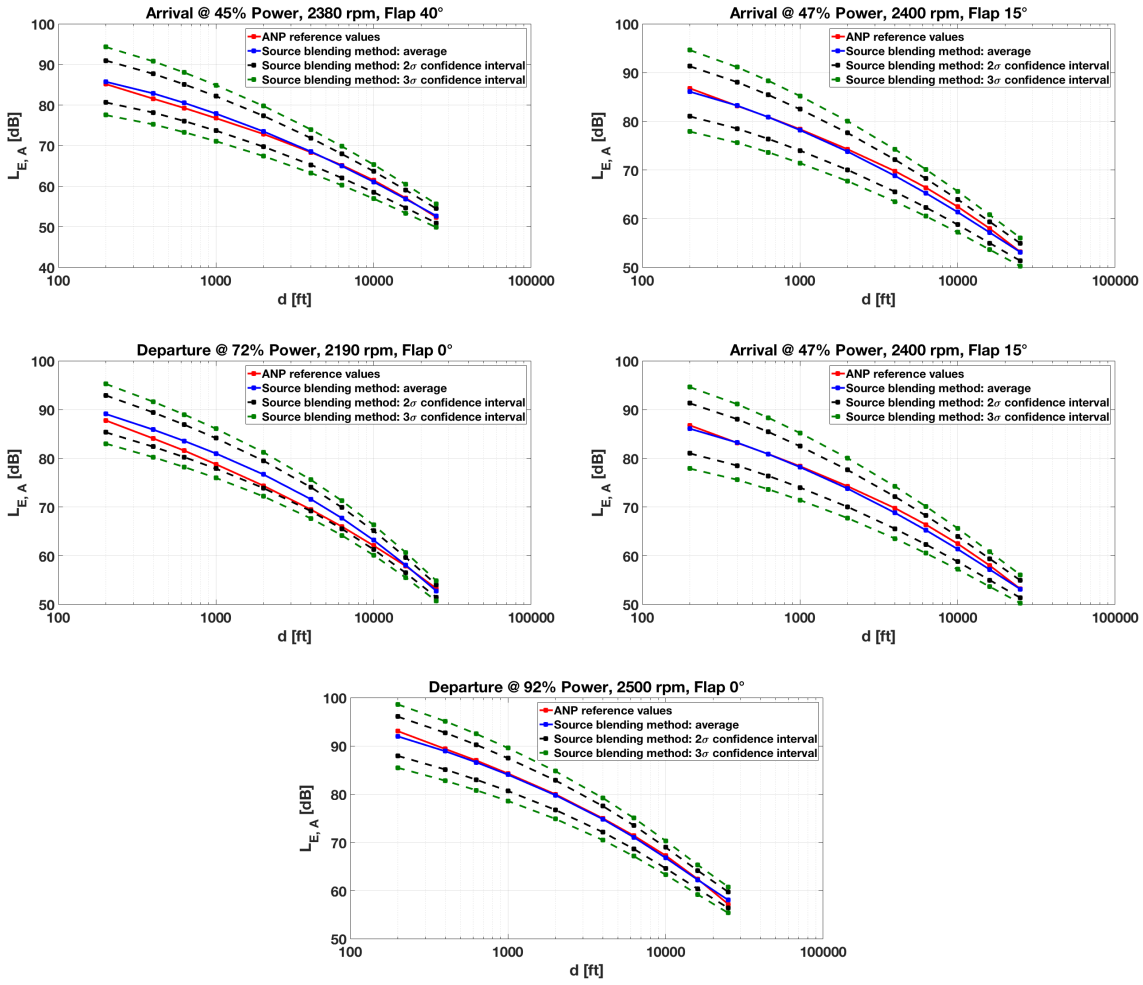

Figure A.2: Sound exposure data relative to Piper PA-31-350 Navajo Chieftain

In this case, the application of the new prediction procedure shows better results with respect to T206H since the ANP reference lines are in general closer to the outcome of the source blending method.

The higher level of accuracy in the application to this airplane is also confirmed by the target ANP values, which are always inside the 2σ bilateral confidence band.

Appendix B

Noise contours dependence on the power-train operational mode

When every acoustic analysis is performed, one of the most significant results is represented by the noise emission maps as they give a visually-effective idea of sound exposure in the proximity of an airport.

They necessarily result from the computation of the sound exposure level in a grid of ground receptors and basically display the isolines characterized by the same exposure value.

Figures from B.1 to B.7 refer to the standard traffic pattern at Milan Bresso airport, performed for each of the seven operational modes typical of the analysis on power management.

In particular, the black lines correspond to the circuit legs in all-electric mode, while the red lines refer to the activation of the internal combustion engine.

Moreover, the left contour plots are relative to Cessna T206H Stationair, the right ones to Piper PA-31-350 Navajo Chieftain.

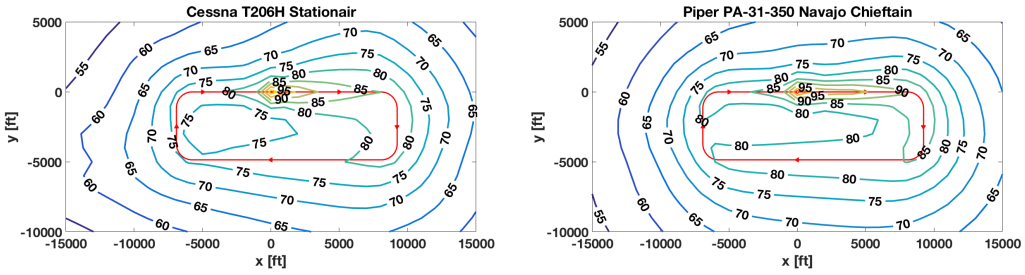

Figure B.1: ICE activation in all legs

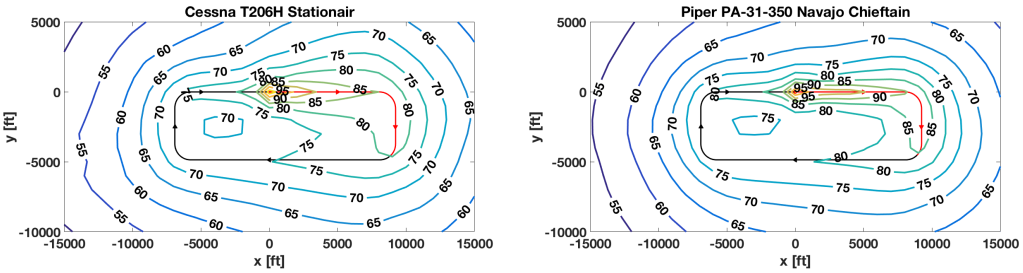

Figure B.2: ICE activation in the departure and crosswind legs

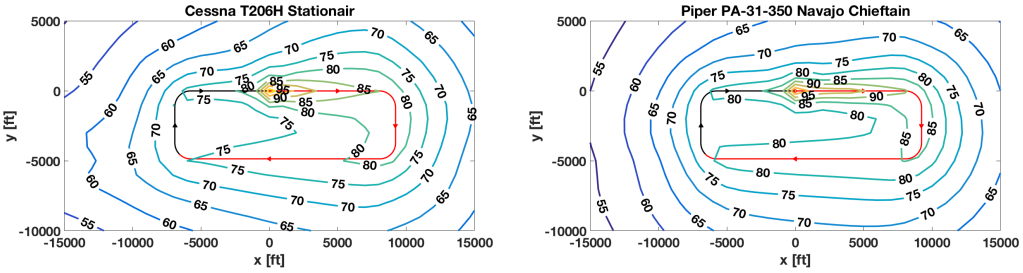

Figure B.3: ICE activation in the departure, crosswind and downwind legs

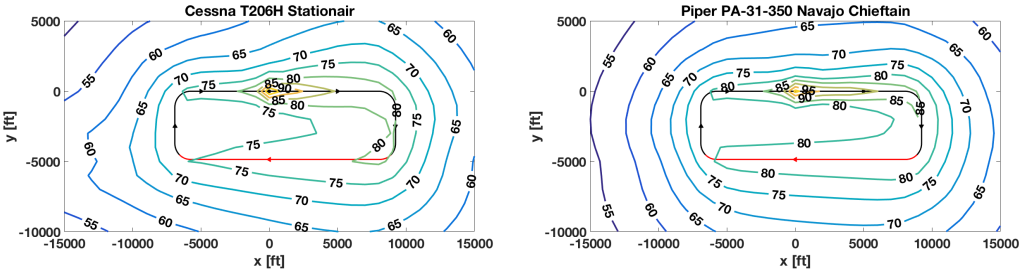

Figure B.4: ICE activation in the downwind leg

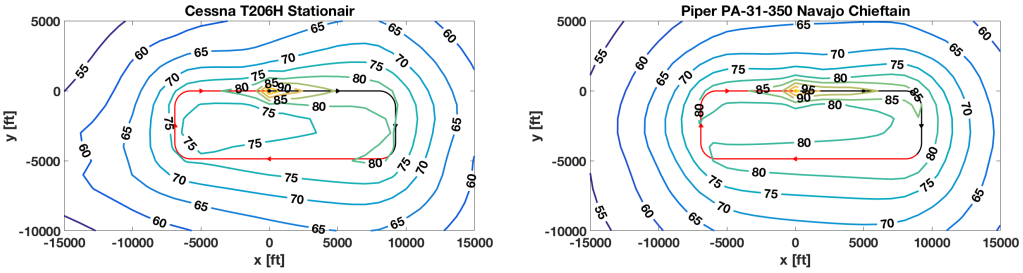

Figure B.5: ICE activation in the downwind, base and final legs

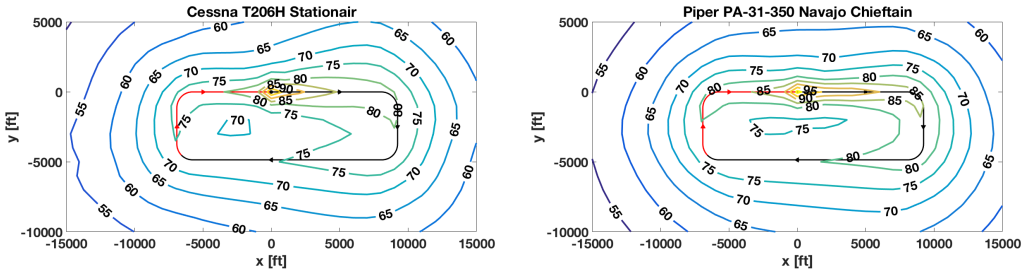

Figure B.6: ICE activation in the base and final legs

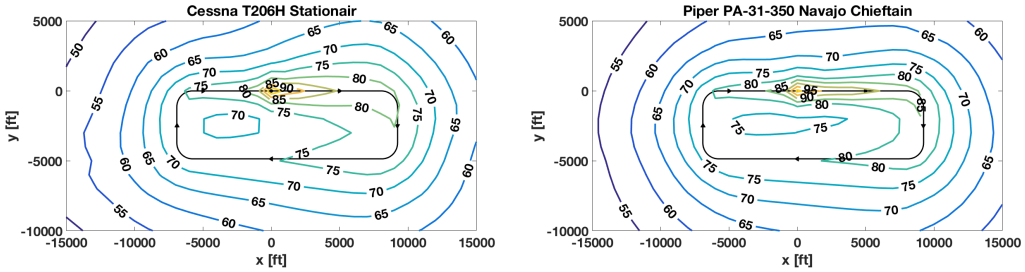

Figure B.7: No ICE activation

Though very effective from a visual point of view, the comparison of the different maps is quite complicated and can be made just is qualitative terms.

In general, the noise contours relative to PA-31 show larger sound exposures with respect to T206H as a result of the different size and number of propulsion units.

Looking at the ground track for the five hybrid-electric modes, it is interesting to notice the presence of an emission line in proximity of the point where power source changes.

In particular, sound exposure increases when the engine is turned on, as in the base-final cases: in proximity to the point of engine activation, noise increments to at least 75 dB for T206H, to 80 dB for PA-31.

The opposite situation occurs when the engine is turned off as can be seen in the downwind, but above all in the departure-crosswind case, where a noise contour is located exactly in the point of engine shutdown both for T206H and for PA-31.

Acknowledgements

After an impersonal and critical tone as it should be, it is the moment for the author to become Luca and open up his heart to thank all those people contributing to the realization of this work. Honestly, I used to think this was the most boring and useless part of a thesis, something to be done just by convention and nothing else. However, all the effort deployed during the preparation of this work has made me fully aware of the importance of people trusting and supporting me during this sort of nine-month journey.

Special thanks go to my supervisor, professor Carlo E. D. Riboldi, for his great availability and his precious advice on the realization of this work. I have particularly appreciated your combination of competence with a positive and proactive attitude even towards the most problematic situations. An important support has also been given by his working team, composed of prof. Rolando and prof. Trainelli, whom I value for your professionalism and for your directness. My gratitude also extends to Ing. Salucci for his psychological support and understanding in the most critical moments. Finally, a particular thought goes to all professors, even the ones I have appreciated less, for having spent a lot of time and effort in teaching me something important for my future.

The most heartfelt thanks are dedicated to my beloved Valentina, the person who has changed my life, making it something awesome. Your psychological contribution to the thesis has been inestimable since when I am with you, I feel safe, I feel understood, I simply feel perfect no matter the possible problems. In the realization of the thesis, I have realized that you have always had the right words to say in every occasion and you have encouraged me to face the problems, to go ahead, to never feel satisfied. Another non-obvious aspect concerns your extreme patience in supporting and listening to me although you study radically different subjects.

I am also extremely grateful to my family from both a psychological and even economical point of view. I am certain that money can not buy happiness, but I personally consider your economical effort as a sign of your faith in me and of your love in seeing me do what I aim to. I thank you for your desire to give me a good education and for your psychological support, which has been great all over the thesis work. Finally, a special thought goes to my granny for having me taught to strive for life and for the most important things against all diseases and possible problems.

Another relevant contribution to this thesis has been made by all my friends, from the ones living in my area to those I have known at university. As for the former, your support has been extremely important since I am at ease when we spend time together. I am aware I am not the most outgoing person ever existed, but I am very grateful to you as you have always found a way to make me smile and feel well. As for the latter, the distance between our homes have made us see just a couple of times during the thesis period, but the joy I have experienced in our rare meetings has made me realize how important you are.

A final dedication goes to all the people I have met during the preparation of this work and in general to all inhabitants of this wonderful planet, in the hope this work will contribute to the preservation of the natural beauties with which we are surrounded.